JOTCS A
Journal of the Turkish Chemical Society
Section: A
Chemistry

TURKISH CHEMICAL SOCIETY

Study on the Preparation and Drug Release Property of Modified PEG-DA Based Hydrogels

Sebnem Senol[1], Emel Akyol[1]*

[1]Department of Chemical Engineering, Yildiz Technical University, Istanbul, Turkey.

Abstract: The aim of the present study is to develop hydroxyapatite-modified PEG-DA and PEG-DA/HEMA based hydrogels for release of Donepezil HCl for potential treatment of Alzheimer's disease. [2,2-Dimethoxy-2-phenyl-acetophenone] (Irgacure 651), 1 hydroxycyclohexyl phenyl ketone (Irgacure 184) and 2-hydroxy-4'-(2-hydroxyethoxy)-2-methylpropiophenone (Irgacure 2959) were used as photo-initiators in the synthesis of hydrogels and hydroxyapatite was used for modifying hydrogels. Fourier transform infrared spectroscopy (FT-IR), scanning electron microscope (SEM) and digital microscope were utilized to investigate the characteristic properties of hydrogels. Photopolymerization technique was selected for the synthesis of hydrogels. Swelling and drug release studies have been performed under different pH conditions.

Keywords: Alzheimer's Disease, Hydrogels, Photopolymerization, Donepezil HCl, Polyethylene diacrylate, 2-Hydroxyethyl methacrylate.

Submitted: November 20, 2018. **Accepted:** January 03, 2019.

Cite this: Senol S, Akyol E. Study on the Preparation and Drug Release Property of Modified PEG-DA Based Hydrogels. JOTCSA. 2019;6(1):1–14.

DOI: http://dx.doi.org/10.18596/jotcsa.485817.

***Corresponding author. E-mail:** eakyol@yildiz.edu.tr.

INTRODUCTION

Many new classes of materials have been used to improve different innovative applications. Hydrogels, being cross-linked three-dimensional polymeric materials, have the ability to absorb large amounts of water. In recent years, hydrogels have an increasing demand for drug delivery systems. The purpose of the drug delivery systems is to maintain drug concentration in the blood or in target tissues at prolonging drug-release times (1-6).

Polyethylene glycol diacrylates (PEG-DA) based polymers possess highly attractive properties that cause widely using in variety of applications

such as tissue engineering, controlled drug delivery, and medicine areas. Polyethylene glycol diacrylate is non-volatile, non-toxic, environmentally friendly, and also tailor-made into various shapes. Polyethylene glycol diacrylate acts as potential stabilizers and matrices for the formation of functional hydrogels (7-10).

Poly(2-hydroxyethyl methacrylate) (pHEMA), one of the synthetic water-soluble polymer, has been largely preferred, especially in various biomedical applications due to its chemical stability (11-12).

Hydroxyapatite (HAp), $Ca_{10}(PO_4)_6(OH)_2$, is a double salt of tri-calcium phosphate and calcium hydroxide, and it is the main inorganic component of human bones and teeth. However, hydroxyapatite has an excellent biocompatibility and tissue bioactivity (13-16).

UV light polymerization is one of the main methods used in the synthesis of hydrogels in biomedical field. Considerable attention has been focused on photopolymerization method due to its broad applications. Nowadays, free radical polymerization with UV light is utilized in different applications such as coatings, information storage systems, films, contact lenses, and biomaterials. In the photopolymerization, the primary radicals were generated from light absorption of photoinitiator at a suitable wavelength thus polymerization and into highly cross-linked structures of multifunctional acrylates occurs (17-18).

Alzheimer's disease (AD) is the most common type of dementia that cause cognitive impairment and memory loss (19). The number of patients with AD is projected to more than double by 2050. Although the etiology of AD has been elucidated, multiple questions remain unanswered (20-21).

Donepezil is a piperidine-based, reversible acetylcholinesterase (Ach) inhibitor generally used in the treatment of Alzheimer patients. Donepezil prevents the hydrolysis of the residual Ach in the brain so it is the best pharmacological tool to decrease cognitive deficits in AD patients. Donepezil has been investigated to be sufficient for enhancing of cognitive impairment and memory loss in patients with Alzheimer's disease. It is well efficient when 5 mg of the drug is used once daily (22-27).

In this study, we aimed to develop prolonged drug release systems enhanced with HAp. We synthesized PEG-DA/HEMA based hydrogels with modified Hap via photopolymerization. Fourier transform infrared spectroscopy (FT-IR), scanning electron microscope (SEM) and digital microscope were utilized to investigate the characteristic properties of hydrogels. Modified PEG-Da/HEMA hydrogels were used for prolonging the release time.

EXPERIMENTAL

Materials

2-Hydroxylethyl methacrylate (HEMA), polyethylene glycol diacrylates M_n=700 (PEG-DA), ethylene glycol dimethacrylate, 2,2-dimethoxy-2-phenyl-acetophenone (Irgacure 651, 99% purity), 1-hydroxycyclohexyl phenyl ketone (Irgacure 184, 99% purity), 2-hydroxy-4'-(2-hydroxyethoxy)-2-methylpropiophenone (Irgacure 2959, 98% purity), hydroxyapatite (powder, 5 μm and surface area ≥ 100 m^2/g), were supplied by Sigma-Aldrich. Donepezil HCl was a kind gift by Abdi İbrahim Company. Sodium chloride and hydrochloric acid were purchased from Merck. Sodium hydroxide and monobasic potassium phosphate were supplied from J.T Baker. All chemicals were used as received without further purification.

Preparation and characterization of PEG-DA/HEMA hydrogels

PEG-DA/HEMA based hydrogels were prepared in the presence of a photo-initiator (Irg 184, Irg 651, Irg 2959) and a crosslinking agent (ethylene glycol dimethacrylate), as shown in Table 1. The reactant mixtures were added to petri plates which consist of olive oil, using a micropipette. The reactant mixtures were deaerated by bubbling nitrogen gas during the reaction. Photopolymerization was performed at 365 nm under UV irradiation for a short time.

According to hydrogel type, 50% (w/v) PEG-DA, 25% (w/v) PEG-DA- 25% (w/v) HEMA and predetermined ratios of photo-initiators were mixed by using a magnetic stirrer at 50 rpm. Then, 0.07% (w/v) Donepezil HCl and deionized water were added. 0.5% ethylene glycol dimethacrylate was then introduced. After photopolymerization, hydrogels were washed with n-hexane and dried at room temperature.

Table 1: Synthesis conditions for the PEG-DA/HEMA based hydrogels.

Hydrogels	PEG-DA	HEMA	EGDMA	Irg 651	Irg 184	Irg 2959	HAp
Hydrogel 1 (H1)	50%	-	0.5%	1%	-	-	1%
Hydrogel 2 (H2)	50%	-	0.5%	-	1%	-	1%
Hydrogel 3 (H3)	50%	-	0.5%	-	-	1%	1%
Hydrogel 4 (H4)	25%	25%	0.5%	1%	-	-	1%
Hydrogel 5 (H5)	25%	25%	0.5%	-	1%	-	1%
Hydrogel 6 (H6)	25%	25%	0.5%	-	-	1%	1%

The equilibrium swelling ratios of the swollen hydrogels were measured using a gravimetric method in deionized water, pH 1.2, 6.8, and 7.4. Drug loaded hydrogels were used for swelling behavior at 37 °C. At predetermined time points, the hydrogels were taken out and weighed after removal of surface water. Swelling and release analyses were repeated three times. A UV–Vis spectrophotometer (Analytikjena Specord 200/Plus) at 270 nm was used for release studies.

The determination of swelling ratio and preperation of buffer solution procedure has been reported previously in detail (4,28).

RESULTS AND DISCUSSIONS

FT-IR Analyses of Hydrogels

For the imaging of photo-crosslinked PEGDA-based hydrogels, the attenuated total reflectance-FTIR (ATR-FTIR) scan was performed with a Perkin Elmer Spectrum 100 FTIR spectrometer. For each sample, a spectrum is obtained using the ATR utilizing a diamond internal reflection element mounted on a holder at a resolution of 4 cm^{-1} in the range 4000-400 cm^{-1} for a total of 16 scans.

FT-IR spectra of the hydrogels are shown in Figure 1. In the PEG-DA spectrum, there was an –OH at 3600 cm^{-1}, a CH_2 at 2853 cm^{-1}, a C=O at 1728 cm^{-1}, and a C=C at 1628 cm^{-1}. For the PEG-DA/HEMA based hydrogels, there was an –OH bond at 3500 cm^{-1}, a CH_2 at 2853 and 2956 cm^{-1} , a C=O at 1730 cm^{-1} , a C=C at

1610 cm^{-1}, a C–OH at 1059 cm^{-1}. The bands at 1090 and 960 cm^{-1} are used for the characterization of phosphate stretching vibration and the bands observed at 598 and 559 and at 1020 cm^{-1} are due to the phosphate being in vibration. FT-IR analyses results confirm the combination of PEG-DA and HEMA.

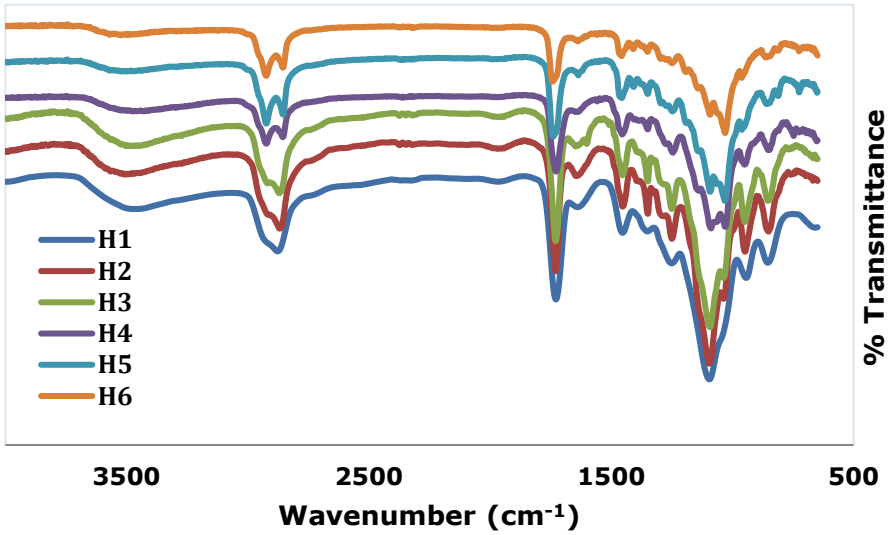

Figure 1. FT-IR spectra of the hydrogels.

SEM Analysis of Hydrogels

The sizes of hydrogels were obtained by digital microscope (Veho, VMS- 004 USB) Microscope (Figure 4). The textures of the hydrogels were examined by a conventional scanning electron microscopy (JEOL JSM 6335F). Figure 2 shows the SEM micrographs of PEG-DA based hydrogels using HAp as modified. The SEM morphology of H1 hydrogel showed a surface devoid of pores and cracks. Figure 3 shows the effect of incorporation of HEMA and PEG-DA on structure of hydrogels. While microparticles were formed in the presence of PEG-DA, the presence of HEMA revealed a spherical structure. The hydroxyapatite modified PEG-DA hydrogels were very different from and PEG-DA/HEMA based hydrogels.

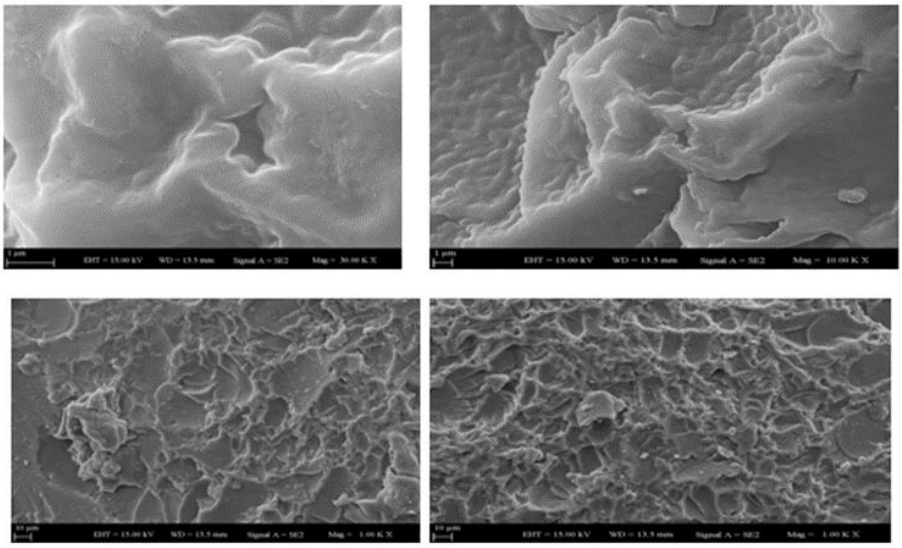

Figure 2: Scanning electron micrographs of H1 hydrogel.

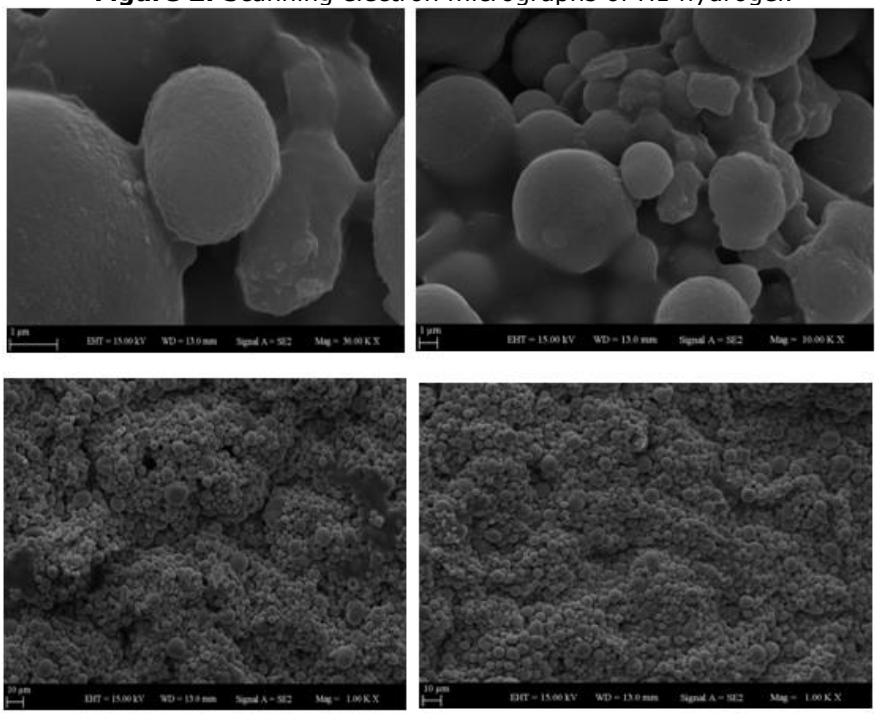

Figure 3: Scanning electron micrographs of H6 hydrogel.

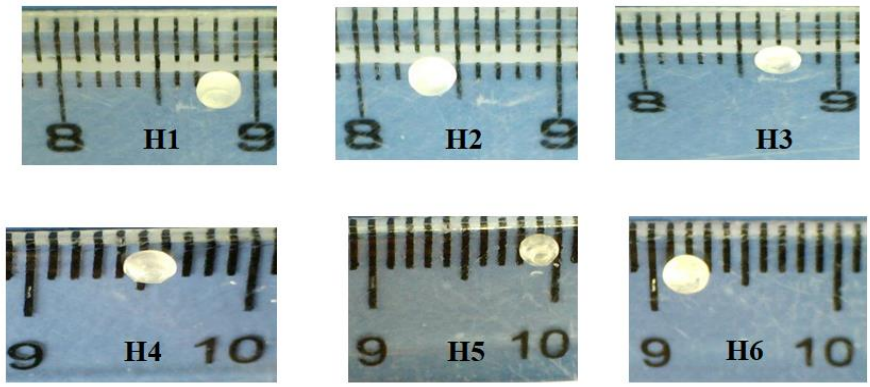

Figure 4: Digital microscope photos of synthesized hydrogels.

Swelling tests

In order to investigate the influence of the presence of HAp and pH, swelling kinetics of PEG-DA and PEG-DA/HEMA based hydrogels were studied. Swelling ratios of the studied hydrogels after 240 minutes of immersion in water and solutions with of pH 1.2, pH 6.8 and pH 7.4 at 37 °C were summarized in Figures 5-8. As seen in the figures, higher swelling ratios were observed for PEG-DA hydrogels according to PEG-DA/HEMA based hydrogels. The swelling ratio of hydrogel decreased significantly with the incorporation of HEMA to PEG-DA. While the values of swelling percentage of PEG-DA hydrogels were ranged between 80 and 86%, swelling percentage of PEG-DA/HEMA hydrogels were ranged between 43 and 49%. The swelling of hydrogels usually depends on the pH. As illustrated in these figures, at pH 6.8 has the highest swelling ratio for all hydrogels.

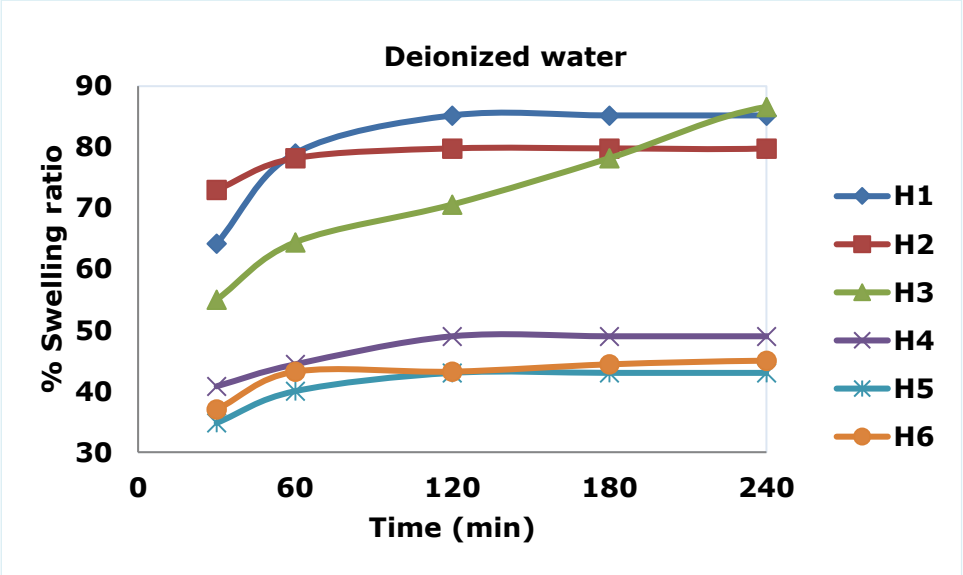

Figure 5: Swelling weight ratio of the studied hydrogels in deionized water.

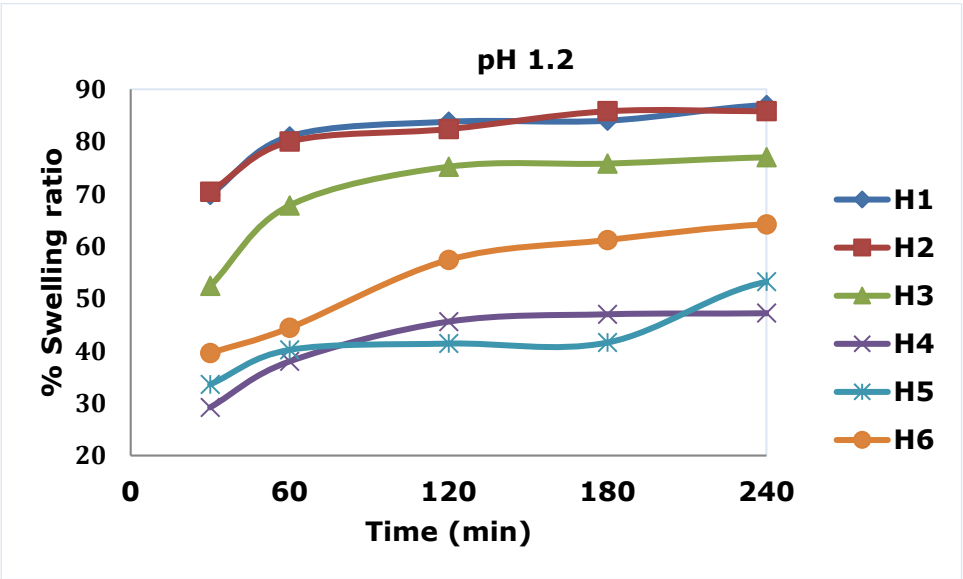

Figure 6: Swelling weight ratio of the studied hydrogels in pH 1.2.

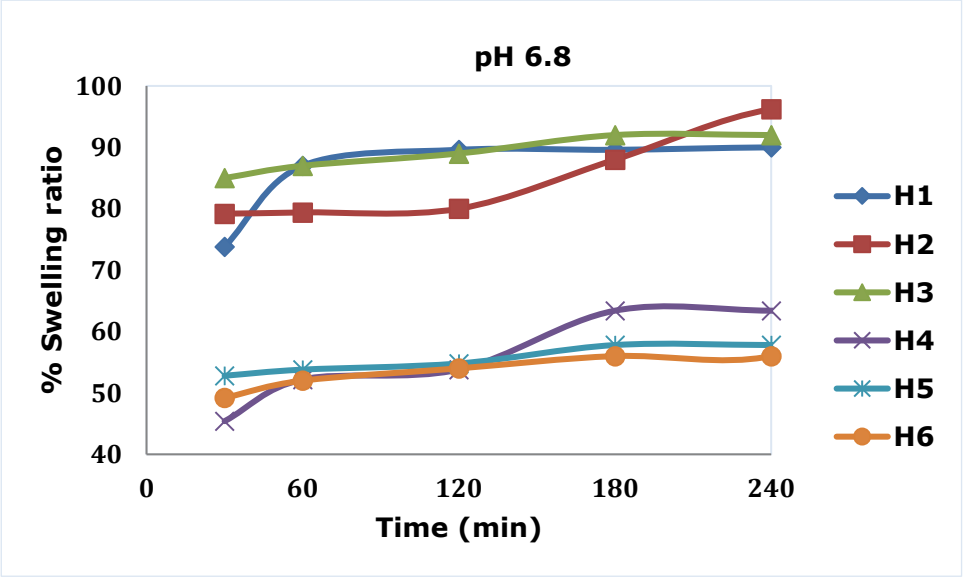

Figure 7: Swelling weight ratio of the studied hydrogels in pH 6.8.

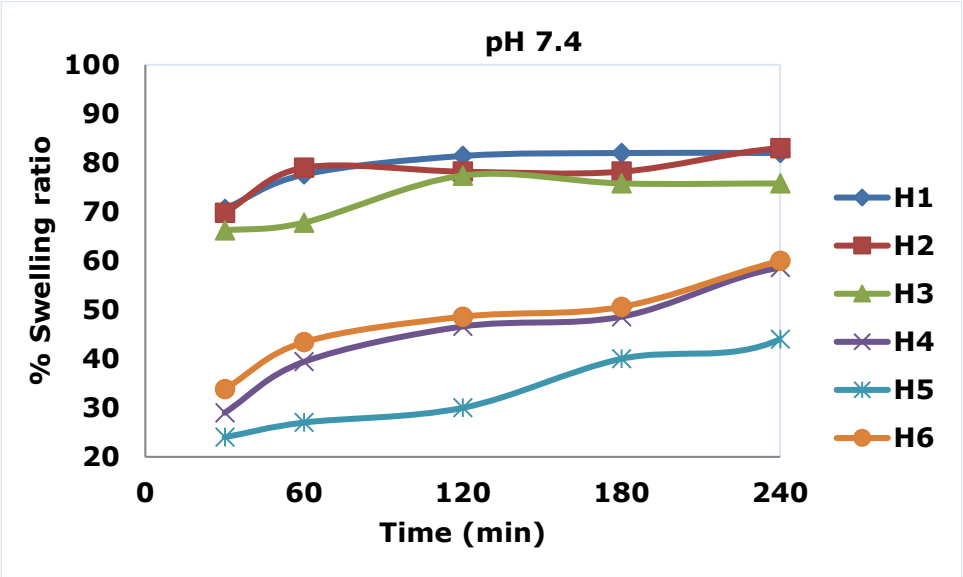

Figure 8: Swelling weight ratio of the studied hydrogels in pH 7.4.

Donepezil HCl release analyses

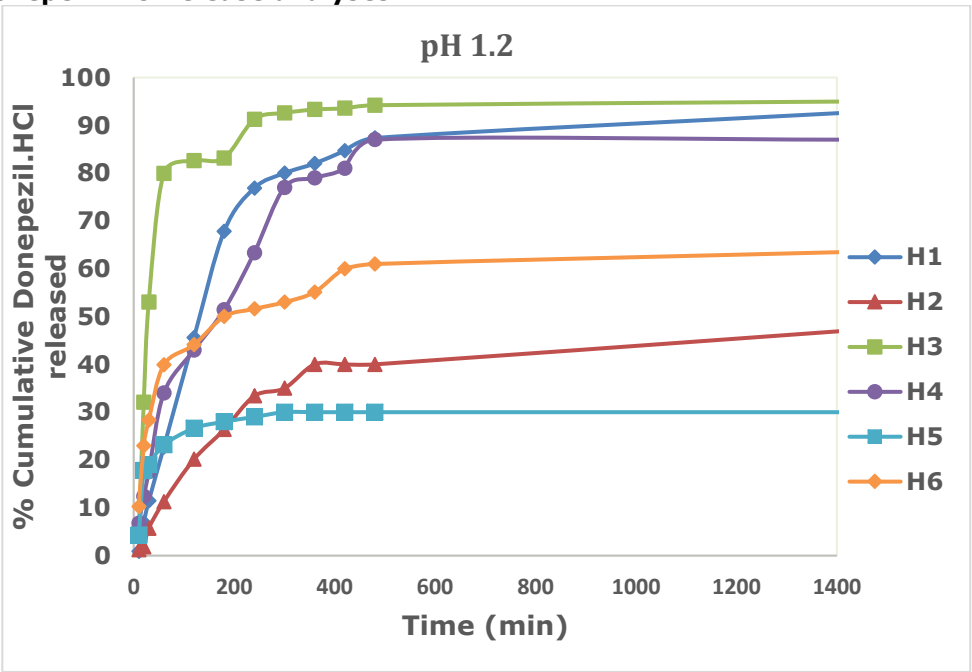

Figure 9: Release ratio of hydrogels in pH 1.2.

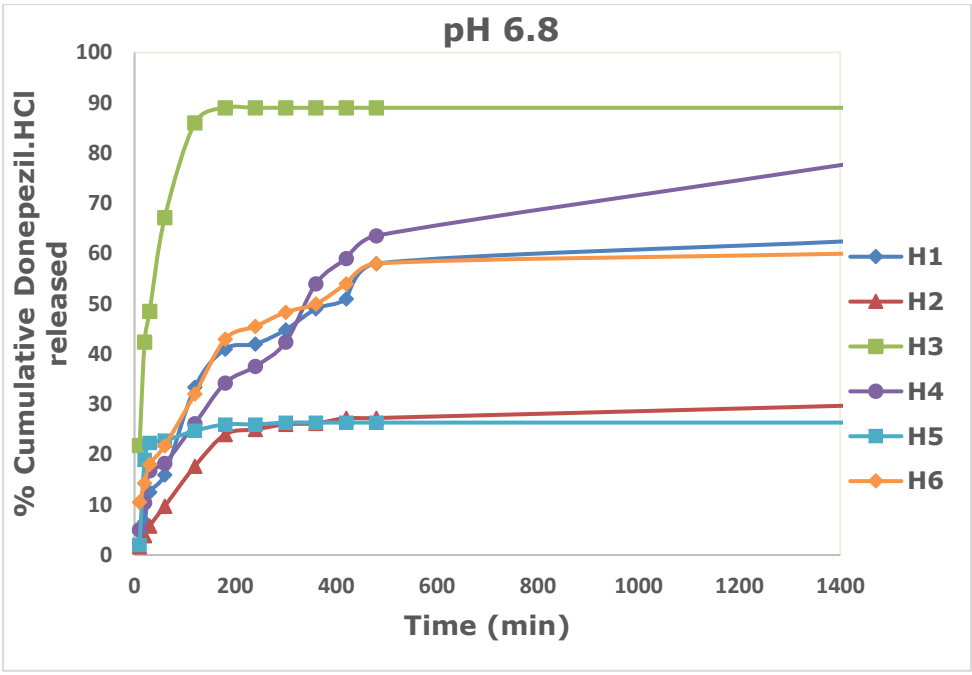

Figure 10: Release ratio of hydrogels in pH 6.8.

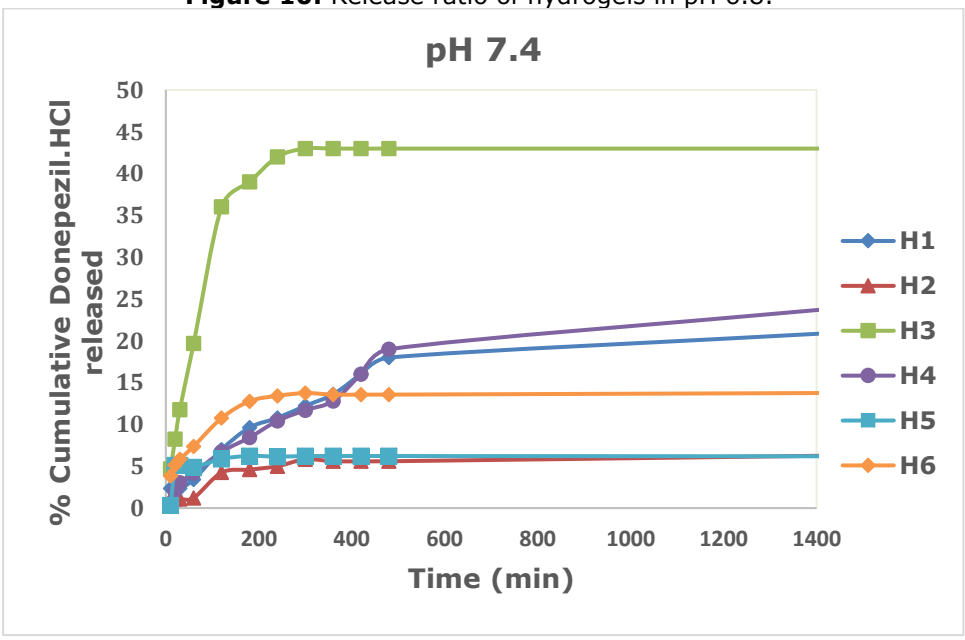

Figure 11: Release ratio of hydrogels in pH 7.4.

Figures 9, 10 and 11 show the percent cumulative release of the pharmaceutical ingredient from synthesized hydrogels at simulated media, at 37 °C. It has been found that H3 hydrogel (hydroxyapatite modified PEG-DA, in the presence of Irgacure 2959 as a photo-initiator shows the highest release. The results demonstrated that synthesized hydrogels using Irg 184 released the minimum amount of donepezil

hydrochloride. Also, PEG-DA/HEMA hydrogels were very pH sensitive. The amount of drug released increased with increasing pH. Similar results obtained from our previous studies (4,29).

CONCLUSION

In the presented study, the synthesis of PEG-DA/HAp and PEG-DA-HEMA/HAp hydrogels was achieved by UV photopolymerization. According to swelling and release analysis of hydrogels in different pH environments, the synthesized hydrogels exhibited a pH sensitive behavior. The release was slower when the pH was lower. Morever, both swelling and release behavior of hydrogels were highly influenced by the type and amount of photo-initiators. The results in the present investigation confirm the controlled release of Donepezil HCl. These data suggested that, this kind of hydrogels may be useful for utilization in the release of drug.

REFERENCES

1. Hagel V, Haraszti T, Boehm H. Diffusion and Interaction in PEG-DA Hydrogels. Biointerphases. 2013;8:36.

2. Rahimi S, Khoee S, Ghandi M. Development of Photo and pH Dual Crosslinked Coumarin-Containing Chitosan Nanoparticles for Controlled Drug Release, Carbohydrate Polymers. 2018;201:236-45.

3. Dash S, Murthy P.N, Nath L, Chowdhury P. Kinetic Modeling On Drug Release From Controlled Drug Delivery Systems. Polish Pharmaceutical Society. 2010;67:217-23.

4. Senol S, Akyol E. Synthesis and Characterization of Hydrogels Based on poly(2-hydroxyethyl methacrylate) for Drug Delivery Under UV Irradiation. Journal of Materials Science. 2018; 53:14953-63.

5. Akyol E, Senol S, Dogan O. Controlled Release of Donepezil Hydrochloride From the Ternary Sodium Alginate Based Hydrogels. Bulgarian Chemical Communications. 2017;49:57-63.

6. Wang Z, Zhang H, Chu J.A, Jackson J, Lin K, lim C.J, Lange D, Chiao M. Mechanically Enhanced Nested-Network Hydrogels as a Coating Material for Biomedical Devices. Acta Biomaterialia. 2018;70:98-109.

7. Ponnuvelu D.V, Kim S, Lee J. Polyethyleneglycol Diacrylate Hydrogels with Plasmonic Gold Nanospheres Incorporated via Functional Group Optimization. Micro and Nano Systems Letters. 2017;5:21.

8. Chiu Y-C, Brey E.M, Pérez-Luna M.B. A Study of the Intrinsic Autofluorescence of Poly(ethylene glycol)-co-(L-Lactic acid) Diacrylate. J Fluoresc.2012;22:907–13.

9. Ayhan H, Ayhan F. Photocrosslinked Poly(Ethylen Glycol) Hydrogels for Controlled Drug Delivery. Turk J Biochem. 2014; 39(4):403–15.

10. Ural-Kayalık H, Çetin S. Synthesis and Drug-release Properties of Biodegradable Hydrogels Having b-cyclodextrin. JOTCSA. 2017;4(1):415–30.

11. Bat E. Hydroxyethyl Methacrylate-based Nanocomposite Hydrogels with Tunable Pore Architecture. JOTCSA. 2016;3(3):607–22.

12. Garćıa-Uriostegui L, Delgado E, Melendez-Ortiz H.I., Camacho-

Villegas T.A. , Esquivel-Solís H, Gatenholm p, Toriz G. Carbohydrate Polymers.2018; 201:490-9.

13. Islas L, Burillo G, Ortega A. Graft Copolymerization of 2-Hydroxyethyl Methacrylate onto Chitosan Using Radiation Technique for Release of Diclofenac. Macromolecular Research. 2018;26:690-5.

14. Cao X-Y, Wen F, Bian W, Cao Y, Pang S-J, Zhang W-K. Preparation and comparison study of hydroxyapatite and Eu-hydroxyapatite. Front. Mater. Sci. 2009;3:255–8.

15. Sani T, Adem M, Fetter G, Bosch P, Diaz I. Defluoridation Performance Comparison of Nanohydrotalcite/Hydroxyapatite Composite with Calcined Hydrotalcite and Hydroxyapatite. Water Air Soil Pollut. 2016;227:90.

16. Verma D, Kattı S-K, Kattı D-R. Effect of Biopolymers on Structure of Hydroxyapatite and Interfacial Interactions in Biomimetically Synthesized Hydroxyapatite/Biopolymer Nanocomposites. Annals of Biomedical Engineering. 2008;36:1024-32.

17. Göktürk S. Effect of Hydrophobicity on Micellar Binding of Carminic Acid. Journal of Photochemistry and Photobiology A: Chemistry. 2005: 169:115-21.

18. Ayhan H, Ayhan F. Water based PHEMA Hydrogels for Controlled Drug Delivery. Turk J Biochem. 2017;43:3.

19. Kamoun E-A, Abu-Seaid M.A., Doma A.S., Menzel H, Chen X. Influence of Degree of Substitution and Folic Acid Coinitiator on pullulan-HEMA Hydrogel Properties Crosslinked Under Visible Light Initiating system. Biomac. 2018;116:1175-85.

20. Liew K-B, Tan Y.T.F, Peh K-K. Characterization of Oral Disintegrating Film Containing Donepezil for Alzheimer Disease. AAPS PharmSciTech. 2012;13:134-42.

21. Zheng H, Niu S, Zhao H, Li S, Jiao J. Donepezil Improves the Cognitive Impairment in a Tree Shrew Model of Alzheimer's Disease Induced by Amyloid-β1–40 via Activating the BDNF/TrkB Aignal Pathway. Metabolic Brain Disease.2018;1-14.

22. Wang Y-R, Yang Y-H, Lu C-Y, Lin S-H, Chen S-H. Trace Analysis of Acetylcholinesterase Inhibitors with Antipsychotic Drugs for Alzheimer's Disease by Capillary Electrophoresis with on Column Field-Amplified Sample Injection , Anal Bioanal Chem.2013;405:3233–42.

23. Cutuli D, Bartolo P.B., Caporali P, Tartaglione A-M.,Oddi D, D'Amato F-R, Nobli A, D'Amelio M, Petrosini L. Neuroprotective Effects of Donepezil Against Cholinergic Depletion. Alzheimer's Research & Therapy.2013;5:50.

24. Choi Y, Rhee S-J, Jang I-J, Yu K-S, Yim S-V, Kim B-H. Bioequivalence Study of Donepezil Hydrochloride in Healthy Korean Volunteers. Transl Clin Pharmacol. 2015;23(1):26-30.

25. Abonassıf M.A, Hefnawy M.M, Kassem M.G, Mostafa G.A.E. Determination of Donepezil Hydrochloride In Human Plasma and Pharmaceutical Formulations by HPLC with Fluorescence Detection. Acta Pharm. 2011; 61:403–13.

26. Barot T.G., Patel P.K. RP-HPLC Method for the Estimation of Donepezil Hydrochloride Dosage Form. E-Journal of Chemistry. 2009;6(2):594-600.

27. Chothe P.P, Subramanian R.C., Kadam V.J. Stability Assessment Of Donepezil Hydrochloride Using Validated RP-HPLC Method. Research Journal of Pharmaceutical, Biological and Chemical Sciences. 2010;1(3):296.

28. Lakka NS, Goswami N. Solubility and Dissolution Profile Studies of Gliclazide in Pharmaceutical Formulations by HPLC. Int Res J Pharm. 2012; 3(6):126–9.

29. Senol S, Akyol E. Controlled Release of Donepezil Hydrochloride From PEG-DA Hydrogels. Bulgarian Chemical Communications. 2018; 50:12-17.

JOTCS A
Journal of the Turkish Chemical Society
Section: A
Chemistry
TURKISH CHEMICAL SOCIETY

Determination of Antimicrobial and Biological Activities of *Salvia sclarea* L. (Lamiaceae) Extracts

Sevim Küçük[1]*, Pervin Soyer[2], Yağmur Tunalı[2]

[1]Anadolu University, Faculty of Pharmacy, Department of Pharmaceutical Botany, 26470, Eskişehir, Turkey.
[2]Anadolu University, Faculty of Pharmacy, Department of Pharmaceutical Microbiology, 26470, Eskişehir, Turkey.

Abstract: Therapeutic plant species of genus Salvia are important and highly recommended medicinal plant, due to their pharmaceutical properties. In the present study, S*alvia sclarea* L. was collected during its flowering stage in 2016, Sarıcakaya (Eskişehir/Turkey) and dried medicinal plant material were macerated with 70% MeOH. The antimicrobial activity of *Salvia sclarea* extracts was determined with minimum inhibitory concentration (MIC) assay against *Staphylococcus aureus* ATCC 29213, *Staphylococcus epidermidis* ATCC 14990, *Enterecoccus faecalis* ATCC 51299, *Bacillus subtilis* NRRL B478, *Escherichia coli* ATCC 35218, *Candida albicans* ATCC 90028 and *Candida krusei* ATCC 6258. The antibiofilm activity of *Salvia sclarea* extracts was determined against *Staphylococcus aureus* ATCC 29213 and *Staphylococcus epidermidis* ATCC 14990 *Candida albicans* ATCC 90028 and *Candida krusei* ATCC 6258. In addition, the preliminary cytotoxicity assessment of extracts was tested with Brine Shrimp Lethality Assay against model organism *Artemia salina* nauplii. As a result, *Salvia sclarea* extract showed remarkably antimicrobial antibiofilm efficacy to all tested microorganisms. The cytotoxicity concentrations of S*alvia sclarea* plant extract also was determined. These results suggest the potential use of the S*alvia sclarea* L. extract as natural medicine in pharmaceutical industry.

Keywords: *Salvia sclarea;* antimicrobial; antibiofilm; cytotoxicity.

Submitted: September 25, 2018. **Accepted:** January 09, 2019.

Cite this: Küçük S, Soyer P, Tunalı Y. Determination of Antimicrobial and Biological Activities of Salvia sclarea L. (Lamiaceae) Extracts. JOTCSA. 2019;6(1):15–20.

DOI: http://dx.doi.org/10.18596/jotcsa.463681.

***Corresponding author.** E-mail: salan@anadolu.edu.tr

INTRODUCTION

Plant derivates are an important source of natural products and considered as new treatments of various diseases. They have a wide variety of structural and biological attributes. They have played a significant role in traditional medicine of various countries. *Salvia sclarea* L. is an important genus of the *Lamiaceae* family that has approximately 1000 species and represented by nearly 99 species with 58 taxa endemic species in Turkey. *Salvia sclarea* is locally known as "Paskulak" (1,2). S*alvia sclarea* L. general plant view is shown in Figure 1. Turkey is an important country for export and usage of Salvia species in the world (3). Salvia species are used in medicine for the treatment of many popular illnesses such as stomach aches, colds and pain in the throat as herbal tea (4). They possess a number of biological activities including antiseptic, antibacterial (5,6), antibiofilm, antioxidant (7), anti-inflammatory (3,8,9), antiviral (10,11), antitumoral (12) cytotoxic (6,13,14), spasmolitic, anticonvulsant (15) antimycobacterial (4), and carminative activities (16). Nowadays, with the increasing of antibiotic resistance in microorganisms, it became a necessity to find effective alternatives. Therefore, in the current study antimicrobial, antibiofilm and lethality activities of *Salvia sclarea* L. was defined by using different biological methods.

Figure 1: General plant view of S*alvia sclarea* (Photo: Sevim Küçük)

MATERIALS AND METHODS

Plant Materials

S*alvia sclarea* L. was collected during the flowering stage in 2016, Sarıcakaya (Eskişehir/Turkey). Collected plant samples were identified and prepared voucher specimens are kept at the Herbarium of Faculty of Pharmacy of Anadolu University, Turkey (ESSE NO:14701). Plants were dried with medicinal plant materials and macerated with 70% MeOH. Aqueous extracts were evaporated at 80 °C, 90 rpm with a rotary evaporator and crude extract was gained. Then, plant extracts were lyophilized. 50 g of plant extract was obtained as a result. Different concentrations of dried extracts were resuspended in dimethyl sulfoxide (DMSO).

Determination of Minimum Inhibitory Concentration (MIC)

The MICs were defined as the lowest concentrations necessary for the inhibition of growth. Clinical Laboratory Standards Institute (CLSI) microdilution broth methods (17,18) were used. Five different concentrations of *Salvia sclarea* extracts were applied to the *Staphylococcus aureus* ATCC 29213, *Staphylococcus epidermidis* ATCC 14990, *Enterecoccus faecalis* ATCC 51299, *Bacillus subtilis* NRRL B478, *Escherichia coli* ATCC 35218, *Candida albicans* ATCC 90028 and *Candida krusei* ATCC 6258 species by using 96 well plate assay. *Salvia sclarea* extracts were weighed and dissolved in dimethyl sulfoxide (DMSO). Proper concentrations were 3000, 1500, 750, 375 and 187.5 µg/mL. Overnight microorganism cultures were adjusted to McFarland 0.5 standard (approximately 10^8 colony-forming units (CFU)/mL) 100 µL of extract and 100 µL of each microorganism cultures were inoculated to the well plates and incubated at 37 °C, 24 hours. Ketoconazole for yeast species (*Candida albicans* and *Candida krusei*), chloramphenicol for bacteria species (*Escherichia coli, Staphylococcus aureus Staphylococcus epidermidis, Enterecoccus feacalis, Bacillus subtilis*) and ethanol (C_2H_5OH) were used as positive control at 6000, 3000, 1500, 750, 375, 187.5, 93.75, 46.875, 23,437 and 11.718 µg/mL. Sterile distilled water was also used as negative control. After incubation period wells were stained by 20 µL resazurin dye to observe the color difference between dead and living cells.

Biofilm eradication assay (Determination of Minimum Biofilm Eradication Concentration (MBEC))

Microbial biofilms are communities of microorganisms that are embedded in a self-producing matrix, forming on living and nonliving surfaces. The antibiofilm activity of *Salvia sclarea* extract was determined by using the minimum biofilm eradication concentration (MBEC) assay. The eradication effect of *Salvia sclarea* extracts on biofilm formation was evaluated in 96-well plates. Briefly, overnight *Staphylococcus aureus* ATCC 29213, *Staphylococcus epidermidis* ATCC 14990, *Candida albicans* ATCC 90028 and *Candida krusei* ATCC 6258 cultures were adjusted to McFarland 0.5 standard standard (approximately 10^8 colony-forming units (CFU)/mL). 200 µL of each bacteria were inoculated to the well plates and incubated at 37 °C, for 48 hours to form the biofilm at the bottom of the wells. After incubation period, wells were gently washed two times with 100 µL of %0.90 NaCl (physiological saline). 100 µL of *Salvia sclarea* extract (3000, 1500, 750, 375 and 187.5 µg/mL) was added to each well and incubated at 37 °C, 24 hours. Ethanol (C_2H_5OH) and sterile distilled water were used as positive and negative controls. After the incubation period, wells were stained by 20 µL resazurin dye.

Brine Shrimp Lethality test

A 24-h LC_{50} bioassay was performed in a 96 well plate using nauplii of the Brine shrimp *Artemia salina* (19). Commercially sold ROTIFISH *Artemia* mix was used. Eighteen grams of *Artemia* mix was poured into 500 mL of distilled water and incubated 48-52 hours at 30 °C. After the incubation period, larvae were taken and counted. Brine shrimp lethality bioassay was determined with *Salvia sclarea* extract concentrations (3000, 1500, 750, 375, 187.5, 93.75, 46.87, 23.43, 11.71, 5.85 µg/mL) with ten (10) *Artemia salina* larvae in each concetration well. After 24 hours of incubation period, the alive larvae were counted.

RESULTS AND DISCUSSION

Extraction Yield

S*alvia sclarea* L. plant samples were extracted by 70% MeOH extraction method. The extraction yields were 62.5% by weight.

Determination of Minimum Inhibitory Concentration (MIC)

The MIC values of *Salvia sclarea* extracts were determined to be 750 µg/mL for *Staphylococcus aureus* ATCC 29213, *Staphylococcus epidermidis* ATCC 14990, *Bacillus subtilis NRRL B478*,

Escherichia coli ATCC 35218 and 1500 µg/mL for *Enterecoccus faecalis* ATCC 51299. Moreover, 750 µg/mL for *Candida albicans* ATCC 90028 and *Candida krusei* ATCC 6258 was determined. These results indicated that plant extract has strong broad-spectrum antimicrobial activity. All of the MIC values showed that *Enterecoccus faecalis* ATCC 51299 is more resistant than other test micoorganisms. Results are represented in Tables 1 and 2. *Salvia sclarea* plant extract showed equal bacteriostatic activity against test bacteria and yeast strains. Our results are similar to observations that previously reported in the literature, indicating that Gram-positive, Gram-negative bacteria and yeasts showed same activity with same MIC values.

Table 1: MIC values of *Salvia sclarea* plant extract and chloramphenicol against bacteria species.

Test Strains	**MIC values of *Salvia sclarea extract* (µg/mL)**	**Chloramphenicol (µg/mL)**
Staphylococcus aureus ATCC 29213	750	23.43
Staphylococcus epidermidis ATCC 14990	750	NG
Enterecoccus faecalis ATCC 51299	1500	187.5
Bacillus subtilis NRRL B478	750	NG
Escherichia coli ATCC 35218	750	93.75

*NG: No growth.

Table 2: MIC values of *Salvia sclarea* plant extract and Ketoconazole against yeast species.

Test Strains	**MIC values of *Salvia sclarea extract* (µg/mL)**	**Ketoconazole (µg/mL)**
Candida albicans ATCC 90028	750	187.5
Candida krusei ATCC 6258	750	48.875

Biofilm eradication assay (Determination of Minimum Biofilm Eradication Concentration (MBEC))

Antibiofilm studies demonstrated a dose-dependent activity. The antibiofilm activity of *Salvia sclarea extract* was examined by minimum biofilm eradication concentration (MBEC) assay. The MBEC values were determined to be 3000 µg/mL for all test microorganisms. It means that, *Salvia sclarea* extract has same antibiofilm effect against the selected bacteria and yeast species as shown in Table 3. It is very difficult to eradicate and treat microbial biofilms. *Salvia sclarea* plant extract should be considered of great value in treating biofilms due to its minimum biofilm eradication concentrations (MBEC).

Table 3: MBEC values of *Salvia sclarea* plant extract against test microorganisms.

Test Strains	**MBEC values of *Salvia sclarea extract* (µg/mL)**
Staphylococcus aureus ATCC 29213	3000
Staphylococcus epidermidis ATCC 14990	3000
Candida albicans ATCC 90028	3000
Candida krusei ATCC 6258	3000

Brine Shrimp Lethality test

The Brine Shrimp Lethality test results were determined at 3000, 1500, 750, 375, 187.5, 93.75, 46.87, 23.43, 11.71, 5.85 µg/mL concentrations. After 24 hours incubation period, live larvae were counted and the results are shown in Table 4. The Brine Shrimp Lethality test concentrations were determined at 93.75 and 46.87 µg/mL.

Table 4: Lethality values of *Salvia sclarea* plant extract against *Artemia salina* larvae.

***Salvia sclarea* plant extract concentrations (µg/mL)**	**3000**	**1500**	**750**	**375**	**187.5**	**93.75**	**46.87**	**23.43**	**11.71**	**5.85**
Number of *Artemia salina* larvae out of 10	All dead	All dead	All dead	All dead	All dead	6	8	All alive	All alive	All alive

CONCLUSION

Antimicrobial, antibiofilm and cytotoxicity methods are extensively used to investigate the biological activities of natural substances. There are limited data in the literature about the biological activities of *Salvia sclarea* L. plant extracts. The results of this study revealed that *Salvia sclarea* L. plant extract exhibited significant antimicrobial and antibiofilm activity against all tested microorganism strains in vitro. The mechanisms of antimicrobial and antibiofilm activities of natural compounds and extracts are still not fully understood. Previous studies reported that there is a relationship with the chemical composition of the plants and the antimicrobial activities. These chemical components exerted their toxic effect against microorganisms by disruption of membrane integrity (20). The mechanism of these disruption molecules in plants is not accurately determined. In addition, these studies provided an experimental basis of practical application of *Salvia sclarea* plant extract as a natural antimicrobial and antibiofilm agent. The Brine Shrimp lethality test is an important bioassay which is an indication of cytotoxicity, pesticidal effects and various pharmacological and biological activities of natural substances. The cytotoxic effects of plants are principally contributed by the presence of secondary metabolites like alkaloid, glycoside, steroid, tannin and flavonoid in their extract (21). This is also revealed with our results that *Salvia sclarea* L. plant extracts showed cytotoxic activities at some concentrations.

In conclusion, plant extracts of *Salvia sclarea* growing in Turkey, have significant pharmacological importance. Different *Salvia sclarea* plant extract concentrations and microorganism cultures may be used in further studies to obtain better results. And for the determination of cytotoxic activity lower *Salvia sclarea* plant extract concentrations may be used.

ACKNOWLEDGMENT

This study was supported by Anadolu University Scientific Research Projects (BAP) Commission and (AUBİBAM). Project number is 1304S069. We greatly acknowledge the financial support. This article is presented as a poster presentation at Chem.Bio.Con'18 congress.

REFERENCES

1. Güner A, Aslan S, Ekim T, Vural M., Babaç MT. Türkiye Bitkileri Listesi (Damarlı Bitkiler). Nezahat Gökyiğit Botanik Bahçesi ve Flora Araştırmaları Derneği Yayını, İstanbul. 2012.

2. Walker JB., Sytsma KJ. Staminal evolution in the genus Salvia (Lamiaceae): Molecular phylogenetic evidence for multiple origins of the staminal lever. Ann Bot. 2007; 100: 375–91.

3. Akkol EK., Göger F, Koşar M, Başer KHC. Phenolic composition and biological activities of *Salvia halophila* and *Salvia virgata* from Turkey. Food Chemistry. 2008; 108: 942–949.

4. Aşkun T, Başer KHC, Tümen G, Kürkçüoğlu M. Characterization of essential oils of some Salvia species and their antimycobacterial activities. Turk J Biol. 2010; 34: 89-95.

5. Yang Z, Kitano Y, Chiba K, Shibata N, Kurokawa H, Doi Y. Synthesis of variously oxidized abietanediterpenes and their antibacterial activities against MRSA and VRE. Bioorg Med Chem. 2001; 9: 347-56.

6. Abd-Elmageed MAM., Hussein BA. Cytotoxicity and antimicrobial activity of *Salvia officinalis* L flowers. 2008; 3: 127-30.

7. Lima CF, Andrade PB, Seabra RM, Fernandes-Ferreira M, Pereira-Wilson C. The drinking of a *Salvia officinalis* infusion improves liver antioxidant status in mice and rats. J Ethnopharmacol. 2005; 97: 383–9.

8. Baricevic D, Sosa S, Della LR, Tubaro A, Simonovska B, Krasna A, Zupancic A. Topical antiinflammatory activity of *Salvia officinalis* L. leaves: The relevance of ursolic acid. J Ethnopharmacol. 2001; 75: 125-32.

9. Çadirci E, Süleyman H, Gürbüz P, Kuruüzüm UA, Güvenalp Z, Demirezer LÖ. Anti-inflammatory effects of different

extracts from three Salvia species. Turk. J. Biol. 2012; 36:59-64.

10. Tada M, Okuna K, Chiba K, Ohnishia E, Yoshiia T. Antiviral diterpenes from *Salvia officinalis*. Phytochemistry. 1994; 35: 539-41.

11. Smidling D, Mitic-Culafic D, Vukovic-Gacic B, Simic D, Knezevic-Vukcevic J. Evaluation of antiviral activity of fractionated extracts of Sage *Salvia officinalis* L (Lamiaceae). Arch BiolSci Belgrade. 2008; 60: 421–9.

12. Fiore G, Nencini C, Cavallo F, Capasso A, Bader A, Giorgi G, Micheli L. In vitro antiproliferative effect of six Salvia species on human tumor cell lines. Phytother Res. 2006; 20: 701-3.

13. Ryu SY, Lee CO, Choi SU. In vitro cytotoxicity of tanshinones from *Salvia miltiorrhiza*. Planta Med. 1997; 63: 339-42.

14. ZareShahneh F, Valiyari S, Baradaran B, Abdolalizadeh J, Bandehagh A, Azadmehr A, Hajiaghaee R. Inhibitory and cytotoxic activities of *Salvia officinalis* L. Extract on human lymphoma and leukemia cells by induction of apoptosis. Adv Pharm Bull. 2013; 3: 51-5.

15. Coelho DE, Souza GP, Elisabetsky EI. Ethnobotany and anticonvulsant properties of Lamiaceae from Rio Grande de Soul (Brasil). In: Harley R, Payton A, Harvey T, eds. Lamiales Newsletter Royal Botanic Gardens, Kew. 1998; 10.

16. Lawrence, B. M.The Antimicrobial /Biological Activity of Essential Oils, Allured Publishing Corp. USA: Carol Stream, IL. 2005.

17. CLSI M27-A2. Reference method for broth dilution antifungal susceptibility testing of yeasts. Approved standard. 2nd ed. 2002.

18. CLSI M7-A7. Methods for dilution antimicrobial susceptibility tests for bacteria that grow aerobically. Approved standard. 7th ed. 2006.

19. Meyer BN, Ferrigni NR, Putnam JE, Jacobsen LB, Nichols DE, Mclaughlin JL. Journal of Medical Plant Research.1982; 45: 31-4.

20. Knobloch K, Pauli A, Iberal B, Weis N, Weigand H. Antibacterial activity and antifungal properties of essential oil components. J Essent Oil Res. 1989; 1:119– 28.

21. Özçelik B, Kartal M, Orhan I. Cytotoxicity, antiviral and antimicrobial activities of alkaloids, flavonoids, and phenolic acids. Pharmaceutical Biology, 2011; 49(4), 396-402.

JOTCS A
Journal of the Turkish Chemical Society
Section: A
Chemistry
TURKISH CHEMICAL SOCIETY

Determination and Evaluation of Methanol, Ethanol and Higher Alcohols in Legally and Illegally Produced Alcoholic Beverages

Orhan DESTANOĞLU*, İsmail ATEŞ

Council of Forensic Medicine (ATK), Department of Chemistry, 34196 Bahçelievler, İstanbul, TURKEY

Abstract: In this paper, we demonstrated the results of ethanol, methanol and higher alcoholic contents of the legally and illegally produced alcoholic samples. For investigation, the samples, which were collected as evidence by officers from the crime scenes or illicit production sites, were sent to our laboratories by prosecutions. 96 Turkish Rakı samples, 8 beer samples, 1 wine sample, 101 other strong drink samples, thus totaling 206 samples, and 2 industrial ethanol samples were examined between years 2015-2017. Fast and reliable analysis of the alcoholic beverages, especially in terms of methanol concentration, has vital importance primarily due to the cases of death arose from metabolic acidosis after consumption of illicit alcoholic beverages with high concentration of methanol produced in clandestine laboratories. In the autumn of 2015, an outbreak of mass methanol poisonings took place and so many people died in Istanbul. An HS-GC-MS system was utilized for qualitative analysis of the higher alcohols and for scanning any volatile compound, whereas the determination of ethanol and methanol concentrations an HS-GC-FID system was performed. So, after all results were investigated in detail, mentioning the key points for evaluations, it was clearly described whether the drinks comply with criteria set by Turkish Food Codex Communiqué on Distilled Alcoholic Beverages. 89 of 96 Rakı samples and 90 of 101 strong alcoholic beverages were not definitely compliant with the Communiqué since they contained either tert-butanol, which is a denaturant, or high levels of methanol.

Keywords: Analysis, gas chromatography, methanol poisoning, alcoholic beverages, forensic chemistry.

Submitted: November 11, 2018. **Accepted:** January 13, 2019.

Cite this: Destanoğlu O, Ateş İ. Determination and Evaluation of Methanol, Ethanol and Higher Alcohols in Legally and Illegally Produced Alcoholic Beverages. Journal of the Turkish Chemical Society, Section A: Chemistry. 2019;6(1):21–32.

DOI: http://dx.doi.org/10.18596/jotcsa.481384.

***Corresponding author.** destanoglu@itu.edu.tr

INTRODUCTION

Fermentation-based alcoholic beverage production has been carried out from ancient times throughout the world. However, as in Turkey, other countries have the issue of illegal alcoholic drink production, which is very serious. Informally produced alcohol consumption is very high in Eastern Europe, followed by South America and Africa (1).

According to the 2010 report of World Health Organization Global Information System on Alcohol and Health (WHO-GISAH), 30% of Turkish alcohol consumption is unrecorded. In 2010, consumption percentages to the type of alcoholic drink are 63% beer, 9% wine and 28% spirits, whereas in the year 2016, beer was consumed 57.6%, wine's consumption was 8.6% and of the spirits were 33.8%. 73% of total population is composed of adults (older than 15 years old) in Turkey and according to the 2016 statistics of WHO-GISAH, 11% of adult males consumed alcohol while this was 3% for females. In addition, 2010 and 2016 statistics of WHO-GISAH tell that males (15+) consumed 4.1

L and 3.7 L pure alcohol per year, respectively. For females, both years recorded the same value, 0.4 L. On the other hand, according to year 2016 data, only alcohol-consuming males had 29 L pure alcohol per year and females had 10.4 L pure alcohol. The data for the same year showed that daily consumed alcohol was 71.9 g for the males and 25.8 g for females. In the year 2016 in Turkey, it was reported that the ratio of alcohol-related deaths to the total was 2.1% for males and 0.5% for females (2,3).

For alcohol addicts, cheap alcoholic drinks are considered more attractive than the others. However, non-institutional markets sell alcoholic beverages at prices which are very much cheaper than the market value might be demanded by insensible customers. Increasing unemployment and economic burdens make alcohol addicts to be increasingly forced to find any cheaper drinks. However, there is a problem; ethyl alcohol which is not agricultural origin can be added into the cheap drinks produced by illicit means in clandestine laboratories, and some unscrupulous people add methanol into these drinks to increase the amount of alcohol and decrease the cost. The fact that methanol is cheaper than ethanol further decrease the cost of these counterfeit drinks. The beverages containing high concentration levels of methanol gives rise to serious health problems or deaths when consumed.

In addition, the number of cases of death attributed to consumption of traditionally fermented beverages, which are contaminated with methanol, increase in many countries including Nigeria, India, and Indonesia. The presence of methanol in traditionally fermented drinks is claimed to occur via microbial routes. Pectin methyl esterase-producing microbes are able to produce methanol from pectine-containing fruits. In fact, during classical fermentation process, different types of microbes might produce a mixture of alcohols (4).

Methanol is metabolized to formaldehyde with alcohol dehydrogenase (ADH), followed by formic acid by aldehyde dehydrogenase quickly (5,6). These metabolites are very toxic. Methanol causes depression in the central nervous system and leads to toxicity, whereas formic acid is suppressively toxic. Therefore, these two must be considered together in toxicity cases. Formic acid is a strong cytotoxic molecule, inhibiting mitochondrial cytochrome c oxidase activation. Formic acid accumulation results in metabolic acidosis, greatly damaging the retinal surface and optical nerves (7,8). Excessive metabolic acidosis results in death. It is reported that toxic level of methanol changes between persons, but it is generally accepted that 10 – 20 mL methanol intake causes ocular disruption or loss, while 30 – 100 mL of methanol leads to death. In addition, literature points out that methanol-intoxicated and survived patients had blood methanol concentration greater than 10 mg/dL (9). In addition, it was reported that the lethal methanolic dose is 20 – 60 g or 25 – 75 mL for a 60-kg adult, whereas ethanol dose is 300 g or 384 mL (10).

According to the UN and Turkish Food Codex Communiqué on Distilled Alcoholic Beverages, ethanol to be used in spirits must be of agricultural origin, at least 96% by volume, and methanol content must not be greater than 30 g (0.038%, d_{MeOH} = 0.792 g/mL) per hectoliter of 100% alcohol (11,12).

The Republic of Turkey, Tobacco and Alcohol Market Regulatory Authority released a definition named Regulation of the Production of Ethyl Alcohol and Methyl Alcohol and Procedures and Principles about Domestic and Foreign Commerce, and all types of non-alcoholic beverages and the beverages having equal to or greater than 60% ethyl alcohol are termed as "alcoholic mixtures" (13). If one or more of the following chemicals are added into ethyl alcohol or methanol to create color, smell, and flavor, the action is coined as "denaturation" and the chemicals added are termed as "denaturant": Thiophene, denatonium benzoate, tert-butanol, isopropanol, Color Index (CI) reactive red 24, methyl ethyl ketone, and diethylphthalate are most commonly used denaturants. In this Regulation, "food alcohol" term means agricultural ethyl alcohol (12,13). In addition, industrial ethyl alcohol is denaturated and released as such. Paragraph 20 of this Regulation tells that ethyl alcohol must be released to the market in six different ways: I) Domestic ethyl alcohol (food alcohol), II) Generic use ethyl alcohol (cleaning material, domestic fuel, *etc*, they are fully denatured ethyl alcohol for general uses), III) Medical ethyl alcohol (used in pharmacy stores and hospitals; they are not denatured), IV) Analytically pure ethyl alcohol for analysis purposes (as laboratory chemical), V) Ethyl alcohol with industrial input (for food and drug uses, packaged or bulk ethyl alcohol, and for cosmetics, chemical and other production industry uses, they are denatured, in packaged or bulk form), VI) Fuel bioethanol (for mixing with gasoline types, in denatured form to mix with unleaded gasoline) (13).

The denaturation process of ethyl alcohol is performed by adding the following chemicals into 100 liters of ethyl alcohol as calculated for absolute alcohol by considering the uses:
a) To release generic use ethyl alcohols, for full denaturation, 125 g of thiophene, 0.8 g of denatonium benzoate, 3 g of CI Reactive Red 24 (25% aqueous solution by weight), and 2 L of methyl ethyl ketone are added into 100 liters of

ethyl alcohol (calculated for at least 90% ethanol) calculated as absolute alcohol.

b) Including eau de cologne, cosmetic-aimed agricultural ethyl alcohol samples add one of the following denaturant group. One denaturant type includes 0.8 g of denatonium benzoate and 78.0 g of tert-butanol, whereas the other type uses 0.5 kg of diethylphthalate and 78.0 g of tert-butanol.

c) 0.8 g of denatonium benzoate + 78.0 g of tert-butanol and 0.5 kg of diethylphthalate + 78.0 g of tert-butanol denaturant mixtures also are used for ethyl alcohol for industrial purposes.

d) Bioethanol as an additive to gasoline types are denatured by adding at least 1% gasoline by volume (13).

In this study, we investigated, and reported in detail, alcoholic drinks prepared by illegally or legally, their analysis methods, analysis results, and the suitability of an alcoholic beverage to the UN and Turkish Food Codex.

A Headspace-Gas Chromatography-Mass Spectrometry (HS-GC-MS) system was utilized for qualitative analysis of higher alcohols and any volatile compound, whereas the determination of ethanol and methanol concentrations were measured with a Headspace-Gas Chromatography-Flame Ionization Detection (HS-GC-FID) system. 96 rakı samples, 8 beer samples, 1 wine sample, 101 other strong drink samples, totaling to 206 samples, and 2 non-agricultural ethanol samples (used in manufacture of illegal alcoholic beverages) were thoroughly investigated.

MATERIALS AND METHODS

Instruments

The qualitative analyses of the alcoholic beverages were performed with a Perkin Elmer Clarus 680 gas chromatograph equipped with a Clarus SQ 8 T Mass Spectrometer and HS40 headspace (HS) autosampler. Separations were achieved using a Perkin Elmer Elite-FFAP capillary GC column (Crossbond Carbowax-PEG). The column was 30 m long, its i.d. was 0.25 mm, and df was 0.5 µm. Helium was used as the carrier gas at 1 mL/min constant flow rate with an HS pressure of 35 psi. The HS oven set at 90 °C for 15 min. The temperature of HS needle was 100 °C.

Injections were made by adjusting needle time of the loopless HS. After the incubation time finished, pressure was applied to the vial with the needle for 1.0 min and then the gas was taken from vapor phase of the vial for 0.12 min. The temperature of transfer line was set at 110 °C. The GC oven temperature program was as follows: I) initially 40 °C for 8 min, II) elevated from 40 °C to 140 °C at rate of 10 °C min^{-1} and held at 140 °C for 3 min, III) elevated from 140 °C to 240 °C at rate of 30 °C min^{-1} and held at 240 °C for 3 min. Equilibration time of GC oven was 0.5 min. GC injector temperature was 150 °C during total analysis time was 21 min. Mass detection was performed at 200 °C and electron energy was 70 eV of EI+ source with both full scan between 10 – 300 amu for identification for 27 min.

Ethyl acetate, methanol, tert-butanol (2-methyl-2-propanol), ethanol, n-propanol, n-butanol, isobutanol (2-methyl-1-propanol), isoamyl alcohol (3-methyl-1-butanol) and anethole were analyzed both in the total ion chromatogram (TIC) and mass chromatograms for sensitive detection. Besides, standard solution analyses were performed to determine the retention times of the peaks (t_R). The t_R values and parent ions (*m/z*) of the analytes are given in Table 1. In addition to the targeted compounds, some other compounds were scanned if they were detected.

A TurboMass version 6.1.0.1963 software was utilized for data acquisition and instrumental control for GC and MS while headspace autosampler was controlled by computer using PerkinElmer HS Driver v2.5.0.0125 software.

For the quantitative determination of ethanol and methanol concentrations in alcoholic beverages, a Perkin Elmer Clarus 580 HS-GC-FID system was performed in the accredited alcoholmetry laboratory. In the HS part, the oven temperature was set to 70 °C for 15 minutes, needle and transfer line temperatures were set to 75 °C and 110 °C, respectively. Injection pressure was 30 psi. Carrier gas was He, and it was applied at 30 psi pressure.

Samples

Permission and sample collection

This study was conducted by permission of the Council of Forensic Medicine (ATK) Chairmanship, Education and Scientific Research Commission (decision number: 2018/737; date: September 18, 2018). After the samples of evidence were collected from the illicit laboratories or crime scenes by officers, the prosecutions sent the samples to our laboratories for examination.

Sample preparation

For qualitative scans, 0.1 mL of alcoholic beverage was taken and transferred into a vial of 22 mL.capacity The vial was tightly sealed with gas-tight polytetrafluoroethylene (PTFE)-lined rubber septum cap. This sample was loaded into HS-GC-MS for analysis. For quantitative analysis, 1 mL of n-propanol (64 mg/dL) was transferred into a 22 mL-HS vial. Then, 0.2 mL of the alcoholic beverage was added. The vial was immediately capped tightly. Since ethanol concentration in the alcoholic

beverages is very high, ethanol determination in the calibration range was conducted after appropriate dilution with deionized water. After applying to the HS-GC-FID system, the analysis was performed under aforementioned chromatographic conditions.

Table 1. The t_R and main ion (*m/z*) values of the analytes when HS-GC-MS system was employed.

Ethyl acetate		methanol		tert-butanol (2-methyl-2-propanol)		ethanol		n-propanol	
t_R (min)	*m/z*	t_R (min)	*m/z*	t_R (min)	*m/z*	t_R (min)	*m/z*	t_R (min)	*m/z*
3.04	43	3.22	31	3.14	59	3.82	31	6.70	31
n-butanol		isobutanol (2-methyl-1-propanol)		isoamyl alcohol (3-methyl-1-butanol)		anethole			
t_R (min)	*m/z*	t_R (min)	*m/z*	t_R (min)	*m/z*	t_R (min)	*m/z*		
8.11	*56*	9.14	*43*	12.39	*55*	22.54	*148*		

RESULTS AND DISCUSSION

Depending on Communiqués and Regulations (vice versa), ethyl alcohols for medical, pharmaceutic, domestic, and food uses must not be denaturized. Tert-butanol is a denaturant that can be detected during alcoholic analysis with GC. Therefore, when tert-butanol is detected during alcoholic beverage analyses, the presence of denaturant must be noted. In addition, tert-butanol is an organic substance with anthropogenic source (14) and there is no information about tert-butanol's natural occurrence. Consequently, tert-butanol is not present in food alcohols.

In food alcohols, the major constituent is ethanol per 100% total food alcohol and when calculated with Communiqué criteria, methanol is present at 0.004% and higher alcohols are present at 6.5 x 10^{-5}%. Namely, methanol and higher alcohols are minor ingredients. When methanol or inappropriate ethanol is added to an alcoholic beverage, trace higher alcohols will be further diluted. In this study, methanol concentration was expressed as methanol to total value of methanol plus methanol concentration ratio. According to this approach, the formula below was derived. In this formula, m_{MetOH} and m_{EtOH} value is directly written from HS-GC-FID result (mg/dL).

$$Methanol\ in\ total\ alcohol\ (g/hL) = \frac{m_{MetOH}}{(m_{EtOH}/0.789 + m_{MetOH}/0.792)} \times 10^5$$

In Table 2, minimum ethyl alcohol concentrations and maximum methanol concentration limits set by Turkish Codex for Turkish Rakı, distilled gin, cider, perry spirits, fruit brandy, distilled fruit residue beverage, distilled grape pulp beverage, brandy, wine distillate and vodka were given.

Table 2. The min. total alcohol concentration limits and max. methanol concentration limits of the different types alcoholic beverages which is set by Turkish Food Codex Communiqué on Distilled Alcoholic Beverages.

Rakı		Distilled gin		Cider, Perry Spirits	
Min alcohol (%)	Max MeOH[a]	Min alcohol (%)	Max MeOH[a]	Min alcohol (%)	Max MeOH[a]
40	150	37.5	5	37.5	1000
Fruit Brandy[b]		Distilled Fruit Residue Beverage		Distilled Grape Pulp Beverage	
Min alcohol (%)	Max MeOH[a,b]	Min alcohol (%)	Max MeOH[a]	Min alcohol (%)	Max MeOH[a]
37.5	1000	37.5	1500	37.5	1000
Brandy		Wine Distillate		Vodka	
Min alcohol (%)	Max MeOH[a,b]	Min alcohol (%)	Max MeOH[a]	Min alcohol (%)	Max MeOH[a]
36	200	37.5	200	37.5	10

[a] g methanol per hectoliter of 100% total alcohol

[b] This value varies up to 1350 g depending on the type of fruit used.

Turkish Rakı

Rakı is a strong alcoholic beverage and is termed as Turkey's national drink. Pastis, ouzo, sambuca, arak and aguardiente are the other rakı-like aniseed-containing beverages around the world (1).

Turkish Food Codex (Communiqué no 2016/55) states that Rakı is a Turkish distilled alcoholic beverage by distilling suma only or suma plus agricultural ethyl alcohol mixture in 5000 L or smaller copper stills, along with Turkish aniseed (*Pimpinella anisum*) (12). As seen in Table 2, it is imperative that methanol content must not be greater than 150 gram per hectoliter of 100% total alcohol in rakı samples and total alcohol content must be at least 40% per volume.

Evaluation of Rakı-Based Results

In this study, 96 rakı samples were analyzed and the results were evaluated. All results of rakı samples are given in Table S1 (see the supplementary material). Both methanol and ethanol were detected in 16 samples, while ethanol was determined alone in the rest of Rakı samples (N = 80). Anethole was detected in all of these 96 samples. The first 16 results in Table S1 were organized by sorting by the methanol results in an increasing order. The first result had methanol in a very low concentration, but denaturant (tert-butanol) was present, and no higher alcohols (which were present in food alcohols) were found, therefore this sample does not conform to the Communiqué. The number eight rakı sample showed n-propanol and ethyl acetate in the analysis, but since denaturant was present, this sample too does not conform to the Communiqué like sample #1. Among 16 rakı samples with methanol detected, only 7 of them had higher alcohols, and they are suitable in terms of codex criteria.

Figure 1 exhibits the total ion chromatogram of the rakı sample #2, in Table S1, row 2, which conforms the Turkish Food Codex. Rakı samples in Table S1, rows 10 – 16 do not conform the criteria of methanol concentration limits, and even it is very clear that these samples are at very high concentration. It can be easily concluded that food ethanol was not used in these alcoholic beverages. The peaks of ethyl acetate and methanol seems to be very close each other in the Figure 1, but as seen in Figure S1 in the supplementary file no overlap is observed in the chromatograms if *m/z* 31 and *m/z* 43 are scanned. The mass library search results and definitions of the analytes presented in this sample are given in supplementary material, please see from Figure S2 to Figure S8.

Ethanol concentration range was 41.9 – 65.1% in the rest of 80 rakı samples, which did not contain methanol (See Table S1, from #17 to #96). All of these 80 samples had tert-butanol, which is a denaturant, so they do not comply with the criteria. A sample contained isobutanol and ethyl acetate whereas two samples only contained n-butanol.The TIC of a Rakı sample (Table S1, row 68) was given in Figure 2. Overlaid ion chromatograms are demonstrated in Figure S9 and the library definitions are given in Figure S10-12. Though the peaks of tert-butanol and ethanol appear allocated in Figure 1, the *m/z* 59 and *m/z* 45 ion chromatograms allow successful separation and analysis (see Figure S9).

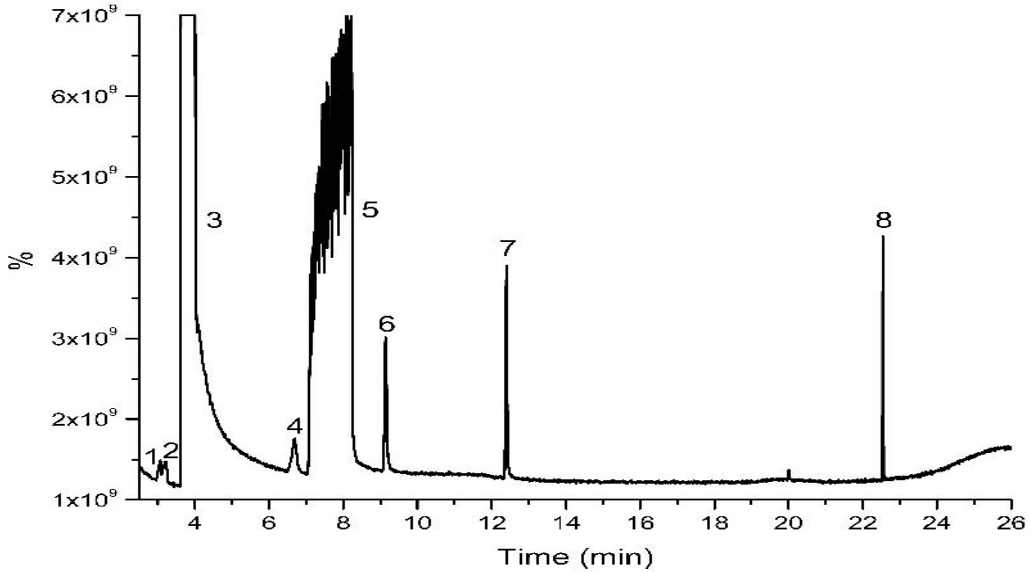

Figure 1. Total ion chromatogram of a rakı sample which is suitable to the Codex. 1) Ethyl acetate, 2) methanol (0.02% in the drink), 3) ethanol (43.9% in the drink), 4) n-propanol, 5) water peak, 6) 2-methyl-1-propanol, 7) 3-methyl-1-butanol, 8) anethole.

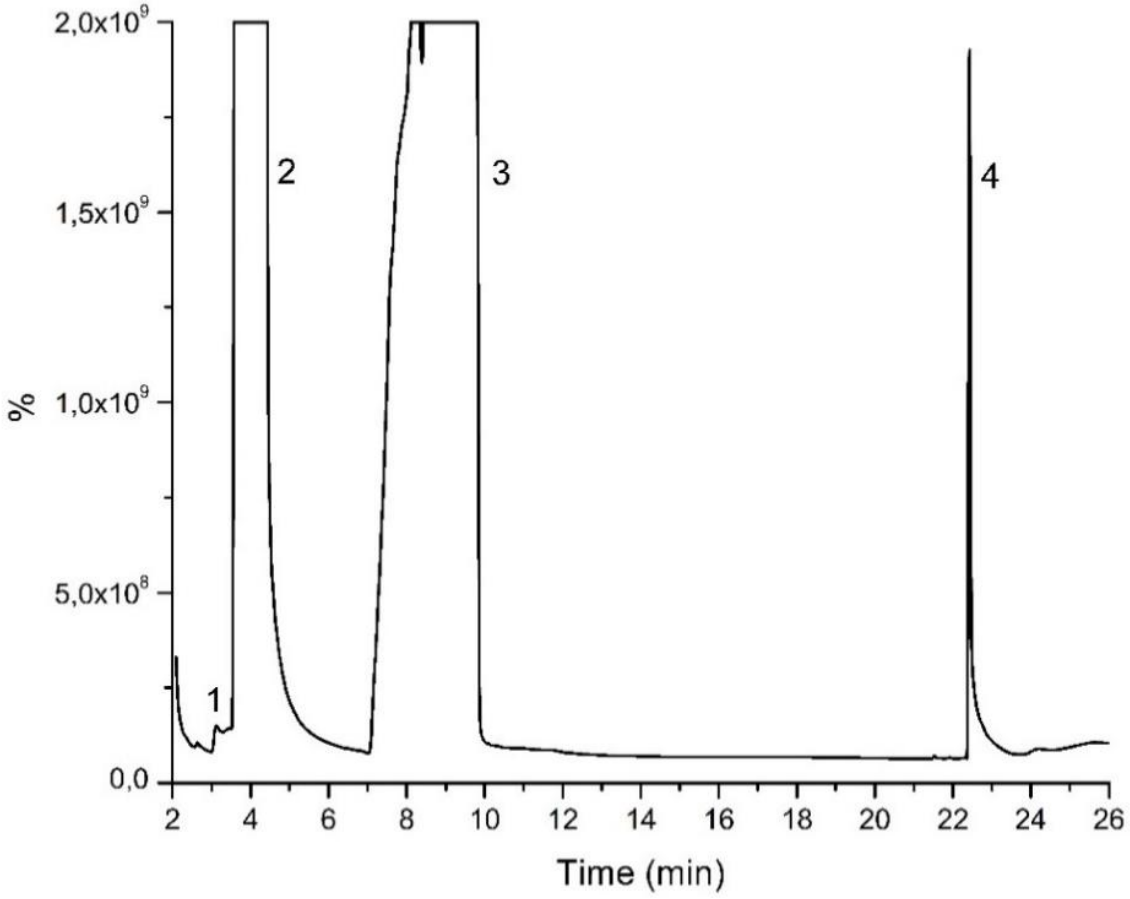

Figure 2. A total ion chromatogram of a sample (Table S1, row 68) containing denaturant, but no methanol. 1) Tert-butanol, 2) ethanol (51.5%), 3) water peak, 4) anethole.

In brief, a rakı sample must obey the following criteria: I) Food grade alcohol must be used and it must not contain any denaturant. II) It must have higher alcohols (fusel oil). III) Methanol concentration must not be greater than 150 g/hL for 100% total alcohol. IV) Even though a Rakı sample does not contain methanol, when a non-agricultural-originating ethanol was used for production, only ethanol, anethole and tert-butanol were detected in the sample.

The commercial and legal "Rakı" beverages (A traditional Turkish alcoholic beverage) are about five times more expensive than the homemade ones. In Turkey, methanol intoxication-related deaths were reported by consumption of homemade alcoholic beverages (1). Arslan *et al.* investigated 56 different types of rakı samples called as "Bogma Rakı" were obtained from local informal manufacturers and 12 types of different rakı samples were bought from markets in Hatay (Mediterranean region in Turkey). Both rakı types are produced with the same method, but the distillation procedure of commercial rakı samples is more sensitive. They reported that the methanol concentration was 0.220% ± 0.089 in the uncontrolled rakı samples (1). This level seems to be a bit more from the limits. However, methanol can be purposely added to some illegally produced drinks (see Table S1, rows 10 – 16) and, unfortunately, this can lead to deaths.

Beer and Wine Results

In Table S2, analysis results of eight beer samples and one wine sample were demonstrated. The concentration range of ethanol in the beer samples was 4.2 – 5.2%, and no methanol was detected. Beer samples also had n-propanol, isoamyl alcohol, isobutanol, n-butanol, and ethyl acetate. Additionally, 11.3% ethanol and 0.023% methanol were determined in the wine sample, along with n-propanol, isoamyl alcohol, isobutanol, and ethyl acetate. For wine, low methanol concentration (180 mg/L), presence of higher alcohols, and no denaturant shows that these comply with the Codex. In the literature, Hodson *et al.* carried out a research about methanol levels in wine samples. In red wine, methanol concentration range was reported to be 120 – 250 mg/L while in white wine, this range was lower and was 40 – 120 mg/L. In addition, depending on the type of grape, methanol concentration could be changed and in fact, it could reach to 364 mg/L (15).

Results of Strong Alcoholic Beverages

The results of 101 strong alcoholic beverages and 2 non-food-ethanol containing liquids

analyzed in our Institute are summarized in Table S3. First seventeen rows of the table contained methanol and sorted by increasing order. Drink samples collected in the areas of crime are sometimes sent in some other flasks than original bottles, therefore we preferred to use "strong alcoholic beverages" definition. However, the presence of a label on the flask or bottle helps determination and evaluation, because the criteria outlined in the Communiqué for the investigated beverage are considered. The key issues that need to be considered, when a sample is investigated, are classified step-by-step in Table S3.

Since the first four samples in Table S3 have very low methanol concentrations, but the presence of tert-butanol (denaturant) and no higher alcohols that should be at trace concentrations, lead us to conclude that they are not compliant with Turkish Food Codex criteria. Table S3, rows 5 – 7 demonstrate that the data about them are compliant to the Communiqué. However, if they are labeled and the label reads "vodka" or "gin", their methanol concentrations are not compliant to the Communiqué. Tulashie *et al.* conducted a research in Ghana and they reported that methanol concentration range in methanol-containing homemade and foreign beverages was 0.003 – 0.161% (10). Osobamiro reported that, after GC analyses of alcoholic beverages purchased from the supermarkets in Lagos – Nigeria, methanol was not detected in three spirit samples while other three types of spirits had 18, 22, and 176 mg/L methanol and the concentrations were within the allowed range (16).

High methanol concentrations and the absence of higher alcohols, which are given in Table S3, rows 8 – 11, are striking. In some strong alcoholic beverages (*vice versa*), it is allowed to contain 1000 – 1500 g methanol in hectoliter of 100% total alcohol, but for rows 8 – 11 in Table S3 the methanol results are 8400 – 12200 g/hL. Moreover, the Communiqué states that ethanol concentrations for samples containing high concentrations of methanol must be minimum 37.5%, but for samples in the rows 8 – 11 showed that the maximum ethanol concentration was 32.5%. One can easily conclude that these four samples are not compliant with the Communiqué with many aspects. The following rows, 12 – 16 had samples with isoamyl alcohol and isobutanol and it indicates that agricultural ethanol was used, but most probably the producer malevolently added methanol to decrease the production costs. The reason why the other higher alcohols were not detected, it could be claimed that methanol addition dilutes these ingredients. The samples in Table S3, rows 12 – 16 are apparently not suitable according to the Communiqué. Table S3, row 17 had the highest methanol concentration in the series, ethanol concentration was 17.4% in the sample and no higher alcohols were detected. Sample 17 is definitely not suitable to the Communiqué. On the other hand, no methanol was detected in the samples with row no 18 – 93, so we sorted them by possessing denaturant tert-butanol. Some samples in Table S3, rows up to 53 had higher alcohols, either all or some of them. Table S3, rows 54 – 93 had no higher alcohols, only tert-butanol was present. Thus, Table S3, rows 18 – 93 are not suitable to the Communiqué and Regulations since denaturant was detected in them. Ethanol concentrations ofliquid samples stated in rows 102 and 103 in Table 4 were 80.3% and 99.3%, respectively, and only tert-butanol was detected in them. So, these liquids were concluded to be used in the production of liquors of 18 – 93 in the Table S3, as non-food alcohol. On the other hand, Table S3, rows 94 – 101 are suitable alcoholic beverages with all aspects of criteria.

CONCLUSION

In this paper, we point out the key points of evaluation with the HS-GC-FID and HS-GC-MS analysis results of the alcoholic beverages, which were collected as evidences by officers from the crime scenes or from clandestine laboratories, and their compliance to the Communiqué and Regulations released by the authorities. The alcoholic beverages containing high concentration of methanol were analyzed after the methanol poisoning cases or outbreak took place in the 2015 Autumn in Istanbul whereas some of the other samples, which are collected in police raids, were examined before the drinks were launched. In terms of evaluation of the results, addition of methanol and/or non-agricultural-origin ethanol gives rise to dilution of higher alcohols (fusel oil) that need to come from agricultural alcohol. Thus, utilizing the appropriate approach described in this paper, the methanol concentrations (g/hL) can be calculated by dividing methanol concentration to the sum of ethanol and methanol concentration values instead of calculating with amounts of the other minor ingredients. It could be said that 7 of 96 Rakı samples were suitable, while methanol concentration levels and denaturant contents make the remaining 89 samples non suitable to the Communiqué and Regulations. Beer and wine samples were all suitable. Only 11 of 101 strong alcoholic drinks were suitable to the Communiqué. Two liquid samples with very high concentrations of ethanol results were also reported, both of which contained tert-butanol, therefore, they are most probably used for production of illicit alcoholic beverages.

ACKNOWLEDGEMENT

The authors are grateful to the Council of Forensic Medicine (ATK) Chairmanship, TURKEY, for permitting, supporting and encouraging us to conduct this research.

REFERENCES

1. Arslan MM, Zeren C, Aydin Z, Akcan R, Dokuyucu R, Keten A, et al. Analysis of methanol and its derivatives in illegally produced alcoholic beverages. J Forensic Leg Med. 2015;33:56–60.

2. World Health Organization. WHO-Turkey [Internet]. 2010 [cited 2018 Sep 3]. Available from: http://www.who.int/substance_abuse/publications/global_alcohol_report/profiles/tur.pdf?ua=1

3. World Health Organization. WHO Global Information System on Alcohol and Health (GISAH) [Internet]. [cited 2018 Sep 3]. Available from: http://apps.who.int/gho/data/node.main.GISAH

4. Ohimain EI. Methanol contamination in traditionally fermented alcoholic beverages : the microbial dimension. Springerplus. 2016;(5):1–10.

5. Akhgari M, Panahianpour MH, Bazmi E, Etemadi-Aleagha A, Mahdavi A, Nazari SH. Fatal methanol poisoning: features of liver histopathology. Toxicol Ind Health. 2013;29(2):136–41.

6. Lee X-P, Kumazawa T, Kondo K, Sato K, Suzuki O. Analysis of methanol or formic acid in body fluids by headspace solid-phase microextraction and capillary gas chromatography. J Chromatogr B Biomed Sci Appl. 1999;734:155–62.

7. Wallage HR, Watterson JH. Formic acid and methanol concentrations in death investigations. J Anal Toxicol. 2008;32:241–7.

8. Zakharov S, Nurieva O, Navratil T, Diblik P, Kuthan P, Pelclova D. Acute methanol poisonings: Folates administration and visual sequelae. J Appl Biomed. 2014;12:309–16.

9. Moffat AC. Clark's Isolation and Identification of Drugs. 2nd ed. London: Pharmaceutical Press; 1986. 744-745 p.

10. Tulashie SK, Appiah AP, Torku GD, Darko AY, Wiredu A. Determination of methanol and ethanol concentrations in local and foreign alcoholic drinks and food products (Banku , Ga kenkey , Fante kenkey and Hausa koko) in Ghana. International Journal of Food Contamination; 2017;14(4):1–5.

11. European Commission. Regulation (EC) No 110/2008 of the European Parliament and of the Council of 15 January 2008 on the definition, description, presentation, labelling and the protection of geographical indications of spirit drinks and repealing Council Regulation (EEC) No. Off J Eur Union. 2008;L39(110):16–54.

12. Turkish Food Codex Communiqué of Distilled Alcoholic Beverages (2016/55) [Internet]. 2016 [cited 2018 Nov 14]. Available from: http://www.mevzuat.gov.tr/Metin.Aspx?MevzuatKod=9.5.23431&MevzuatIliski=0&sourceXmlSearch=alkol

13. The Republic of Turkey, Tobacco and Alcohol Market Regulatory Authority, Regulation of the Production of Ethyl Alcohol and Methanol with Procedures and Principles about Domestic and Foreign Commerce [Internet]. 2011 [cited 2018 Oct 6]. Available from: http://www.mevzuat.gov.tr/Metin.Aspx?MevzuatKod=7.5.15462&MevzuatIliski=0&sourceXmlSearch=#

14. Kingsbury JA, Delzer GC, Hopple JA. Anthropogenic Organic Compounds in Source Water of Nine Community Water System that Withdraw from Streams, 2002-05: U.S. Geological Survey Scientific Investigations Report 2008–5208. Virginia; 2008.

15. Hodson G, Wilkes E, Azevedo S, Battaglene T.Methanol in wine. In: 40th World Congress of Vine and Wine. 2017.

16. Osobamiro T. Analysis of Some Contaminants Commonly Found in Alcoholic Beverages. Am-Euras J Sci Res. 2013;8(1):53–6.

JOTCS A
Journal of the Turkish Chemical Society Section: A Chemistry
TURKISH CHEMICAL SOCIETY

2-Chlorobenzoylthiourea-modified MCM-41 for Drug Delivery

Fatih Mehmet EMEN[1*], Ruken Esra DEMİRDÖĞEN[2], Göktürk AVSAR[3], Derya KILIÇ[1]

[1]Mehmet Akif Ersoy University, Faculty of Arts and Science, Department of Chemistry, TR 15030, Burdur, Turkey
[2]Çankırı Karatekin University, Faculty of Science Department of Chemistry, TR 18100, Çankırı, Turkey
[3]University of Mersin, Faculty of Science, Department of Chemistry, TR 33100, Mersin, Turkey.

Abstract: Mesoporous 2-chlorobenzoylthiourea-modified MCM-41 (2-Cl-BT-MCM-41) was prepared for the first time and loaded with ibuprofen in a supercritical carbon dioxide (sC-CO_2) environment. 2-Cl-BT-MCM-41 was prepared and also characterized via XRD, FT-IR, SEM and BET techniques. The (100) and (110) reflections observed at low angle XRD show the mesoporous SiO_2 structure. The particule size of non-uniform spheres were observed at a range of 250-305 nm. BET surface areas were calculated as 1506 m^2 / g for MCM-41 and 306 m^2/g for 2-Cl-BT-MCM-41, respectively. The absorption and releasing studies of ibuprofen were carried out in simulated body fluid. The result revealed that high adsorption capacity for drug with 2-Cl-BT-MCM-41 and slower drug release rate was achieved.

Keywords: Drug delivery system (DDS), mesoporous MCM-41, 2-chlorobenzoylthiourea.

Submitted: October 04, 2018. **Accepted:** January 18, 2019.

Cite this: Emen F, Demirdöğen R, Avşar G, Kılıç D. 2-Chlorobenzoylthiourea-modified MCM-41 for Drug Delivery. JOTCSA. 2019;6(1):29–34.

DOI: https://dx.doi.org/10.18596/jotcsa.467177.

***Corresponding author.** E-mail: femen106@gmail.com, Tel: +905077681688, Fax: +902482133099.

INTRODUCTION

Controlled drug delivery systems (DDS) are formulations that release a drug in a targeted area in the body. Materials obtained by encapsulation of clinically approved drugs will increase the therapeutic effect of the drug and reduce side effects. Biodegradable polymers, polymeric micelles, liposomes, magnetic nanoparticles, hydroxyapatites, calcium phosphate cement (CPC), xerogels, hydrogels and mesoporous silica are used as drug delivery systems. As a disadvantage, hydrolysis leads to deterioration of the polymer-based carrier structure, resulting in a rapid release of drug molecules and non-homogeneous distribution during the separation process. Research is underway to develop inorganic carriers to overcome these disadvantages of polymer systems. Controlled release of drugs from ordering mesoporous materials is an interesting field of application (1). High-order mesoporous silicates are very promising materials with a wide range of possible applications (2). The porous web of these biocompatible materials can act as a reservoir for the maintenance of drug molecules by increasing the solubility and relative bioavailability of drug molecules. Among the mesopoous silicates, the MCM-41 has a high specific surface area (~ 1150 m^2/g), a larger pore volume (~ 1 cm^3/g), and smaller pore size (2-5 nm), thus being a drug carrier. MCM-41 has attracted more attention as a carrier for drug delivery (2). MCM has been tested for the transport and controlled release of aspirin (3), atenolol (4), captopril (5), coumarin derivatives (6), diflunisal (7), hydrochlorothazide (8), ibuprofen (9–12), methotrexate (13), naproxine (9), sertraline hydrochloride (14), resveratrol (15), and others (16–17). The presence of high concentrations of silanol group on the silica surface makes it possible to modify the pore walls and surfaces by selecting appropriate organic groups. The surface of MCM-41 can be modified with chloropropyl, phenyl, benzyl,

mercaptopropyl, cyanopropyl, and aminopropyl groups (18).

The objective of this work was to study the ibuprofen adsorption and release behavior of 2-Cl-BT-MCM-41 in simulated body fluid. 2-Cl-BT-MCM-41 was prepared and also characterized via XRD, FT-IR, SEM and BET techniques.

MATERIALS AND METHODS

Synthesis of Compounds

Synthesis of MCM-41

Typically, 0.6 g of n-cetyltrimethylammonium bromide (CTAB) was first dissolved in 400 mL of deionized water. Then 3.5 mL of 2 mol/L NaOH was added to the solution, followed by adjusting the solution temperature to 80 °C. Subsequently, 2.5 mL of TEOS was added dropwise to the above solution with vigorous stirring. The mixture was stirred for another 2 h to give rise to white precipitates. The obtained solid product was filtered, washed with deionized water and ethanol, and then dried in air. The dried sample was calcined at 550 °C for 1 h in N_2 and followed by another 3 h in air to remove the organic template.

Synthesis of 2-Cl-BT-MCM-41

The MCM-41 was functionalized with 3-aminopropyltriethoxysilane in the toluene solution (refluxing for 24 h) according to the conventional procedure (19). After cooling, the modified mesoporous material was filtered out and washed several times with small portions of toluene and *i*-propanol to remove an excess of the modifier and possible products of hydrolysis. Finally, the modified mesoporous material was dried overnight in an oven at 95-100 °C under vacuum. The resulting material was designated as MCM-41-NH_2.

2-Cl-BT-MCM-41 was synthesized via a reaction between aminopropyl-functionalized mesoporous silica (MCM-41-NH_2) and benzoyl isothiocyanate, which normally proceeds completely. A typical procedure included reaction of $9.04x10^{-6}$ mmol (2 g) of aminopropylsilica with 0.50 mL of 2-chlorobenzoyl isothiocyanate (25% excess) in toluene. The resulting solid was filtered out, washed with 50 mL of toluene and 50 mL of *i*-propanol, and dried under vacuum for 5 h at 90 °C. The final sample with the attached thiourea functionality had a light yellow color. Schematic illustration of the surface present in the 2-Cl-BT-MCM-41 is given in Figure 1.

Characterization

X-ray diffraction pattern was recorded on a Bruker D8 using CuK_α radiation, with the diffraction angle (2Θ) at range of 10–80°. FT-IR spectrum was recorded on Perkin Elmer FT-IR/FIR/NIR spectrometer Frontier ATR system. SEM measurements were recorded with a Jeol Sem-7100-EDX computer controlled digital model device. BET analyzes were done with Quantachrome Quadrasorb SI device. Absorbance measurements were performed with Pg Instruments UV-Visible spectrometer.

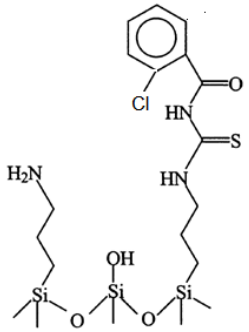

Figure: 1. Schematic illustration of the surface present in the 2-Cl-BT-MCM-41

Ibuprofen loading and release studies

Drug loading studies were carried out via supercritical carbon dioxide ($scCO_2$) system. 1 g of 2-Cl-BT-MCM-41 and 0.8 g ibuprofen were dissolved in 15 mL of ethanol and they were charged to the $scCO_2$ reaction unit at 40 °C and allowed to stand at 200 bar CO_2 for 2 hours. The reaction unit's valve was opened to reduce the CO_2 pressure and the drug loaded nanostructures were obtained.

The in vitro drug delivery was performed by soaking the sample powder into a simulated body fluid, SBF, at 37 °C and at pH of 7.4, maintaining the ratio SBF volume (mL) per adsorbed ibuprofen mass (mg) equal to 0.8:1. Continuous magnetic stirring was maintained during the delivery to avoid limitation of the delivery rate by external diffusion constraints. The delivered ibuprofen concentration was monitored by UV spectrophotometry at 273 nm.

RESULTS AND DISCUSSION

FT-IR studies of MCM-41, MCM-41-NH_2 and 2-Cl-BT-MCM-41

FT-IR spectra of the MCM-41, MCM-41-NH_2 and 2-Cl-BT-MCM-41 are given in Figure 2a-c. Asymmetric vibration band of the O-H group is observed at 3356 cm^{-1}. The stretching and bending vibration bands of Si-O are observed at 1064 cm^{-1} and 801 cm^{-1}, respectively. The results indicate the accuracy of the proposed MCM-41 structure. In the FT-IR spectrum of the MCM-41-NH_2, N-H vibration peaks were observed at 2850-2920 cm^{-1}. In the FT-IR spectrum of the 2-Cl-BT-MCM-41, aromatic C-H vibrations were observed at 3000 cm^{-1}. C=O vibrations also observed at 1700 cm^{-1}. FT-IR spectra confirm that the proposed structures are formed.

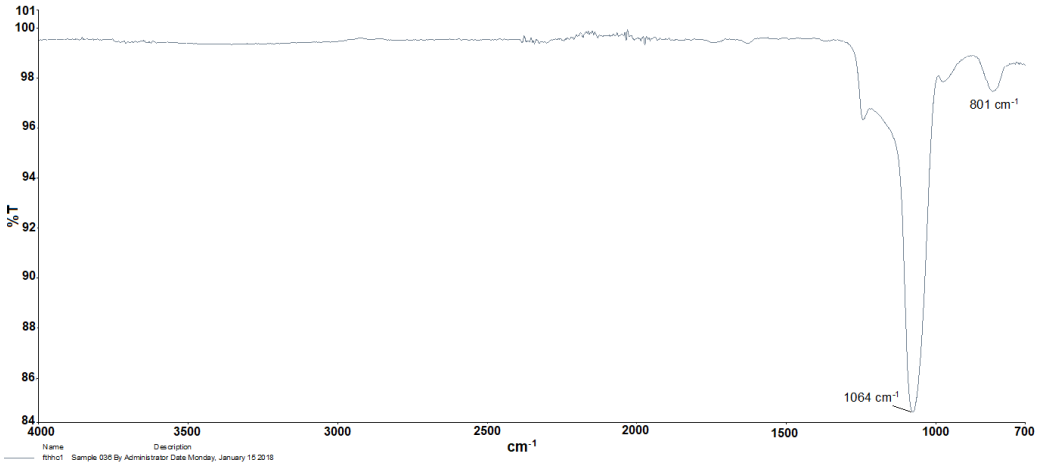

Figure 2: FT-IR spectrum of MCM-41.

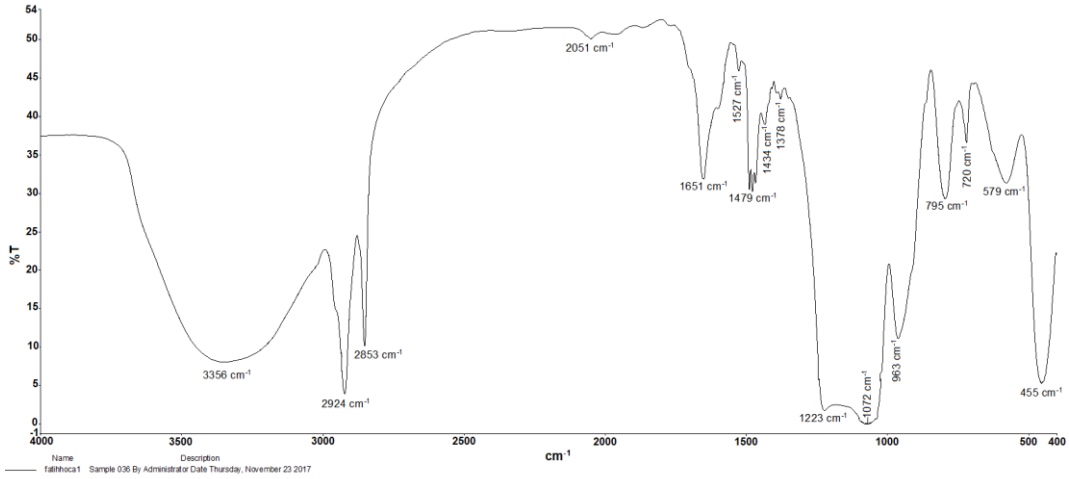

Figure 3: FT-IR spectrum of MCM-41-NH_2.

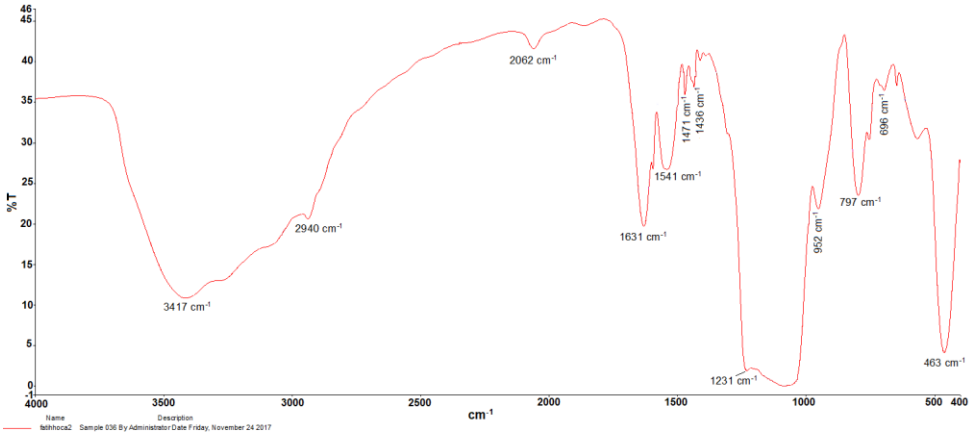

Figure 4: FT-IR spectrum of 2-Cl-BT-MCM-41.

XRD studies

The XRD pattern and low angle XRD patterns of 2-Cl-BT-MCM-41 are given in Figure 5a-b. The (100) and (110) reflections observed at low angle XRD show the mesoporous SiO_2 structure. The broad band observed in the XRD powder pattern at 2 theta = 20° belongs to amorphous SiO_2. XRD results show that mesoporous 2-Cl-BT-MCM-41 has been successfully synthesized.

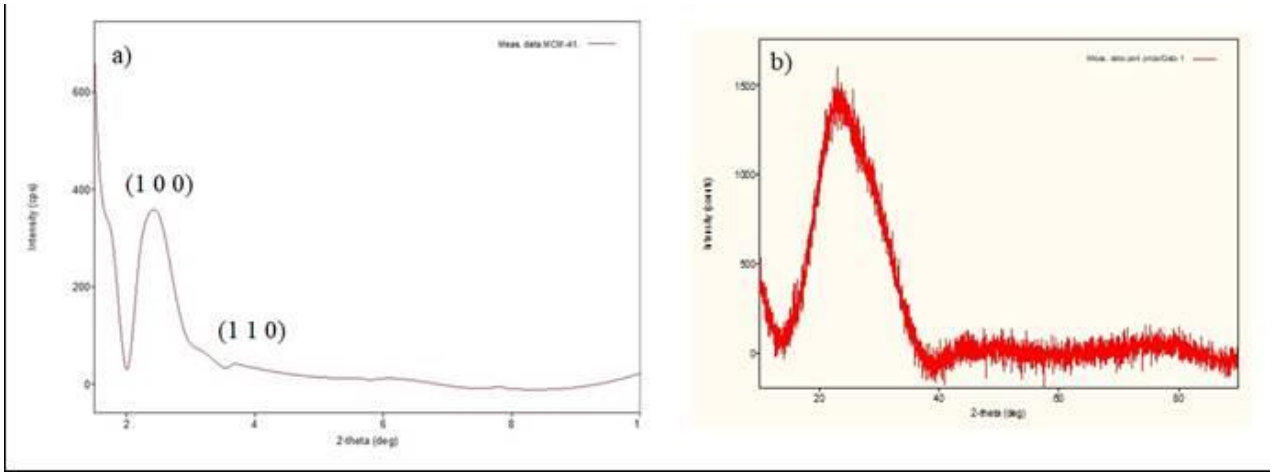

Figure 5: XRD powder patterns of MCM-41 a) Low angle XRD pattern, b) XRD pattern.

SEM studies

Surface investigations of the prepared 2-Cl-BT-MCM-41 were carried out by FE-SEM. SEM micrographs are given in Figure 6. SEM images showed non-uniform spheres at a range of 250-305 nm.

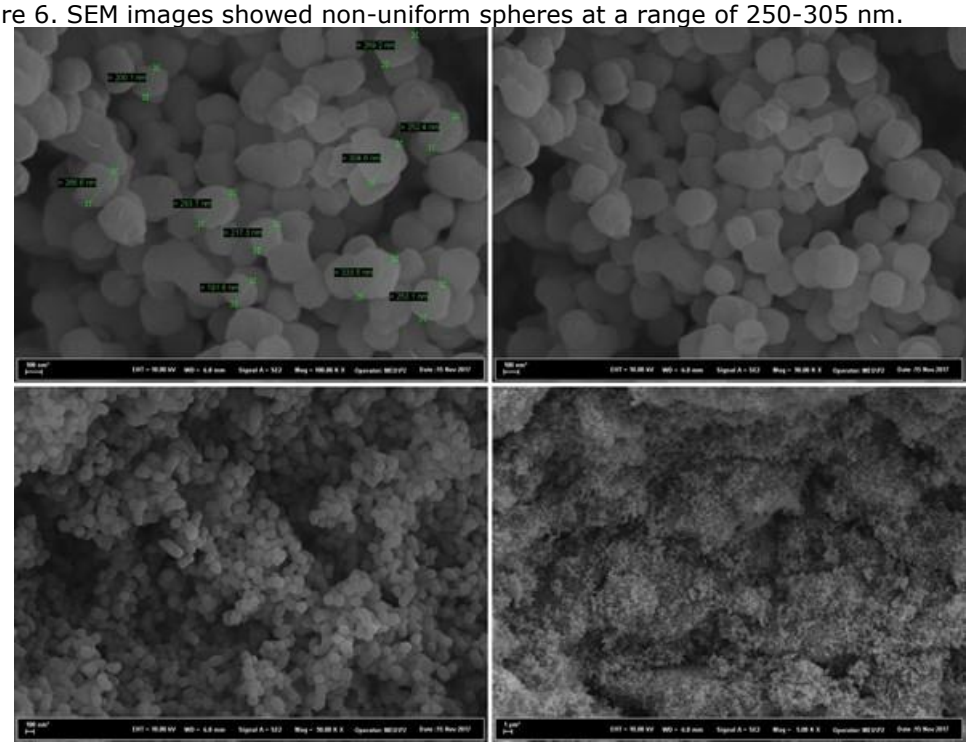

Figure 6: SEM images of 2-Cl-BT-MCM-41.

***In vitro* Ibuprofen Releasing Studies**

To examine the drug release profiles, the cumulative percentages of drug release were plotted against time. The release behavior of ibuprofen from 2-Cl-BT-MCM-41was investigated in the PBS solution for 66 hours. Release of ibuprofen from 2-Cl-BT-MCM-41 in PBS solution (pH = 7.4; 37 ºC) is given in Figure 7. Wave swing is observed in the drug release profiles. This behavior is due to unbalanced distribution of drug molecules from layered matrices, diffusibility, number of layers and thickness, and fluctuations in drug release are observed (20).

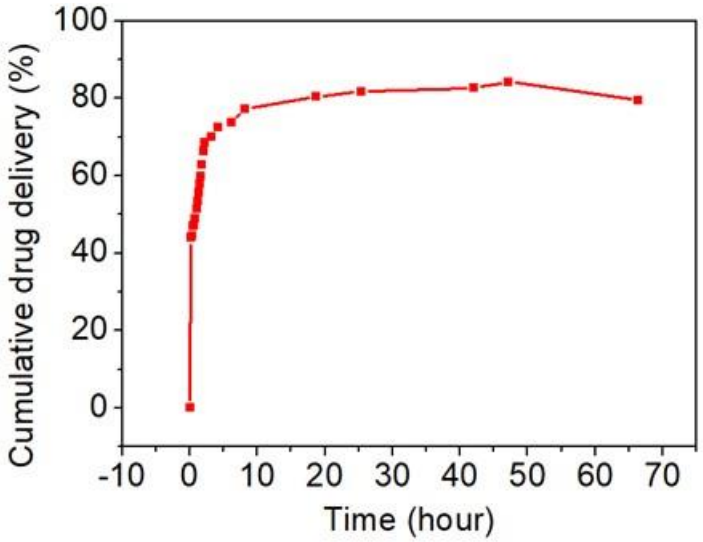

Figure 7: Release of ibuprofen from 2-Cl-BT-MCM-41in PBS solution (pH = 7.4; 37 °C).

BET studies

For the prepared MCM-41, the BET surface area was calculated as 1506 m^2/g and is compatible with the >1000 m^2/g value given in the literature. In addition, the pore diameter of MCM-41 was found to be 3.61 nm according to the literature. The surface area of 2-Cl-BT-MCM-41 was found to be 306 m^2/g. Nitrogen adsorption (black) desorption isotherms of MCM-41 and 2-Cl-BT-MCM-41are given in 8a-b.

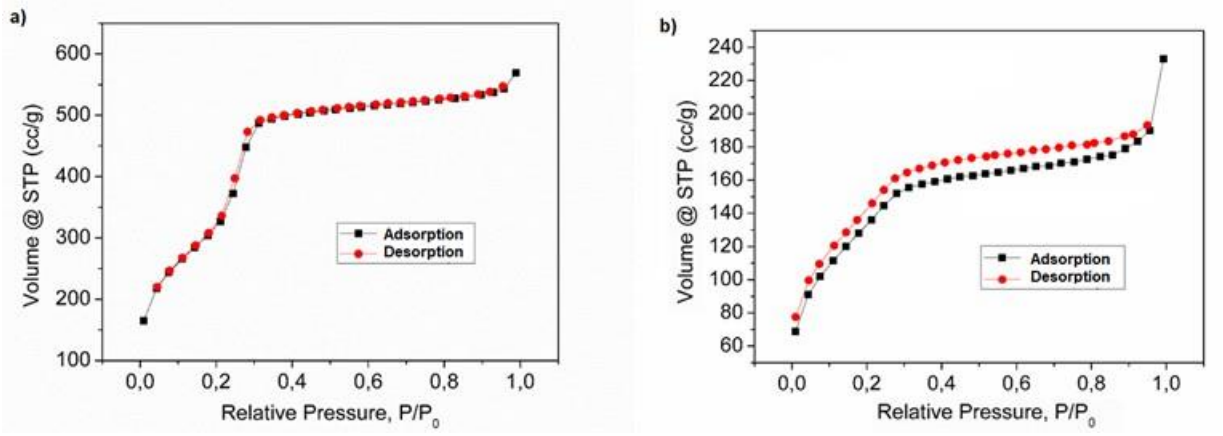

Figure 8: Nitrogen adsorption (black) desorption isotherms of a) MCM-41 and b) 2-Cl-BT-MCM-41.

CONCLUSION

In this study, mesoporous 2-Cl-BT-MCM-41was synthesized by precipitation method. 2-Cl-BT-MCM-41 was characterized via XRD, FT-IR, SEM and BET techniques. FT-IR spectrum of the 2-Cl-BT-MCM-41, the aromatic vibrations (γC-H) were observed at 3000 cm^{-1}. The carbon-oxygen vibrations (γC=O) were also observed at 1700 cm^{-1}. The (100) and (110) reflections observed at low angle XRD show the mesoporous SiO_2 structure. The characterization results confirm that the proposed structures are formed. The surface morphology of the particles was determined by SEM micrographs. The particule size of non-uniform spheres were observed at a range of 250-305 nm. BET surface areas were calculated as 1506 m^2 / g for MCM-41 and 306 m^2/g 2-Cl-BT-MCM-41, respectively. BET surface area is given as > 1000 m^2/g value in the literature. Our BET results are compatible with the literature. Ibuprofen was loaded using supercritical carbon dioxide (sC-CO_2) environment. The absorption and releasing studies of ibuprofen were carried out in simulated body fluid. The result revealed that high adsorption capacity for drug with 2-Cl-BT-MCM-41 and slower drug release rate was achieved. MCM 41 and 2-Cl-BT-MCM-41 bind with ibuprofen over weak hydrogen interactions. This causes slow releasing.

ACKNOWLEDGEMENTS

This study was supported by Mehmet Akif Ersoy University Scientific Research Projects Council (Project Number 0434-Yl-17).

REFERENCES

1. Vallet-Regi M. Ramila A. Del Real RP. Pérez-Pariente J. A new property of MCM-41: drug delivery system. Chem.Mater. 2001; 13(2):308-11.

2. Wang, S. Ordered mesoporous materials for drug delivery. Micropor. Mesopor. Mat. 2009; 117(1-2): 1-9.

3. Zeng W. Qian XF. Yin J. Zhu ZK. The drug delivery system of MCM-41 materials via co-condensation synthesis. Mater. Chem. Phys. 2006; 97(2-3): 437-41.

4. Sousa A. Souza KC. Sousa EMB. Mesoporous silica/apatite nanocomposite: special synthesis route to control local drug delivery. Acta. Biomater. 2008; 4(3): 671-9.

5. Qu F. Zhu G. Huang S. Li S. Sun J. Zhang D. Qiu S.Controlled release of Captopril by regulating the pore size and morphology of ordered mesoporous silica. Micropor. Mesopor. Mat. 2006; 92(1-3): 1-9.

6. Mal NK. Fujiwara M. Tanaka Y. Taguchi T. Matsukata M. Photo-switched storage and release of guest molecules in the pore void of coumarin-modified MCM-41. Chem. Mater. 2003; 15(17): 3385-34.

7. Aiello R. Cavallaro G. Giammona G. Pasqua L. Pierro P. Testa F. Mesoporous silicate as matrix for drug delivery systems of non-steroidal antinflammatory drugs. In Studies in Surface Science and Catalysis Elsevier. 2002; 142:1165-72.

8. Cavallaro G. Pierro P. Palumbo FS. Testa F. Pasqua L. Aiello R. Drug delivery devices based on mesoporous silicate. Drug. Deliv. 2004; 11(1):41-6.

9. Vallet-Regí M. Balas F. Arcos D. Mesoporous materials for drug delivery. Angew. Chem.Int. Edit 2007; 46(40):7548-58.

10. Xu W. Xu Y. Wu D. Sun Y. Ibuprofen delivery systems based on monodispersed spherical MCM-41 materials. In Studies in Surface Science and Catalysis Elsevier. 2007; 170:861-5.

11. Manzano M. Aina V. Arean CO. Balas F. Cauda V. Colilla M. Vallet-Regi M. Studies on MCM-41 mesoporous silica for drug delivery: effect of particle morphology and amine functionalization. Chem. Eng. J. 2008; 137(1):30-7.

12. Carino IS. Pasqua L. Testa F. Aiello R. Puoci F. Iemma F. Picci N. Silica-based mesoporous materials as drug delivery system for methotrexate release. Drug. Deliv. 2007; 14(8):491-5.

13. Nunes CD. Vaz PD. Fernandes AC. Ferreira P. Romao CC. Calhorda MJ. Loading and delivery of sertraline using inorganic micro and mesoporous materials. Eur. J. Pharm. Biopharm. 2007; 66(3):357-65.

14. Vallet-Regi M. Ramila A. Del Real RP. Pérez-Pariente J. A new property of MCM-41: drug delivery system. Chem. Mater. 2001; 13(2):308-11.

15. Popova M. Szegedi A. Mavrodinova V. Tušar NN. Mihály J. Klébert S. Yoncheva K. Preparation of resveratrol-loaded nanoporous silica materials with different structures. J. Solid State Chem. 2014; 219:37-42.

16. Horcajada P. Ramila A. Perez-Pariente J. Vallet-Regı M. Influence of pore size of MCM-41 matrices on drug delivery rate. Micropor. Mesopor. Mat. 2004; 68(1-3):105-9.

17. Rámila A. Munoz B. Pérez-Pariente J. Vallet-Regí M. Mesoporous MCM-41 as drug host system. J. Sol-Gel Sci. Tech. 2003; 26(1-3):1199-202.

18. Vallet-Regí M. Balas F. Arcos D. Mesoporous materials for drug delivery. Angew. Chem.Int. Edit. 2007; 46(40):7548-58.

19. Antochshuk V. Jaroniec M. Adsorption, thermogravimetric, and NMR studies of FSM-16 material functionalized with alkylmonochlorosilanes. J. Phys. Chem. B. 1999; 103(30):6252-61.

20. Dash S. Murthy PN. Nath L. Chowdhury P. Kinetic modeling on drug release from controlled drug delivery systems. Acta. Pol. Pharm. 2010;67(3):217-23.

JOTCS A
Journal of the Turkish Chemical Society
Section: A
Chemistry
TURKISH CHEMICAL SOCIETY

LDH- ɣ-Fe_2O_3-MoS_2 Composite for Vegetable Oil and Pb^{2+} Removal From Water

Fatih Mehmet EMEN[1], Ruken Esra DEMİRDÖĞEN[2], Göktürk AVSAR[3], Ali İhsan KARAÇOLAK[1]

[1]Mehmet Akif Ersoy University, Faculty of Arts and Science, Department of Chemistry, TR 15030, Burdur, Turkey
[2]Çankiri Karatekin University, Faculty of Science Department of Chemistry, TR 18100, Çankırı, Turkey
[3]Mersin University, Faculty of Arts and Science, Department of Chemistry, TR 15030, Burdur, Turkey

Abstract: Water pollution is a global concern. Inorganic and organic pollutants constitute primary pollutants in water resources. Therefore, it is of great concern to develop advanced sorbent materials for effective and efficient removal of metals and oil from water. In this study, synthesis of new LDH composites which would be used for sorption of heavy metals and oils from polluted water. For this purpose, MgAlOH-ɣ-Fe_2O_3-MoS_2 composite was prepared and characterizations were performed by FT-IR and XRD. The XRD powder pattern of the composite showed that it contained γ-Fe_2O_3, $MgAl(OH)14.xH_2O$ and MoS_2. Thermal stability of the composite was investigated via DTA/TG technique. MgAlOH-ɣ-Fe_2O_3-MoS_2 composite showed highly efficient sorption for vegetable oil up to 418% times of its own weight. The ability of MgAlOH- ɣ-Fe_2O_3-MoS_2 composite for removing Pb^{2+} ions from aqueous solution. Pb^{2+} ion analysis was made by ICP-OES. The effect of Pb^{2+} amounts, pH, sorbent amounts, and solvent flow rate on the adsorption capacity of MgAlOH- ɣ-Fe_2O_3-MoS_2 composite were also investigated.

Keywords: ɣ-Fe_2O_3, nanoparticle, composite, MoS_2, LDH.

Submitted: October 02, 2018. **Accepted:** January 18, 2019.

Cite this: Emen F, Demirdöğen R, Avşar G, Karaçolak A. LDH- ɣ-Fe2O3-MoS2 Composite for Vegetable Oil and Pb2+ Removal From Water. Journal of the Turkish Chemical Society, Section A: Chemistry. 2019;6(1):35–40.

DOI: https://dx.doi.org/10.18596/jotcsa.466768.

***Corresponding author.** E-mail: femen106@gmail.com, Tel: +905077681688, Fax:+902482133099.

INTRODUCTION

Water pollution is a global problem. Inorganic and organic pollutants are known as primary pollutants in water resources. Therefore, for eco-efficient and effective removal of metal ions and oil from water advanced sorbent materials should be developed (1). The photocatalytic deterioration which is the solution of environmental problems arising from organic pollutants, has attracted the attention of many researchers in recent years (2). A wide range of synthetic materials have been proposed and applied for this purpose (3–9). Due to its suitable physicochemical and optical properties, TiO_2, ZnO, Fe_2O_3, etc. metal oxide nanoparticles are promising candidates for photocatalytic applications (5,3–9). Molybdenum disulfide (MoS_2) has been widely used in biomedical applications as it has excellent photothermal conversion ability. Transition metal dichalogenes (TMDCs) are a family of two-dimensional layered materials with interesting physical, electronic, and chemical properties (10). The atoms in the layers are held together by strong covalent interactions and the layers are deposited along the van der Waals forces (11, 12). TMDCs have been extensively studied in energy storage, sensors, catalysis and biomedical (13-17). In particular, MoS_2, WS_2 and WSe_2 can be used in a wide variety of biomedical applications because their chalcogenides are less toxic than graphene (18). Oil pollution causing by oil spills has been an environmental and ecological disaster. The oil

spill in the Gulf of Mexico and the Bohai Gulf of China have shown the difficulty of an effective oil spill clearance. Mechanical extraction with sorbents is considered to be one of the most economical and efficient methods (19). In this process, the preparation of efficient, cost-effective materials for oil-water separation has gained importance. To date, different materials such as natural absorbers, microporous polymers, expanded graphite, carbon nanotubes and nanowire membranes have been used for this purpose (20). However, having several disadvantages, such as low oil loading capacity, excessive cost or environmental and ecological risk, limit the extensive application of these materials.

In this study, MgAlOH- ɣ-Fe_2O_3-MoS_2 composite was prepared and characterized via FT-IR and XRD techniques. The sorption studies of Pb^{2+} ion and vegetable oil from polluted water was carried out.

Herein, lightweight, hydrophobic, and porous aerogels made of carbon microbelts (CMBs) are first produced via a facile route by using waste paper as the raw material. Importantly, the CMB aerogel can absorb a wide range of organic compounds.

MATERIALS AND METHODS

Synthesis of Compounds

Synthesis of MCM-41

Typically, 0.6 g of n-cetyltrimethylammonium bromide (CTAB) was first dissolved in 400 mL of deionized water. Then 3.5 mL of 2 mol/L NaOH was added to the solution, followed by adjusting the solution temperature to 80 °C. Subsequently, 2.5 mL of TEOS was added dropwise to above solution with vigorous stirring. The mixture was stirred for another 2 h to give rise to a white solid. The obtained solid product was filtered, washed with deionized water and ethanol, and then dried in air. The dried sample was calcined at 550 °C for 1 h in N_2 and followed by another 3 h in air to remove the organic template.

Sythesis of mesoporous ɣ-Fe_2O_3

$Fe(NO_3)_3$ was dissolved in ethanol and MCM-41 was added to solution and stirred for 2 h. After the fitration, the powder was dried at 100 °C and fired at 550 °C for 3 h. The obtained MCM-41-Fe_2O_3 was added to 10 M NaOH and heated to dissolve MCM-41 phase. The obtained mesoporous Fe_2O_3 was washed and dried.

Preparation of MgAlOH-ɣ-Fe_2O_3-MoS_2

A portion of 50 mL of an aqueous solution containing 56.07 mmol (11.4 g) $MgCl_2$ $6H_2O$ and 28.17 mmol (6.8 g) $AlCl_3$ $6H_2O$ was added to 75 mL of an aqueous solution containing 12.52 mmol (2 g) Fe_2O_3 and $1{,}25x10^{-5}$ mmol (2 g) MoS_2 (12.50 mmol) The pH was raised to a value of 9 by addition of 2 M NaOH and the mixture was sonicated at room temperature for 16 h. The solid was filtered, washed, and dried in a vacuum desiccator.

Characterization

X-ray diffraction pattern was recorded on Bruker D8 using Cu Kα radiation, with the diffraction angle (2Θ) at a range of 10–80◦. FT-IR spectrum was recorded on a Perkin Elmer FT-IR/FIR/NIR spectrometer Frontier ATR system. Thermal stability of the composite was investigated via DTA/TG technique. Heavy metal analysis was made by ICP-OES. Measurements were carried out with a sequential, axially viewed Perkin Elmer Optima 8000 ICP-OES equipped with a meinhard nebulizer, a glass cyclonic spray chamber and ICP WinLab software Data System. Optimized operating conditions for the determination of constituents in water by ICP OES are given in Table 1.

Table 1. Optimized operating conditions for the determination of constituents in water by ICP OES

Rf power (W)	1450
Injector:	Alumina 2 mm i.d.
Sample tubing:	Standard 0.76 mm i.d
Drain tubing:	Standard 1.14 mm i.d.
Quartz torch:	Single slot
Sample capillary:	PTFE 1 mm i.d.
Sample vials:	Polypropylene
Source equilibrium delay:	15 sec
Plasma viewing:	Axial
Processing mode:	Peak area
Gases:	Argon and Nitrogen
Shear Gas:	Air

Sorption of Vegetable Oil

In a typical sorption test, MgAlOH-Fe_2O_3-MoS_2 composite was placed in contact with a vegetable oil emulsion in water until the composite was filled with the oil, which was then taken out for weight measurement. The weight measurement should be done quickly. The weight of a piece of the composite before and after sorption was recorded for calculation of the weight gain.

RESULTS AND DISCUSSION

FT-IR studies of MgAlOH-ɣ-Fe_2O_3-MoS_2

FT-IR spectrum of the MgAlOH-ɣ-Fe_2O_3-MoS_2 is given in Figure 1. Asymmetric vibration band of the O-H group of MgAlOH is observed at 3356 cm^{-1}. FT-IR spectrum of Fe_2O_3 exhibited vibrations in the region of 400-600 cm^{-1} which can be attributed to the vibrations of Fe-O and Mo-S (443 cm^{-1}) which confirms Fe_2O_3 nanoparticles and MoS_2 sheet structure. The results indicate the accuracy of the proposed structure (21-23).

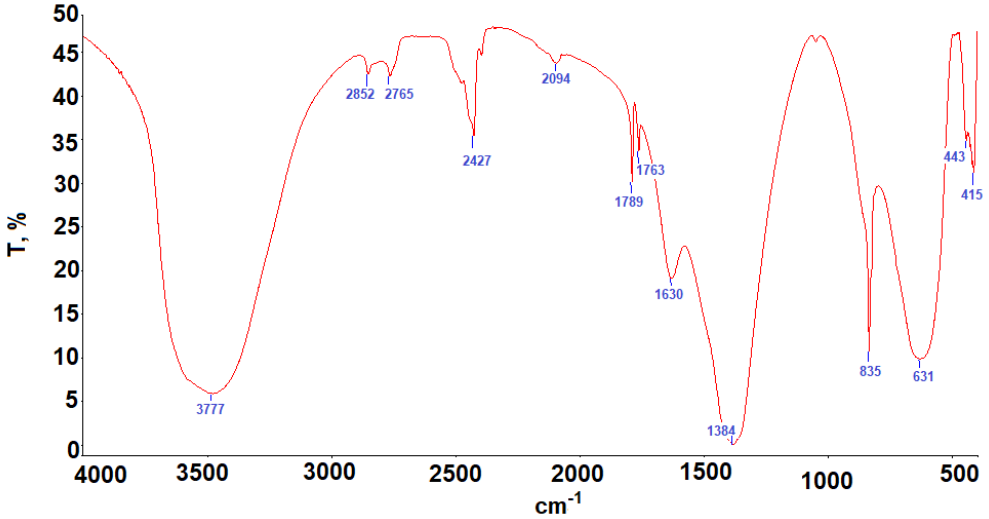

Figure 1: FT-IR spectrum of MgAlOH-Fe_2O_3-MoS_2.

XRD studies of MgAlOH-ɣ-Fe_2O_3-MoS_2

XRD powder diffraction pattern of MgAlOH-ɣ-Fe_2O_3-MoS_2 is presented in Figure 2. The XRD powder pattern of the composite showed that it contained γ-Fe_2O_3 (PDF card no:00-002-1047), $MgAl(OH)_{14}.XH_2O$ (PDF card no:00-043-0072) and MoS_2 (PDF card no:00-037-4492).

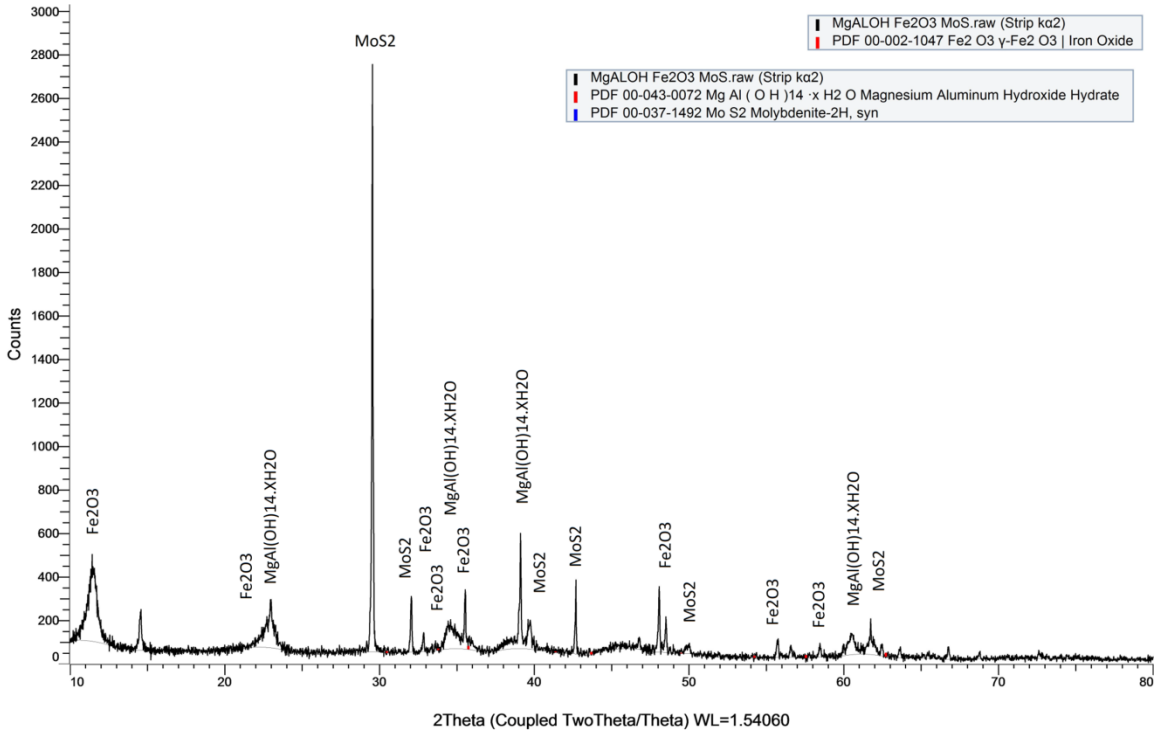

Figure 2: XRD powder diffraction pattern of MgAlOH-ɣ-Fe_2O_3-MoS_2

Thermal Analysis of MgAlOH-ɣ-Fe_2O_3-MoS_2

TG/DTA/DTG curves of MgAlOH-ɣ-Fe_2O_3-MoS_2 are given in Figure 3. In TG and DTG curves, three decomposition stages were obtained between 30 °C and 700 °C for MgAlOH-Fe_2O_3-MoS_2 . These decompositions were attributed to MgAlOH. The remaining products are MgO, Al_2O_3, Fe_2O_3 and MoS_2 mixture. Three endothermic peaks of decomposition stages were observed at 50 °C, 300 °C and 670 °C, respectively.

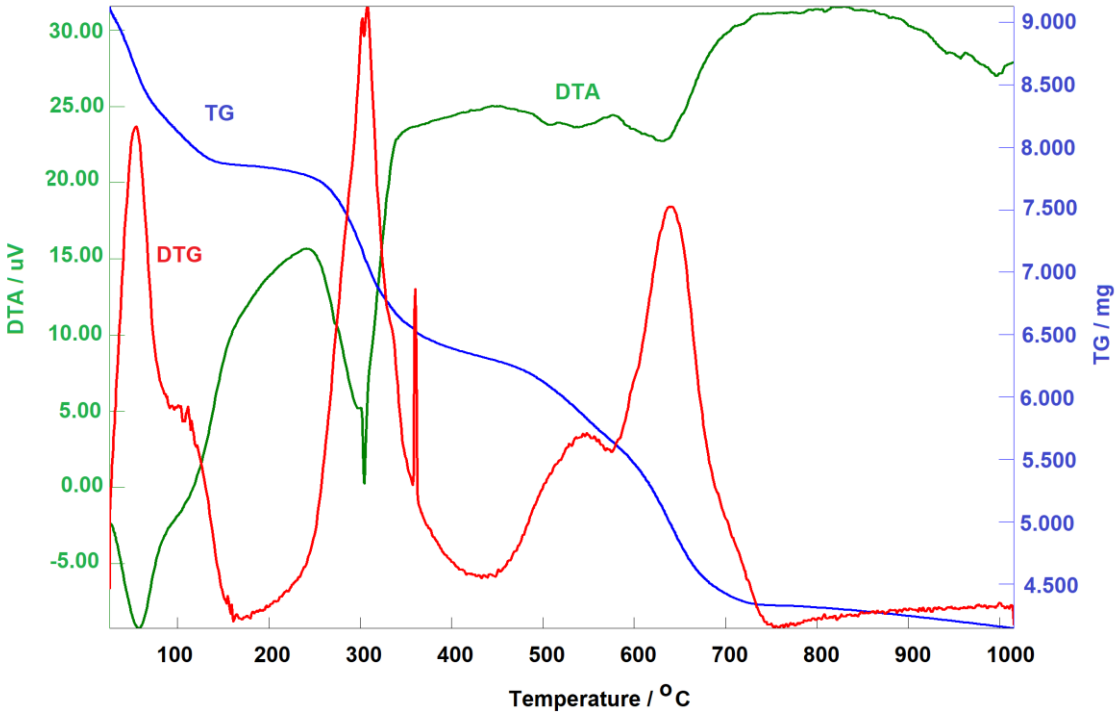

Figure 3: TG/DTA/DTG curves of MgAlOH-Fe_2O_3-MoS_2.

Absorption studies

Lead ion solutions of various volumes ranging from 1.1 mL to 4.2 mL, depending on the concentration of the lead ions in the solution, were passed through the column. The sorbed Pb^{2+} ions were eluted with 0.01 M hot nitric acid solution. Lead determination was made by ICP-OES at 217.0 nm and limit of detection was 0.1 mg/L. Effect of pH and concentration of Pb^{2+} as well as maximum sorption capacity was determined.

The obtained results are given in Tables 2-5.

Table 2. pH effect on adsorption capacity of MgAlOH-ɣ-Fe_2O_3-MoS_2.

MgAlOH-ɣ-Fe_2O_3-MoS_2	Pb concentration in solution	Adsorption	Recovery (%)
pH=3	420 ppm	403.3 ppm	96
pH=6	420 ppm	412.07 ppm	98
pH=7	420 ppm	415.93 ppm	99

Table 3. The effect of Pb^{2+} amounts on adsorption capacity of MgAlOH-ɣ-Fe_2O_3-MoS_2

Pb concentration in solution	Adsorption	Recovery (%)
420 ppm	415.07 ppm	98.1
320 ppm	312,94 ppm	97.6
215 ppm	212.1 ppm	98.2

Table 4. The effect of sorbent amounts on adsorption capacity of MgAlOH-ɣ-Fe_2O_3-MoS_2

Amount of MgAlOH-ɣ-Fe_2O_3-MoS_2	Pb concentration in solution	Adsorption	Recovery (%)
0.2 g	420 ppm	415 ppm	99.2
0.3 g	420 ppm	-	100

Table 5. The effect of solvent flow rate on adsorption capacity of MgAlOH-ɣ-Fe_2O_3-MoS_2

Solvent flow rate	Pb concentration in solution	Adsorption	Recovery (%)
1.1 mL/dk	420 ppm	416.7 ppm	99.4
2.7 mL/dk	420 ppm	413 ppm	98.1
4.2 mL/dk	420 ppm	405 ppm	96

Oil Sorption studies

0.5 g MgAlOH-ɣ-Fe_2O_3-MoS_2 was weighed and added onto water/oil (30 mL/4 mL) and sonicated for 30 min. Then the sorbent material was decanted and dried at 100 °C for 2 h. 0.5 g MgAlOH-ɣ-Fe_2O_3-MoS_2 absorbed 2.05 g oil. These result revealed that oil sorption capacity of MgAlOH-ɣ-Fe_2O_3-MoS_2 is 418%. The images MgAlOH-ɣ-Fe_2O_3-MoS_2 and oil adsorbed MgAlOH-ɣ-Fe_2O_3-MoS_2 are shown in Figure 4.

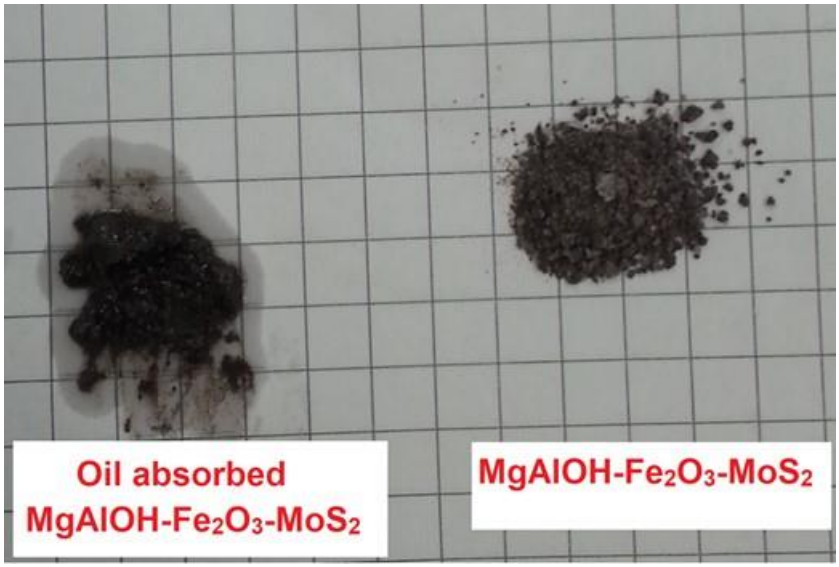

Figure 4. The images of MgAlOH-ɣ-Fe_2O_3-MoS_2 and oil-adsorbed MgAlOH-ɣ-Fe_2O_3-MoS_2.

CONCLUSION

In this study, MgAlOH-ɣ-Fe_2O_3-MoS_2 composite was prepared. The structure of MgAlOH-ɣ-Fe_2O_3-MoS_2 was elucidated by FT-IR and XRD powder pattern methods. The XRD powder pattern of the composite showed that it contained γ-Fe_2O_3, $MgAl(OH)14.xH_2O$ and MoS_2. The thermal behavior of the composite was investigated by DTA/TG combined system. In TG curves, three decomposition stages were obtained between 30 °C and 700 °C for MgAlOH-ɣ-Fe_2O_3-MoS_2. Double layer hydroxides are composed of layers. LDHs have the ability to absorb various cations and anions between layers. In recent years, magnetic nanoadsorbents and magnetic composites (24) have been widely used in the removal of heavy metals, various anions, organic pollutants and dyestuffs from solution media, for the removal of water as well as used in the recovery of these adsorbents and their evaluation after regeneration Furthermore, magnetic nanoadsorbents and magnetic composites (24) have been used for the removal of heavy metals, various anions, organic pollutants and dyestuffs from solution media. Recovering of these adsorbents and evaluation after regeneration are widely studied (25). Fe_2O_3 with the magnetic properties are known to absorb some heavy metal ions. It is also used to remove MoS_2 oils from the water. MgAlOH-ɣ-Fe_2O_3-MoS_2 composite can be used not only to remove heavy metals from contaminated water but also to remove oils. The results revealed that MgAlOH-ɣ-Fe_2O_3-MoS_2 composite was shown highly efficient sorption for vegetable oil up to 418% times weight itself.

REFERENCES

1. Gao X, Wang X, Ouyang X, Wen C. Flexible Superhydrophobic and Superoleophilic MoS_2 Sponge for Highly Efficient Oil-Water Separation. Sci. Rep-UK. 2016; 6:27207.

2. Karimi M, Jahangir V, Ezzati M, Saydi J, Lejbini MB. Zn0. 94Cd0. 06O nanoparticles with various structures, morphologies and optical properties toward MB optodecolorization. Opt. Mater. 2014; 36(3):697-703.

3. Putri LK, Tan LL, Ong WJ, Chang WS, Chai SP. Graphene oxide: exploiting its unique properties toward visible-light-driven photocatalysis. Appl.Mater. Today. 2016; 4:9-16.

4. Li M, Huang H, Yu S, Tian N, Dong F, Du X, Zhang Y. Simultaneously promoting charge separation and photoabsorption of BiOX (X= Cl, Br) for efficient visible-light photocatalysis and photosensitization by compositing low-cost biochar. Appl. Surf. Sci. 2016; 386:285-95.

5. Mazhdi M, Saydi J, Karimi M, Seidi J, Mazhdi F. A study on optical, photoluminescence and thermoluminescence properties of ZnO and Mn doped-ZnO nanocrystalline particles. Optik 2013; 124(20):4128-33.

6. Askari MB, Banizi ZT, Soltani S, Seifi M. Comparison of optical properties and photocatalytic behavior of TiO2/MWCNT, CdS/MWCNT and TiO2/CdS/MWCNT nanocomposites. Optik. 2018; 157:230-9.

7. Bystrov VS, Piccirillo C, Tobaldi DM, Castro, PML, Coutinho J, Kopyl S, Pullar RC. Oxygen vacancies, the optical band gap (Eg) and photocatalysis of hydroxyapatite: comparing modelling with measured data. Appl. Catal. B: Environ. 2016; 196:100-7.

8. Güler SH, Güler Ö, Evin E, Islak S. Electrical and optical properties of ZnO-milled Fe2O3 nanocomposites produced by powder metallurgy route. Optik. 2016; 127(6):3187-91.

9. Yin Q, Qiao R, Zhu L, Li Z, Li M, Wu W. α-Fe2O3 decorated ZnO nanorod-assembled hollow microspheres: Synthesis and enhanced visible-light photocatalysis. Mater. Lett. 2014; 135:135-8.

10. Wang QH, Kalantar-Zadeh K, Kis A, Coleman JN, Strano MS. Electronics and optoelectronics of two-dimensional transition metal dichalcogenides. Nat. Nanotechnol. 2012; 7(11):699.

11. Chhowalla M, Shin HS, Eda G, Li, LJ Loh, KP, Zhang H. The chemistry of two-dimensional layered transition metal dichalcogenide nanosheets. Nat. Chem. 2013; 5(4):263.

12. Voiry D, Mohite A, Chhowalla M. Phase engineering of transition metal dichalcogenides. Chem. Soc. Rev. 2015; 44(9):2702-12.

13. Kalantar-zadeh K, Ou JZ, Daeneke T, Strano MS, Pumera M, Gras SL. (2015). Two-dimensional transition metal dichalcogenides in biosystems. Adv. Funct. Mater. 2015; 25(32):5086-99.

14. Yin W, Dong X, Yu J, Pan J, Yao Z, Gu Z, Zhao Y. MoS2-Nanosheet-Assisted Coordination of Metal Ions with Porphyrin for Rapid Detection and Removal of Cadmium Ions in Aqueous Media. ACS Appl. Mater. Inter. 2017; 9(25):21362-70.

15. Chen Y, Wu Y, Sun B, Liu S, Liu H. (2017). Two-Dimensional Nanomaterials for Cancer Nanotheranostics. Small. 2017; 13(10):1603446.

16. Song JX, Tang XY, Zhou DM, Zhang W, James TD, He XP, Tian H. A fluorogenic 2D glycosheet for the simultaneous identification of human-and avian-receptor specificity in influenza viruses. Mater. Horiz. 2017; 4(3):431-6.

17. Wahiba M, Feng XQ, Zang Y, James TD, Li J, Chen GR, He XP. A supramolecular pyrenyl glycoside-coated 2D MoS 2 composite electrode for selective cell capture. Chem. Commun. 2016; 52(78):11689-92.

18. Teo WZ, Chng ELK, Sofer Z, Pumera M. Cytotoxicity of Exfoliated Transition-Metal Dichalcogenides (MoS2, WS2, and WSe2) is Lower Than That of Graphene and its Analogues. Chemistry. 2014; 20(31):9627-32.

19. Zhu H, Qiu S, Jiang W, Wu D, Zhang C. Evaluation of electrospun polyvinyl chloride/polystyrene fibers as sorbent materials for oil spill cleanup. Environ. Sci. Technol. 2011; 45(10):4527-31.

20. Yuan J, Liu X, Akbulut O, Hu J, Suib SL, Kong J, Stellacci F. Superwetting nanowire membranes for selective absorption. Nat. Nanotechnol. 2008; 3(6):332.

21. Zhang H, Duan X, Ding Y. Preparation and investigation on a novel nanostructured magnetic base catalyst MgAl–OH-LDH/$CoFe_2O_4$, Mater. Chem. Phys. 2009;114(2-3): 795-801.

22. Willis AL. Turro NJ, O'Brien S. Spectroscopic Characterization of the Surface of Iron Oxide Nanocrystals, Chem. Mater. 2005;17:5970-5.

23. Wang H, Chen P, Wen F, Zhu Y, Zhang Y, Flower-like Fe_2O_3@MoS_2 nanocomposite decorated glassy carbon electrode for the determination of nitrite, Sens. Actuators B. 2015;220:749–54.

24. Sivashankar R, Sathya AB, Vasantharaj K, Sivasubramanian V. Magnetic composite an environmental super adsorbent for dye sequestration – A review. Environ. Nanotechnol.Monit. Manage. 2014, 1–2, 36–49.

25. Gómez-Pastora J, Bringas E, Ortiz I. Recent progress and future challenges on the use of high performance magnetic nano-adsorbents in environmental applications. Chem. Eng. J. 2014, 256, 187–204.

JOTCS A
Journal of the Turkish Chemical Society
Section: A
Chemistry
TURKISH CHEMICAL SOCIETY

Phytochemical Evaluation of *Morus alba* Seeds and Cold Pressed Oil

Zeliha Ustun-Argon[1]*, Nihal İlhan [2,3], Ali Gökyer [2,3], Sıdıka Buyukhelvacigil Ozturk [2,3], Beril Koparal [2,3]

[1]Department of Biosystem Engineering, Necmettin Erbakan University, Konya, Turkey,
[2]Zade&Zade Vital İbn-i Sina R&D Center, Konya, Turkey
[3]DUAMER-Natural Products Research and Development Center, Konya, Turkey

Abstract: This study has focused on *Morus alba,* which is grown in Turkey mostly for the production of fruit. *M. alba* seeds' analysis results showed that oil, protein, ash, ash insoluble in hydrochloric acid, and total carbohydrate were, 21.33±0.58 g, 21.58±0.13 g, 3.99±0.13 g, 0.9±0.00 g, 54.76±2.42 g for 100 g of sample respectively; the main minerals were calcium, phosphorus, and potassium. Dominating fatty acids were linoleic acid (80.56±0.22%), palmitic acid (7.96±0.06%), oleic acid (7.11±0.05%). The primary volatiles were l-limonene, 2,2-dimethyldecane, and hexanal. Sterol components were found as beta-sitosterol>delta-5-avenasterol>campesterol>cholestenol and the total sterols' amount was 5501.49±44.26 mg/kg. δ-tocopherol, γ-tocopherol, β-tocopherol, α-tocopherol, total phenolic content, the radical scavenging activity were 257.67±4.51 mg/kg, 18.23±0.11 mg/kg, 6.71±0.13 mg/kg, 3.23±0.06 mg/kg, 137.1±0.36 mgGAE/100 g oil, 19.9±0.46% respectively. Other properties were free fatty acid (1.55±0.89% oleic acid), peroxide value (3.23±0.55 meq O_2/kg of oil), p-anisidine value (1.18±0.55) and refractive index (40 °C) (1.4687±0.00). As a result, *M. alba* seeds and oil along with its fatty acid, tocopherol, sterol and mineral composition can be used as nutritional supplements.

Keywords : *Morus alba*, phytochemical properties, volatile oils, fatty acid composition, sterols and tocopherols

Submitted: October 13, 2018. **Accepted:** January 10, 2019.

Cite this: Ustun-Argon Z, İlhan N, Gökyer A, Büyükhelvacıgil-Öztürk S, Koparal B. Phytochemical Evaluation of Morus alba Seeds and Cold Pressed Oil. JOTCSA. 2019;6(1):41–50.

DOI: https://dx.doi.org/10.18596/jotcsa.470279.

Corresponding author. E-mail: ustun.zeliha@gmail.com, zargon@erbakan.edu.tr. Phone: +90 555 380 44 96, +90 0332 777 00 30 Fax: +90 0332 777 00 40.

INTRODUCTION

The mulberry belongs to the flowering plants' genus Morus which is in the Moraceae family. The Morus genus has 24 species and at least one hundred known varieties belong to one subspecies. Mulberry plants can grow in various climate, soil and topographical conditions. Therefore, it can be found widely in the temperate, tropical or subtropical regions of both the Northern and the Southern hemisphere (1,2). Mulberry trees have been planted in Turkey for more than 400 years. According to the statistics in 2017, 74,383 tons of mulberry were cultivated from 2,713 trees in Turkey (3) and these trees represent three different species: *Morus alba (M. alba)* (%95), *Morus rubra* (3%) and *Morus nigra* (2%) (4). The white mulberry (*Morus alba*) is also found in China, Korea and later naturalized in Asia, Europe and America with a warm climates or subtropical zones. The Middle East, East and Southeast Asian countries are the main cultivation areas (4).

Mulberry fruits have different usages in traditional Turkish food products such as (mulberry fruit leather, mulberry churchkhela,

mulberry molasses), natural dyes and cosmetic products (1,5). The plant also has traditional medicinal purposes not only in Turkey but also in various countries of the world. Mulberry fruits can be used with anthelmintic, odontalgic, expectorant, laxative, emetic, hypoglycaemic effects and as a remedy for dysentery and oral lesions (6,7). In Chinese folk medicine, the fruits have been used for hypertension, arthritis, anemia, and diabetes treatment (2). Morus fruits also reported with their cooling and laxative effects, and applications for sore throat, fever, thirst, melancholia, and dyspepsia in Asian traditional therapies (8,9). Some important phenolic components which are found naturally in mulberries like anthocyanins, and other chemical components such as flavanoids, steroids, volatiles, trace elements, vitamins and amino acids, affect the physical and medical characteristics of the fruits such as color, neuro-protective effects, antioxidant, anti-inflammatory, and antimicrobial properties (2,10). The other parts of mulberries (leaves, bark, and branches) have been used in traditional medicine in various ways to protect the liver, strengthen joints, lower blood pressure, improve eyesight, tonify the blood, treat edema, gray hair and wheezing (10,11).

There have been some studies on some mulberry species' and some different parts of the plant like leaves, root, and bark (1). There are very limited studies which are especially focused on chemical properties of *M. alba* seeds and oil. This study aimed to show that native *M. alba* seeds and oil can be a new natural supplement alternative with its chemical properties. Therefore, in the present study, we have focused on some phytochemical and physicochemical properties of *M. alba*. The seeds were analysed for oil yield, trace elements, protein, total ash, and ash insoluble in hydrochloric acid. The seeds' cold pressed oil was analyzed for fatty acids and sterol compositions, volatile oils, antioxidant capacity, tocopherol compositions, and total phenols. The cold pressed oil was evaluated also for free fatty acid content, refractive index, peroxide, and p-anisidine value. The focus of this study to provide deeper scientific data for *M. alba* and evaluate the availability of native white mulberries for further medicinal and supplemental applications with their phytochemical properties.

MATERIAL and METHODS

Plant and oil samples

Commercially ripened mulberry samples were provided from Adıyaman, in the Tut Region in Turkey. Seeds were seperated from the fruits in place and sun-dried to represent the commercial raw material. Seed oil was extracted with the cold press method at Zade Vital Pharmaceuticals, Inc. The process temperature was under 40 °C. For the extraction no chemicals and heating applications were used and the whole process was completed according to GMP rules.

Chemicals

All the reagents were purchased from J.T. Baker and Sigma–Aldrich products which were of analytical or chromatographic grade. The water used for the analysis was provided by Millipore ultrapure water (Type I).

Determination of Protein, Total Ash, Ash Insoluble In Hydrochloric Acid, and Carbohydrate content

Total protein content was determined using the Kjeldahl's method and for crude protein calculation the nitrogen conversion factor was 6.25 (12). EP 8.0 method 2.4.16 was used for total ash analysis and EP 8.0 method 2.8.1 was used for ash insoluble in hydrochloric acid analysis. The total carbohydrate percentage was calculated by the difference of the total sample amount from protein, ash and ash insoluble in hydrochloric acid .

Determination of Trace Elements content

Trace elements analysis has been completed according to EPA 3051A, EN 14332 methods by using ICP-OES. For the analysis 7 mL HNO_3 65% and 1 mL H_2O_2 %30 were added onto 0.5 g of mulberry seed samples. The microwave digestion is conducted with the Milestone Ethos One oven and the microwave parameters were for steps 1 and 2; T1: 200 ˚C and T2: 110 ˚C Pressure: 45 bar with max power for 15 min. After the digestion process the samples were cooled down to the 25 °C and were diluted to 200 mL. Final analysis was done by using ICP-OES (Shimadzu ICPE-9000).

Fatty Acid Methyl Esters (FAME) Analysis and Sterol Composition

For determination of fatty acid methyl esters content (FAME) COI/T.20/Doc. No 33 for olive oils method was used (13). Retention time was used to identify the fatty acids, and for the quantitative analysis the area ratio under the relevant peak was used . The standard for the retention time was A 37 component mixture of FAME (Supelco). Shimadzu 2010 Plus GC-FID system , and a Restek Rt2560 capillary column (100 m x 0.25 mm ID x 0.2 µm) were used for the analysis. Split ratio was 1:100, injection temperature was 250°C and detector temperature was 260°C. The temperature was programmed as follows: At 140 °C, holding for 1 min and then increased to 240 °C at a rate of 4 °C/min and hold for 5 min.

Sterol analysis was completed with preparation of unsaponifiable matter and then isolation of the sterol fraction of the fatty oil according to EP

8.0 method 2.4.23. Sterol determination was done by using gas chromatography (Shimadzu 2010 Plus). The column was Teknokroma (TRB-Sterol) (30 m x 0.22 mm ID X 0.22 µm). Carrier gas was hydrogen, split ratio was 50:0 and flow rate was 40.0 cm/s. Column, injector, and detector (FID) temperatures were 260, 280 and 290 °C, respectively, and the injection volume was 1 µL for each analysis.

Free Fatty Acids, Peroxide Value, Refractive Index and p-Anisidine Value

Free fatty acid (FFA) content analysis was completed according to EP 8.0 method 2.5.1 and for peroxide value (PV) EP 8.0 method 2.5.5 was applied. Refractive index was determined by using EP 8.0 method 2.2.6 and Rudolph J57WR, for P-anisidine value A.O.C.S Official Method Cd 18-90 was used. The p-anisidine values were calculated using the following equation: p-A.V.=25*(1,2As-Ab)/m

Determination of Volatile Oils

Volatile compounds determined by Gas Chromatography-Mass Spectrometry (GC-MS). The equipment was a Shimadzu model GC – 2010 with mass selective detector QP 2010 plus – MS. The column was Restek Rxi-5ms, with 0.25 µm thickness, 30 m length, and 0.25 mm internal diameter. Volatile oils were identified with the database of the equipment. For analysis oven temperature was set to 40 °C, injection temperature to 250 °C in split mode with the split ratio 20, total flow was 40,8 mL/min, column flow was 1.80 mL/min. Oven temperature programmed as follow; holding the oven temperature at 40 °C for 3 min and increasing the temperature to 240 °C at a rate of 4 °C/min and holding for 5 min.

DPPH Free Radical-Scavenging Assay

The free radical scavenging activity was determined spectrophotometrically by the DPPH assay (14). Briefly, 1.95 mL of DPPH (0.025 mg/mL) which was prepared in methanol was added to 50 µL of methanolic solution of the sample. 30 min later, the absorbance was measured at 515 nm. As the control sample methanol (80%) was preferred. The following equation was used to calculate the capability of scavenging the DPPH radical :

$$DPPH\ radical\ scavenging\ effect\ (\%) = \frac{A\ control - A\ sample}{A\ control}\ x\ 100$$

$A_{Control}$: The initial concentration of the DPPH

A_{Sample} : The absorbance of the remaining concentration of DPPH in the presence of the extract and positive controls.

Determination of Total Phenolic Content (TPC)

Total phenolic content of the samples was determined using the method given in the study of Ferhat *et al.* (14,15). Gallic acid was used as the standard. For the analysis, 5 mL of distilled water and 1 mL of Folin–Ciocalteu reagent were added onto the 0.5 mL of methanolic extract solution in the test tube, and the tube was shaken. Four minutes later, 0.8 mL of Na_2CO_3 (7.5%) solution was added. The mixture was allowed to stand for 2 h and shaken occasionally. Absorbance of the sample was measured at 640 nm. The phenolic compounds concentrations were calculated according to the equation below which was obtained from the gallic acid standard graph.

Absorbance = 0.006 gallic acid (mg) – 0.021 (R^2=0.969)

Tocopherol Content

Tocopherols' stock solutions (1000 µg/mL) were prepared by using n-hexane as the solvent and the working standard solutions were diluted from the stock solution. The concentrations of the calibration solutions were between 1.25-200.00 µg/mL for all tocopherols. 20 µL injections were repeated for three times for each concentrations of tocopherols. Calibration graphs were completed using the data related with the peak areas. The linear regression equations were calculated according to the emission at 330 nm, the excitation at 290 nm wavelengths and corresponding concentrations. Approximately 0.500 g (±0,001 g) of seed oil sample was weighed into 10 mL volumetric flask and 8 mL n-hexane was added. The sample solution was kept in an ultrasonic bath for 5 minutes of sonication. The volume is completed to 10 mL by adding n-hexane and sonication was repeated for 5 minutes (15,16). For the HPLC analysis Lichrosorb Si 60, 250 x 4.0 mm column was used and the column temperature was 25±1 °C, flow rate was 0,8 mL/min, and mobile phase was hexane/2-propanol (99,5/0,5) (v/v). Tocopherol Set (Merck) was used as a standard which is including a four-vial pack containing α, β, γ, and δ-tocopherols.

RESULTS and DISCUSSION

Oil, Protein, Total Ash, Ash Insoluble In Hydrochloric Acid, Carbohydrate Content

The oil content of mulberry seeds was found to be 21%, protein was found to be 21,58±0,13 g, ash content was at 3,99±0,13 g, ash insoluble in hydrochloric acid level was at 0,9±0,00 g and total carbohydrate was at 54,76±2,42 g for 100 g seeds (Table 1). The total carbohydrate and the oil content determined in the seeds were with the highest amounts, respectively.

The results were compatible with the other results in the literature. For example, Absar *et al.* (17) mentioned that mulberry seeds contain 38 g of carbohydrate, 32 g of fat, and approximately 15 g of protein per 100 g of seed . Another study found the total carbohydrate at 47.58-43.17%, total lipid at 29.04-27.15%, total protein at 20.20-21.50%, ash at 6.05-5.10% for *M. alba* and *M. nigra,* respectively (8). In a study by Imran *et al.* (18), total carbohydrates were found with the highest range 13.83±1.20-17.96±1.54 g/100 g and it was followed by protein (0.96 ± 0.16-1.73 ± 0.10 g /100 g), lipid (0.48 ± 0.11-0.71 ± 0.07 g/100 g) and ash (0.46 ± 0.06-0.87 ± 0.12) for four different Morus species of Pakistan. *M. nigra* samples from Turkey showed a similar composition of nutrients with different percentages such as 42.4–46.6% carbohydrate, 27.5–33% crude oil, 20.2–22.5% crude protein and 3.5–6% ash (5). Total ash content gave an estimate of the total mineral content (19) also total ash and acid-insoluble ash contents are important indicators of the quality and the purity of herbal medicines. Total ash content is based on plant tissues and environmental sources such as soil and sand. Determination of total ash is not generally adequate to respresent the quality of the herbal supplements (20), therefore, acid-insoluble ash analysis has been conducted in this study. The contents of nutrients, as mentioned earlier depend on various effects such as variety, soil, geographical conditions, and absorbed minerals during growing season (5,8). Besides, most of the studies have been conducted with the whole fruits not solely with the seeds. The differences in the results can be explained with these factors. When our results are compared with the reported results of other studies it can be accepted that *M. alba* seeds can be a good source of these nutrients.

Trace elements

The main mineral components have essential activities in the body. Calcium and phosphorus are important especially for bones and tooth structure. Calcium has a role in activation of some enzymes and hormones and regulation of blood clotting (21). Phosphorus can be found in the structural composition of nucleic acids, ATP, GTP, nucleotide coenzymes, and is also important in maintenance of osmotic and acid–base balance, enzyme systems, and intermediary metabolism. Potassium has an important activity in excitability regulation of nerves and muscles and can be added to the diet to control the hypertension of people who use diuretics and can help to replace the excessive excretion of potassium (21). Minerals are also vital for physical and mental health and basic components of muscles, hemoglobin, soft tissues, nerves and blood cells (22). The differences in mineral composition of the fruits and the seeds can be explained with the variety of the cultivars and species. It also can be related with the environmental factors such as climate, soil, geographical conditions, fertilizers, cultural management techniques (2), harvesting, and storage conditions (23).

Mulberry seed trace element levels measured for 100 g seed as presented in Table 1 were: calcium (Ca) (821.00 ± 24.58 mg), phoshorus (P) (288.67 ± 7.51 mg), potassium (K) (288.50 ± 10.61 mg), iron (Fe) (11.97 ± 0.61 mg), magnesium (Mg) (243.33 ± 11.59 mg), and sodium (Na) (35.30 ± 0.46 mg). Ca was at the highest amount, and it was followed by P, K, and Mg, respectively. In a study by Liang *et al.* (2) with eight different mulberry cultivars from China (2) it has been found that K level was higher than other elements and it has been followed by P, Ca, Mg, and Fe with similar quantities in our study. Another study, which evaluated the mineral contents of different mulberry species, found the K amount between the range of 1731 ± 11.50 and 1270 ± 9.36 mg, while Ca was–576 ± 7.37-440 ± 3.21 mg , Na was 260 ± 3.86-280 ± 3.50 mg and Mg was 240 ± 2.90-360 ± 4.20 mg/100 g for *M. alba, M. nigra, M. laevigata* black and white fruits. Ercisli and Orhan (1) found the results for *M.alba, M. nigra, M. rubra* between the following ranges: P (226-247 mg/100 g), K (834-1668 mg/100 g), Ca (132-152 mg/100 g), Mg (116-115 mg/100 g), Na (59-61 mg/100 g). These studies also mentioned other elements such as Cu, Mn, Zn, Ni, Se, As, Cr being in lower quantities. The results showed that with its rich mineral composition mulberry seeds could be recognized as a valuable nutritional product.

Table 1. Nutrients profile of *M. alba* seeds (n=3)

Nutrient component	**Amount (g/100 g of seed)**
Total carbohydrate	54.76±2.42
Protein	21.58±0.13
Oil	21.33±0.58
Ash	3.99±0.13
Ash insoluble in hydrochloric acid	0.9±0.00
Trace elements	**Amounts (mg/100 g)**
Calcium	821.00±24.58
Phosphorus	288.67±7.51
Potassium	288.50±10.61
Magnesium	243.33±11.59

Sodium	35.30±0.46
Iron	11.97±0.61

Fatty Acid Composition

In our study, the main fatty acids of mulberry seed samples were found to be linoleic acid (80.56 ± 0.22%), palmitic acid (7.96 ± 0.06%), oleic acid (7.11 ± 0.05%) and stearic acid (3.45 ± 0.02%) and these four components comprised approximately 99% of the fatty acid composition. Fatty acid methyl ester composition can be seen in Table 2. PUFA was 81,07%, MUFA was 7.27%, USFA was 88.34%, and SFA was 11.64%.

In a study about *M. nigra* from Turkey, main fatty acids were found to be linoleic acid (73.74%), palmitic acid (10.25%), oleic acid (8.20%) and stearic acid (4.48%), similar to our study (5). Another study about *M. alba* from Bangladesh found the linoleic acid to be the most dominant fatty acid by 74.29%, and it has been followed by palmitic (10.60%) and stearic (5.61%) acids. This study did not mention oleic acid (24). According to the results of this study mulberry seeds oil contains one of the two essential oils which can not be produced in the human body. *M.alba*'s oil can be considered as a good source of linoleic acid since its deficiency can cause poor wound healing, hair loss, and dry hair (2) and the addition of omega-6 to the daily diet in 5-10% can reduce the cardiovascular disease risk (25).

It can be seen in different studies with different mulberry cultivars from different countries that linoleic, palmitic, oleic, and stearic acids are the most dominant fatty acids generally with different ranges in accordance with our study (1,2,8,26). The differences in the fatty acid compositions may be due to the differences in species and genetics. The environmental conditions are the other factors which affect fatty acid composition and these conditions can be more effective on fatty acid composition more than the plant varieties (2,5).

The other properties of the *M. alba* seeds oil are given at the Table 2. Free fatty acid (FFA) content was found to be 1.55 ± 0.89% oleic acid, peroxide value (PV) was 3.23 ± 0.55 meq O_2/kg oil, p-anisidine value 1.18 ± 0.55 and the refractive index (RI) (40 °C) was 1.4687 ± 0.00. FFA content was found lower than the other studies of Morus varieties in the literature which were between 2.15-2.34 and 2.87 ± 0.17. PV was also lower than the results of the same studies which found the PV as 1.65-2.05 and 6.33 ± 0.22 (5,24) and also was lower than the recommended value of commercially available edible vegetable oils (PV≤10) (27). There was not any study, to our knowledge, with the anisidine value of mulberry seed oil. Therefore, our results were compared with another study which evaluated the raspberry fruits. The values of our study were found to be lower than the other study which was conducted with rasperry samples which p-anisidine value was 14.3 (27). It can be explained with the lower level of the secondary oxidation products. RI was similar with the other studies at 29 °C 1.465-1.468 and 1.469 ± 0.002 at 50 °C (5,8). With the results of the quality parameters *M. alba* seeds oil can be considered safe to use as edible oil and as ingredient for supplements.

Sterol Composition

M. alba seed's oil sterol analysis results revealed beta-sitosterol most abundantly by 78.21±0.61 mg/kg. Other sterol components were delta-5-avenasterol (8.11 ± 0.42 mg/kg), campesterol (6.73 ± 0.42 mg/kg), cholestanol (3.50 ± 003 mg/kg), stigmasterol (1.09 ± 0.04 mg/kg), delta-7-avenasterol (0.90 ± 0.03 mg/kg), sitositanol (0.59 ± 0.06 mg/kg), clerosterol (0.55 ± 0.03 mg/kg) and total sterol was 5501.49 ± 44.26 mg/kg. The study about *M. nigra*'s sterol contents gave the results which indicated that the main sterol components were betasitosterol, Δ5-avenasterol, Δ5,23-stigmastadienol, clerosterol, sitostenol and Δ5,24-stigmastadienol. The rest of the sterol composition contained campesterol, stigmasterol, cholesterol and Δ7-stigmasterol in small amounts (5). Our results show similarity with the previous study. With the knowledge that consuming enriched foods with with phytosterols can help lowering the plasma cholesterol (21) and has many benefits for human health (5), with our results it can be said that mulberry seeds' oil can be considered as a source of phytosterols.

Tocopherol Content

Results of the analysis showed that *M. alba* seed oil contains four different types of tocopherols. These were δ-tocopherol, γ-tocopherol, β-tocopherol, α-tocopherol and their levels were 257.67 ± 4.51, 18.23 ± 0.11, 6.71 ± 0.13, 3.23 ± 0.06 mg/kg, respectively. Total tocopherol content was 285.84 ± 4.80 mg/kg. While δ-tocopherol was with the highest value, α-tocopherol showed the lowest value. Compared with other studies our results found higher than the parsley and cardamom cold pressed oils' tocopherol levels (28), also α-tocopherol level of Gecgel *et al.* (5)'s work which reported as 0.18 ± 0.01 mg/100 g value. Yılmaz and Durmaz's study (26) showed the same gradation among tocopherols with higher percentages. The optimal tocopherol contents in vegetable oils are needed for the stabilization and technological quality of these oils (26,29). From the nutritional perspective, tocopherols intake in daily diet is considered beneficial for different

treatments such as cardiovascular problems, cataract, and tocopherols show neuroprotective and anticancer properties with antioxidant activities (21).

Volatile Oils

In our study, we identified 34 different volatile components which are dominated with monoterpenes (54.46%), alkanes (16,91%) and aldehydes (10.97%). Alcohols (3.75%), acids (3.44%), esters (2.72%), ethers (2.58%), benzenes (2.54%), other components (1.68%), ketones (0.51%), miscellenous components (0.18%) also have been analyzed in *M. alba* volatile oil (Table 3). For the monoterpenes l-limonene, alpha pinene and 2-beta-pinene were found with the highest amount. Looking into the components generally l-limonene was found with the highest percentage and it has been followed by 2,2-dimethyl-decane and hexane. Among the other components propanoic acid, 1-hexanol, hexanal, 4-ethyl-1,2-dimethylbenzene, 2,2-dimethyl-1-propanol acetate and anethole percentage were more than 1%. The most dominant compound limonene is generally found in citrus fruits and it has been used in different treatments with its antibacterial, hepatoprotective, anticancer, gallstones dissolving and gastric acid neutralizing effects (30–32).

Table 2. Physicochemical properties of *M. alba.*

Fatty Acids (%)*		**Sterols (%)****	
Palmitic acid C 16:0	7.96±0.06	Beta-sitosterol	78.21±0.61
Palmitoleic acid C 16:1	0.07±0.01	Delta-5-avenasterol	8.11±0.42
Margaric acid C 17:0	0.07±0.00	Campesterol	6,73±0.42
Stearic acid C 18:0	3.45±0.02	Cholestanol	3.50±003
Oleic acid C 18:1	7.11±0.05	Stigmasterol	1.09±0.04
Linoleic acid C 18:2	80.56±0.22	Delta-7-avenasterol	0.90±0.03
Gamma linolenic acid C 18:3	0.01±0.02	Sitositanol	0.59±0.06
Alpha linolenic acid C 18:3	0.47±0.01	Clerosterol	0.55±0.03
Arashidic acid C 20:0	0.12±0.01	Total sterol (mg/kg)	5501.49±44.26
Eicosenoic acid C 20:1	0.08±0.01		
Eicosadienoic acid C 20:2	0.03±0.00	**Tocopherols (mg/kg)**	
Behenic acid C 22:0	0.04±0.00	δ-tocopherol	257.67±4.51
Erusic acid C 22:1	0.01±0.02	γ-tocopherol	18.23±0.11
Lignoseric acid C 24:0	0.01±0.02	β-tocopherol	6.71±0.13
		α-tocopherol	3.23±0.06
Free fatty acid (% oleic acid)	1.55±0.89	Total tocopherol	285,84±4.80
Peroxide value (meq O_2/kg oil))	3.23±0.55		
p-anisidine value	1.18±0.55		
Refractive index (40 °C)	1.4687±0.00.		

*Percentage of the fatty acids in the oil
** Percentage of the sterols in total sterols

Table 3. *M. alba* volatile oil components (n=3)

Acids	**(%)*****
Propanoic acid	2.61±0.08
Heptanoic acid	0.62±0.03
Isovaleric acid	0.21±0.01
Alcohols	
1-Hexanol	2.59±0.24
1-Octen-3-ol	0.51±0.04

Benzeneethanol	0.24±0.07
1-Pentanol	0.22±0.04
Benzenemethanol	0.18±0.01
Aldehydes	
Hexanal	9.15±0.26
Heptenal	0.94±0.05
Nonanal	0.32±0.02
Heptenal	0.30±0.09
Benzaldehyde	0.26±0.05
Alkanes	
2,2-dimethyldecane	15.25±0.36
Decane	0.68±0.10
2,2,3,3-tetramethylpentane	0.37±0.02
Dodecane	0.30±0.04
Pentylbenzene	0.17±0.03
3,3,4-trimethylhexane	0.12±0.02
Benzenes	
4-ethyl-1,2-dimethylbenzene	1.39±0.81
Styrene	0.98±0.13
1,2-dimethylbenzene	0.17±0.06
Esters	
2,2-dimethyl-1-propanol acetate	2.13±0.15
3-methyl-1-butanol acetate	0.60±0.04
Ethers	
Anethole	2.58±0.11
Ketones	
2-Heptanone	0.51±0.13
Monoterpenes	
l-limonene	49.50±0.88
Alpha pinene	2.63±0.09
2-beta-pinene	1.15±0.14
Alloocimene	0.34±0.02
Alpha thujene	0.32±0.03
Camphene	0.31±0.01
Delta-3-Carene	0.21±0.09
Miscellaneous	
Dihydro-2(3H)-Furanone	0.18±0.06

***The percentage of the specific oil among the total volatile oil content

Total Phenolic Content

In our study, total phenolic content was found to be 137.1 ± 0.36 mg GAE/100 g. Our results are competent with the study of Gecgel *et al.*(5) which analyzed the different mulberry seeds and found the total phenolic content to be in the range of 112.2–152.0 mg GAE/100 g. The results of Yilmaz and Durmaz's study (26) found the phenolic content for purple mulberry and black mulberry as 193 mg GAE and 178 mg GAE for 100 g seed oil respectively. The phenolic content in different studies changed between 100–150 mg GAE/100 g oil similar with our results. Our results were generally lower than the other studies as we used the seeds for analysis while the other studies were conducted with the whole fruits. Comparing the seeds and the whole fruit, mulberry fruits were found to be with one of the most powerful phenolic contents among ~~the~~ other fruits. Different mulberry cultivars showed very rich content of the total polyphenols such as *Morus atropurpurea* Roxb. (189.67-246.00 GAE mg/100 mg DW) (2), *M. alba* (1650±12.25 mg/100 g FW) (18), *M. nigra* (1422 mg GAE/100 g) and *M. rubra* (1035 mg GAE/100 g) (1). The differences between the

total phenolic contents depend on the varieties of the mulberries and the amount of the phenolics which passed to the oil during extraction (26). Also other factors can affect the level of the phenolic compound such as genotype, maturity at harvesting and environmental conditions (1,2,18).

Free Radical-Scavenging Activity

Free radicals are accepted to have an important role for health problems such as cardiovascular diseases and chronic pathologies also have a major effect on lipid peroxidation. The compounds with the antioxidant effects can be used to reduce the radicals (18). Edible oils are known with their antioxidant effects and also therefore it has been important to include these oils in the daily diet (26). In our study we evaluated the *M. alba* seeds' cold pressed oil for their antioxidant capacity with the DPPH radical which is mostly preferred for natural products. The antioxidant capacity was found 19.9±0.46%. In the studies which compared different mulberry cultivars, *M. alba* and mulberry pomace were found with the highest antioxidant capacity (18,26). Another study which focused on eight different mulberry cultivars from China found the free radical scavenging activity rates between 50-96%. In this study the whole fruits have been evaluated and it has been implicated that phenolic compounds such as anthocyanins, phenolic acids, and flavonoids are accepted as the major responsible component of the antioxidant activities in the fruits (2). The difference can be explained with the different parts of the fruits which were used for the analysis. Also different varieties of the fruits can effect the results (2).

CONCLUSION

The study analyzed M. alba seeds' ash levels and ash insoluble in hydrochloric acid, indicating that with the quality and purity of the material, *M. alba* seeds can be considered an appropriate raw material for herbal medicines. Trace elements of the seeds such as calcium, phosphorus, and potassium also can be accepted as a source of some minerals in the diet which are important for bones, dental structure and treatment of hypertension. Seeds contain approximately 21% of oil content with the dominance of linoleic acid (80.56%). Therefore cold pressed oil can be used in diets for supplementing this essential fatty acid. Volatile oils consist mostly of monoterpenes, alkanes and aldehydes and mulberry seed oil can be used with its l-limonene content for phytotherapeutical applications. Tocopherols and sterols, which have preventive effects for cardiovascular problems and antioxidant effects, were also found in remarkable amounts. *M. alba* seeds and its oil can be used in diets and nutritional supplements with its nutritional and phytotherapeutic effects. Since the studies about the mulberry seeds oil have been very limited, more researches with different cultivars are needed for further applications.

CONFLICT OF INTEREST

The authors declare no conflict of interest.

ACKNOWLEDGEMENTS

This study was supported by the Zade – Zade Vital İbn-i Sina R&D Center and DUAMER-Natural Products Research and Development Center. The authors wish to thank the Zade Vital Pharmaceutials for supplying the raw material and cold pressed oil.

REFERENCES

1. Ercisli S, Orhan E. Chemical composition of white (Morus alba), red (Morus rubra) and black (Morus nigra) mulberry fruits. Food Chemistry. 2007;103(4):1380–4.

2. Liang L, Zhu M, Li F, Yang L, Wu X, Zhao W, et al. Chemical composition, nutritional value, and antioxidant activities of eight mulberry cultivars from China. Pharmacognosy Magazine [Internet]. 2012;8(31):215. Available from: http://www.phcog.com/text.asp?2012/8/31/215/99287

3. TUIK TSI. Other fruits , 1988-2017 [Internet]. 2018. Available from: http://www.tuik.gov.tr/PreTablo.do?alt_id=1001

4. Ercisli S. A short review of the fruit germplasm resources of Turkey. Genetic Resources and Crop Evolution. 2004;51(4):419–35.

5. Gecgel U, Velioglu SD, Velioglu HM. Investigating some physicochemical properties and fatty acid composition of native black mulberry (Morus nigra L.) seed oil. JAOCS, Journal of the American Oil Chemists' Society. 2011;88(8):1179–87.

6. Baytop T. Therapy with medicinal plants in Turkey (Past and Present). Second. İstanbul: Publications of the Istanbul University; 1999.

7. Elmacı Y, Altug T. Flavour evaluation of three black mulberry (Morus nigra) cultivars using GC/MS, chemical and sensory data. Journal of the Science of Food and Agriculture. 2002;82(6):632–5.

8. Rahman M, Akther A, Yeasmin S, Rahman S, Ferdousi S, Das K, et al. Comparative Studies on the Physicochemical Characteristics, Nutritional Value and Antimicrobial Activities of

Two Varieties Indigenous Mulberry (Morus alba L. and Morus nigra L.) Seeds. International Journal of Current Research in Chemistry and Pharmaceutical Sciences. 2014;1(7):44–50.

9. Shukla RK, Painuly D, Shukla A, Kumar V, Singh J, Porval A, et al. Physical evaluation, proximate analysis and antimicrobial activity of Morus Nigra seeds. International Journal of Pharmacy and Pharmaceutical Sciences. 2015;7(1):191–7.

10. Jha S, Srivastava AK. Antibacterial , Antifungal and Pesticidal Activity of Plant Morus Alba-a Novel Approach in Po .... International Journal of Agricultural Science and Research. 2013;3(1):157–62.

11. Katsube T, Yamasaki M, Shiwaku K, Ishijima T, Matsumoto I, Abe K, et al. Effect of flavonol glycoside in mulberry (Morus alba L.) leaf on glucose metabolism and oxidative stress in liver in diet-induced obese mice. Journal of the Science of Food and Agriculture. 2010;90(14):2386–92.

12. El-Shurafa MY, Ahmed HS, Abou-Naji SE. Organic and inorganic constituents of date palm pit (seed). Date Palm Journal. 1982;1(2):275–84.

13. Gumus ZP, Ertas H, Yasar E, Gumus O. Classification of olive oils using chromatography, principal component analysis and artificial neural network modelling. Journal of Food Measurement and Characterization [Internet]. 2018;12(2):1325–33.

14. Ferhat R, Lekbir A, Ouadah H, Kahoul MA, Khlalfa L, Larouni S, et al. Effect of extraction solvent on total phenolic content, total flavonoid content, and antioxidant activities of Algerian pomace olive oil. Ifrj. 2017;24(6):2295–303.

15. AğŞelecï D, Gümüş ZP, Yavuz M, ŞELECİ M, Bongartz R, Stahl F, et al. A case study on in vitro investigations of the potent biological activities of wheat germ and black cumin seed oil. Turkish Journal of Chemistry. 2015;39:801–12.

16. U. Celenk V, Gumus ZP, Ustun Argon Z, Buyukhelvacigil M, Karasulu E. Analysis of Chemical Compositions of 15 Different Cold-Pressed Oils Produced in Turkey : A Case Study of Tocopherol and Fatty Acid Analysis. JOTCSA. 2018;5(1):1–18.

17. Absar N, Yeasmin T, Raza MS, Sarkar SK, Arisaka F. Single step purification, characterization and N-terminal sequences of a mannose specific lectin from mulberry seeds. The Protein Journal. 2005;24(6):369–77.

18. Imran M, Khan H, Shah M, Khan R, Khan F. Chemical composition and antioxidant activity of certain Morus species. Journal of Zhejiang University SCIENCE B [Internet]. 2010;11(12):973–80. Available from: http://www.springerlink.com/index/10.1631/jzus.B1000173

19. Fennema OR. Food Chemistry [Internet]. 3rd ed. New York: Marcel Dekker Inc.; 1996. 632-650 p. Available from: http://linkinghub.elsevier.com/retrieve/pii/0260877488900556

20. Rao Y, Xiang B. Determination of total ash and acid-insoluble ash of Chinese herbal medicine Prunellae spica by near infrared spectroscopy. Journal of the Pharmaceutical Society of Japan. 2009;129(7):881–6.

21. Sardesai V. Introduction to Clinical Nutrition. Third. Boca Raton, FL: CRC Press Taylor & Francis Group; 2012.

22. Dini I, Tenore GC, Dini A. Chemical composition, nutritional value and antioxidant properties of Allium caepa L. Var. tropeana (red onion) seeds. Food Chemistry. 2008;107(2):613–21.

23. Ustun Argon Z, Gokyer A. Determination of Physicochemical Properties of Nigella sativa Seed Oil from Balıkesir Region , Turkey. Chemical and Process Engineering Research. 2016;41:43–6.

24. Rahman MM, Akhter A, Mounuddin M, Yeasmin SM, Rahman M, Rahman S, et al. Investigation Some Physicochemical Properties, Lipids, Glycerides and Fatty acid Composition of Mulberry (Morus Alba L) Seed oil of three Different Regions of Bangladesh. American Journal of Applied Chemistry [Internet]. 2014;2(3):38–41.

25. Harris WS, Mozaffarian D, Rimm E, Kris-Etherton P, Rudel LL, Appel LJ, et al. Omega-6 fatty acids and risk for cardiovascular disease: A science advisory from the American Heart Association nutrition subcommittee of the council on nutrition, physical activity, and metabolism; council on cardiovascular nursing; and council on epidem. Circulation. 2009;119(6):902–7.

26. Yilmaz MA, Durmaz G. Mulberry seed oil: A rich source of δ-Tocopherol. JAOCS, Journal of the American Oil Chemists' Society. 2015;92(4):553–9.

27. Oomah BD, Ladet S, Godfrey D V., Liang J, Girard B. Characteristics of raspberry (Rubus idaeus L.) seed oil. Food Chemistry. 2000;69(2):187–93.

28. Parry Jr. JW. Value-adding factors in cold-pressed edible seed oils and flours. University of Maryland; 2006.

29. Kamal-eldin A. Effect of fatty acids and tocopherols on the oxidative stability of vegetable oils. Eur J Lipid Sci Technol. 2006;58:1051–61.

30. Chen Q, McGillivray D, Wen J, Zhong F, Quek SY. Co-encapsulation of fish oil with phytosterol esters and limonene by milk proteins. Journal of Food Engineering [Internet]. 2013;117(4):505–12.

31. Rathore SS, Saxena SN, Singh B. Potential health benefits of major seed spices. International Journal of Seed Spices [Internet]. 2013;3(2):1–12. Available from: http://isss.ind.in/pdf/2013volume/1.pdf

32. Gould MN. Cancer chemoprevention and therapy by monoterpenes. Environmental Health Perspectives. 1997;105(SUPPL. 4):977–9.

JOTCS A
Journal of the Turkish Chemical Society
Section: A
Chemistry
TURKISH CHEMICAL SOCIETY

Salvadora persica Extract-laden Jellyfish Collagen Hybrid Constructs for Periodontal Tissue Regeneration

Yavuz Emre Arslan* **and Ilkim Kantarcioglu**

Regenerative Biomaterials Laboratory, Department of Bioengineering, Engineering Faculty, Canakkale Onsekiz Mart University, Canakkale 17100, Turkey

Abstract: Considerable effort in the field of periodontal tissue engineering has been expended in the construction of advanced biomatrix for the treatment of periodontal diseases caused by poor oral hygiene, malnutrition, genetic factors, and systemic disorders. With these in mind, the ultimate goal of this investigation is to fabricate sophisticated scaffolds using jellyfish collagen (JC) and aqueous *Salvadora persica* (Miswak) extracts. *Rhizostoma pulmo* species JC was isolated and characterized in depth. Miswak was extracted using two different methods. The extraction yield was calculated to be 14.2 ± 0.9% and 17.1 ± 0.4% for Methods I and II, respectively. Gas chromatography-mass spectroscopy (GC-MS) results revealed the extract to be composed of 1,8-cineole (49.3%), benzyl nitrile (36.2%), benzyl isothiocyanate (5.9%), limonene (2.4%), eugenol (0.8%), and palmitic acid (0.3%). Total phenolic content and antioxidant capacities of the extracts were also determined by spectrophotometric means. Human periodontal ligament fibroblast cells were isolated and expanded. Cell viability on JC and miswak extract-laden JC scaffolds was determined by 3-(4,5-dimethylthiazol-2-yl)-2,5-diphenyltetrazolium Bromide (MTT) assay. Microarchitectures of the JC, 0.05 and 0.1% miswak extract-laden JC scaffolds and also cellular behaviors on these surfaces were evaluated by scanning electron microscopy (SEM) analysis. This study suggests that miswak extract-laden JC scaffolds would present new opportunities for periodontal tissue engineering.

Keywords: *Salvadora persica*, Miswak, Jellyfish collagen, Human periodontal ligament fibroblasts, Periodontal tissue engineering, Translational medicine

Submitted: November 19, 2018. **Accepted:** January 22, 2019 .

Cite this: Arslan Y, Kantarcioglu I. Salvadora persica Extract-laden Jellyfish Collagen Hybrid Constructs for Periodontal Tissue Regeneration. JOTCSA. 2019;6(1):51–62.

DOI: https://dx.doi.org/10.18596/jotcsa.484936.

***Corresponding author: E-mail:** yavuzea@gmail.com. Tel.: +90-286-218-0018; Fax: +90-286-218-0541.

INTRODUCTION

Periodontal ligament fibroblast (PDLF) cells, embryologically-derived from the ectomesenchymal tissue of the dental follicle and embedded in the periodontal tissue, are a connective tissue element with spindle-shaped fibroblastic morphology (1,2). The periodontal tissue is a complex structure, which consists of gingiva, periodontal ligament (PDL), cementum and the alveolar bone (3). When the microbial equilibrium shifts in favor of pathogens due to deteriorating oral hygiene, also referred to as the periodontitis, a common chronic inflammatory gingival disease, causes loss of tooth-supporting constituents (e.g., PDL, alveolar bone) (3,4). In the pathogenesis of the periodontitis, there are gingival inflammation, gingival pocket formation, periodontal ligament destruction and finally alveolar bone resorption. With the progression of the disease, loss of tooth may also occur. Interestingly, recent studies have demonstrated that periodontitis is related to many systemic diseases such as *diabetes mellitus*, cardiovascular diseases, and rheumatoid arthritis (5,6).

Current treatment approaches for maintenance or regeneration of damaged tooth-supporting constituents caused by periodontal diseases aim at fabricating novel

bioengineered scaffolds by taking advantage of translational medicine & tissue engineering concepts which employ the knowledge of cells, materials, soluble factors, and so on for their use in clinical arena (7,8). Different synthetic or naturally-derived biopolymers and/or their composites with biominerals have evolved since last decades in periodontal tissue engineering applications (9–11).

Collagen is a structural extracellular matrix protein and can easily be extracted from many tissue types (e.g., skin, tendon). It has unique properties such as self-assembling into fibrillar structures under physiological conditions, high level biocompatible and biodegradability, mechanical and homeostatic qualities, which make it a significant candidate in regenerative medicine applications (12–14). However, there are limitations in the use of mammalian-derived collagen in clinical purposes because they tend to carry some risks such as bovine spongiform encephalopathy and foot-and-mouth disease. In addition, collagen from porcine skin or tendon is not preferred by the patients due to religious concerns (15,16). Thus, marine-derived collagen is considered to be an alternative and probably a safer source in the construction of bioengineered scaffolds compared to mammals. In the current literature, jellyfish-derived collagen has been used as a hybrid construct for chondrogenesis of human mesenchymal stem cells (hMSCs) (15,17), a composite scaffold for osteogenic differentiation of human adipose-derived MSCs (18) and an aptasensor substrate for detection of blood thrombin levels in different neurological diseases (19). Furthermore, it has been reported that jellyfish-derived collagen has the potential to activate bone marrow-derived dendritic cells, which also proves its immunoregulatory function (20).

Medicinal plants, which are almost as old as human history, have been used in various civilizations of the world for thousands of years to treat many health problems (21–23). Miswak, also recommended by the World Health Organization as an oral hygiene tool for mechanically removing plaque and food residues from the teeth, has great potential due to its substantial components such as minerals (e.g., sulfur, chlorides, fluorides, silica) and phytochemicals (e.g., tannins, benzyl isothiocyanate) which are related to dental care (24,25). Although aqueous, alcoholic, or nonpolar extracts of miswak contain various antimicrobial agents, it was reported that the aqueous extract had shown better antimicrobial activity compared to other solvents (26).

In this work, 3-dimensional (3D) hybrid constructs were fabricated using marine-derived collagen and miswak extracts for periodontal tissue engineering applications. Aqueous extracts from miswak sticks were prepared using two different methods to evaluate the extraction yield. The bioactive constituents in the miswak extracts were then analyzed by GC-MS. Total phenolic contents and antioxidant activities were also determined spectrophotometrically. Jellyfish collagen was isolated and well-characterized using different analysis methods (e.g., SDS-PAGE, GC-MS, Lowry assay, TGA and ATR-FTIR). Human periodontal ligament fibroblast cells were isolated, expanded and seeded on jellyfish collagen and miswak extract-laden jellyfish collagen scaffolds. MTT assay was applied to determine the number of viable cells on prepared scaffolds. Finally, the scaffold and cell/scaffold constructs were observed by scanning electron microscopy to evaluate the micro-architecture and cellular behaviors on these surfaces.

MATERIALS AND METHODS

Materials

S. persica sticks (origin of Pakistan) were purchased from a local seller of medicinal herbs in vacuum bags in the wet form. *Rhizostoma pulmo* species jellyfishes were collected from the coast of Dardanelles (Abydus), Çanakkale, Turkey. All chemicals were provided from Merck (Millipore-Sigma, Germany) unless otherwise noted.

Preparation of miswak extracts

The extraction process was carried out according to the procedure described by Abhary and Al-Hazmi (26), with slight modifications. Briefly, the outer layer of miswak sticks was carefully removed, and the sticks were cut into small pieces, then dried in an incubator (Memmert UN55, Germany) at 40 °C for three days. The dried miswak pieces were milled (IKA M20, Germany) to obtain a fine powder. Two different methods were applied in order to obtain aqueous extracts of miswak. The dried miswak powder was suspended in Milli-Q water (Merck-Millipore, Germany) at a ratio of 5 % (w/v), and the suspension was vigorously stirred at room temperature (RT) for three days (described as Method I). Similarly, the suspension (5 %, w/v in Milli-Q water) was infused in a rotary-evaporator (Buchi, Rotavapor R210, Switzerland) at 80 °C for 1 h (described as Method II). The solutions were then centrifuged at 6000 rpm for 15 minutes, and the resulting supernatants were filtered through Whatman No. 43 filter paper (Macherey-Nagel, Germany) under reduced pressure. The solutions were then concentrated using Rotary-evaporator and the miswak extracts were frozen at -26 °C, then freeze-dried (LyoQuest, Telstar, Spain) for overnight to obtain water-soluble miswak extracts. The lyophilized extracts were kept at -26 °C until the time of analysis. The

extraction yields were calculated using the equation given below. Step-by-step procedure of miswak extraction can be seen in Figure 1.

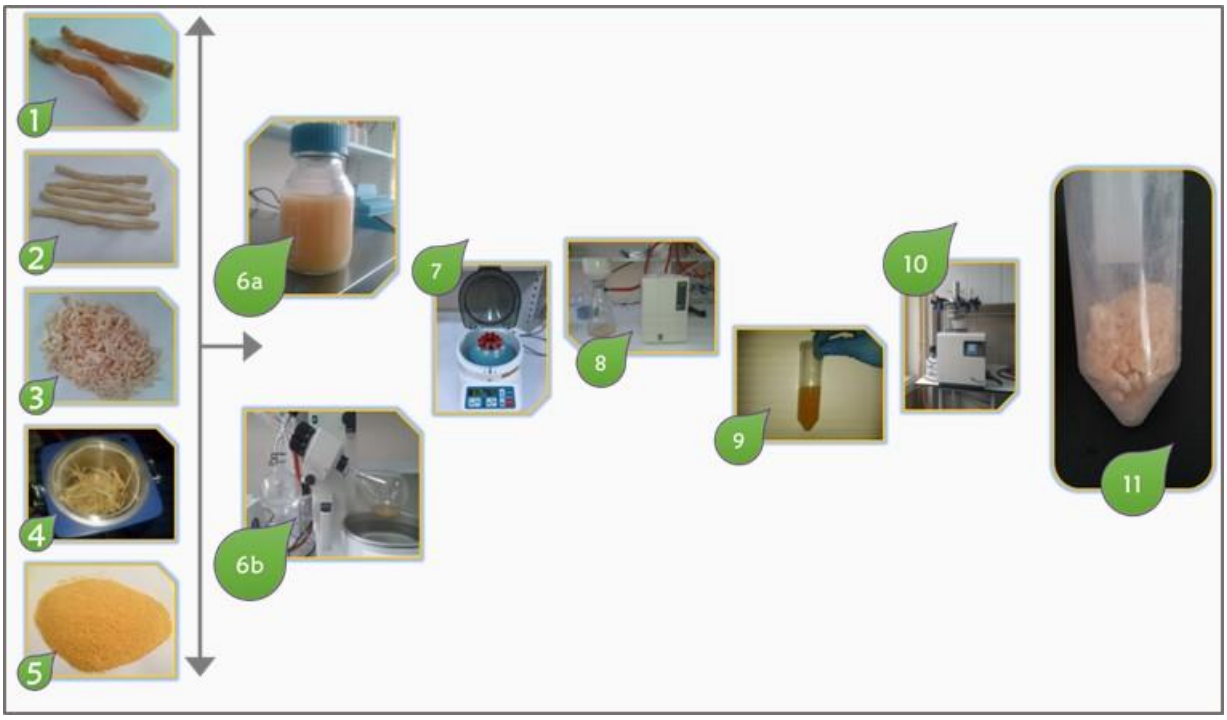

Figure 1. Step-by-step representation of the extraction process of Salvadora persica (Miswak). Raw miswak sticks (1), removing of outer layer (2), cutting (3), milling (4), obtaining fine powders (5), Method I (6a), Method II (6b), centrifugation (7), filtration (8), concentrated sticky miswak solution (9), lyophilization (10) and obtaining dry form of miswak extracts (11).

Yield (%) = [(initial weight (dry) – lyophilized weight) / initial weight (dry)] x 100 ***(1).***

Gas Chromatography-Mass spectroscopy analysis of extracts

In order to identify the chemical composition of miswak extracts, the GC-MS analysis was conducted according to our previous study (21). Initially, lyophilized miswak extracts were dissolved in Milli-Q water and filtered through a 0.22 µm sterile filter. Then, the extracts were loaded an instrument (Thermo MS Finnigan Trace DSQ, USA), with a DB-WAX column (30 m x 0.25 mm i.d.; film thickness 0.25 µm). The oven temperature was adjusted as described as follows: 50 °C for 1 minute, followed by an increase rate of 3 °C / minute up to 220 °C. Helium as a carrier gas was set to flow at a rate of 1 mL/minute. All data were evaluated using the Xcalibur software.

Total phenolic content analysis of extracts

The total phenolics of each extract were colorimetrically assessed according to the Folin-Ciocalteu method reported in the literature by Singleton and Rossi (27). In short, each extract (10 mg) was dissolved in 1 mL of Milli-Q water at RT. Then, 900 µL of Milli-Q water, 5 mL of Folin reagent (0.2 N) and 4 mL of sodium carbonate solution (7.5 %, w/v) were added into each 100 µL of sample. The samples were left to stand in the dark at RT for 2 hours for color development and the absorbance at 765 nm was measured against blank solution (Shimadzu UV-mini 1240, Japan). The results were presented as mg of gallic acid equivalent (GAE) per g of dry weight.

CUPRAC assay for antioxidant capacity of extracts

The antioxidant capacity levels of each extract were ascertained using the method described by Apak et al. (28). Following their work, 20 µL of each sample was mixed with 1 mL of $CuCl_2.2H_2O$ (0.01 M, prepared in Milli-Q water), 1 mL of neocuproine ($7.5x10^{-3}$ M, prepared in ethanol), 1 mL of ammonium acetate solution (1 M in Tris-buffer, pH = 7.0) and 1.08 mL of Milli-Q water, each solution was allowed to rest at RT for 30 minutes in the dark. The absorbance was measured at 450 nm against the blank solution and the antioxidant capacity of extracts was expressed in terms of mg Trolox per liter.

Isolation and characterization of marine-derived collagen from R. pulmo

Jellyfish collagen (JC) was isolated from *R. pulmo* and characterized well according to the studies previously published by our group (18,19). Briefly, jellyfish was cut into medium-sized pieces after being caught and transferred to our laboratory. Jellyfish pieces were then

immersed into 99.9 % ethyl alcohol and treated with 0.1 M NaOH for 24 hours in order to dehydrate and remove any non-collagen substances, respectively. Before being digested with pepsin (600–1200 U/mg) for three days, jellyfish pieces were blended (IKA T18 Basic, Germany) in 0.5 M acetic acid (1-gram sheet per 100 mL solution). Following, the viscous solution was centrifuged at 10000 g for 1 minute and dialyzed against 0.02 M dibasic sodium phosphate (pH 8.8) for three days for the purpose of inactivating the enzyme. The pepsin-soluble JC was frozen at -86 °C and freeze-dried overnight. The lyophilized form of the JC was stored at -86 °C until use in the experiments. In order to characterize pepsin-soluble JC, various experiments were carried out such as modified Lowry assay (for determining the protein concentration and purity), SDS-poly acrylamide gel electrophoresis (SDS-PAGE) (for determining the protein size, distribution, etc.), thermogravimetric analysis (TGA) (for determining the thermal properties), ATR-FTIR, contact angle measurement, amino acid composition analysis using GC-MS and also hydroxyproline content analysis (for both raw and pepsin-soluble JC). The results related to the analyses have been pointed out in the papers mentioned above.

Fabrication of hybrid constructs from JC and miswak extracts

To produce hybrid constructs from JC and miswak extracts, JC was first dissolved in Milli-Q water at a ratio of 3 % (w/v). Then, the solution was poured into a 48-well plate, frozen immediately at -86 °C and then freeze-dried overnight (18). In order to enhance the mechanical properties of prepared scaffolds, cross-linking process was conducted using N-hydroxysuccinimide (NHS) / N-(3-dimethylaminopropyl)-N'-ethylcarbodiimide hydrochloride (EDC) prepared in 2-(N-morpholino)ethanesulfonic acid (MES) buffer (pH 5.5) according to the method described by Buttafoco et al. (29), with slight modifications. In short, MES buffer was mixed with 99% ethanol at a ratio of 1:9 (v/v) and cross-linkers were dissolved in this solution. The scaffolds were then immersed in ethanol (≥ 99 %) for 10 minutes and cross-linked for 8 hours at room temperature with gentle agitation (Incu-Shaker Mini, Benchmark Scientific, USA). The scaffolds were then thoroughly rinsed with Milli-Q water to eliminate excess cross-linker and freeze-dried overnight. The dimensions of the cross-linked scaffolds were measured to be h = 3 mm and Ø = 6 mm. Following this, lyophilized miswak extract was separately dissolved in Milli-Q water at ratios of 0.05 and 0.1 % (w/v), 200 µL of each extract solution was loaded into cross-linked scaffolds. Finally, the miswak extract-laden JC hybrid constructs were frozen at -86 °C and lyophilized overnight.

Swelling test

Liquid handling capacities of the JC and miswak extract-laden JC scaffolds were determined by inserting the scaffolds in 30 mL of phosphate-buffer saline (PBS) solution (pH = 7.4) at 37 °C for 10 minutes. Initially, all of the dry scaffolds were weighed (W_o) before being immersed in PBS. After 10 minutes, the scaffolds were removed, gently wiped for any adsorbed buffer and weighed again (W_s). The swelling ratio of scaffolds was calculated using the equation given below. Three independent measurements were carried out for the test (30).

$$\text{Swelling ratio (\%)} = [(W_s - W_o) / W_o] \times 100 \quad \textbf{\textit{(2).}}$$

Isolation and expansion of human periodontal ligament fibroblast cells

Human periodontal ligament fibroblast (hPDLF) cells were isolated from root surfaces of healthy premolars as described previously by Inanc et al. (9), with slight modifications. The experimental design was reviewed and approved by Clinical Research Ethics Committee, Faculty of Medicine, Çanakkale Onsekiz Mart University (permission number: 2016-02-04). Informed written consent was also obtained from each donor. Immediately after extraction, teeth were washed repeatedly (5 – 8 times) using sterile PBS (pH = 7.4) containing 5% penicillin-streptomycin in order to eliminate debris and blood located on dental surfaces. The periodontal layers were then scraped off gently middle third of the teeth roots and minced using a sterile surgical blade. Minced tissues were enzymatically digested in 0.1 % collagenase (Type I, 0.25 - 1.0 FALGPA units/mg solid) for 45 minutes in a CO_2 incubator (Panasonic, Japan), and the cell suspension was centrifuged (Hettich, Germany) at 300 g for 5 minutes. The pellet was then re-suspended in a culture medium consisting of DMEM (Dulbecco's modified Eagle's medium) supplemented with 10% fetal bovine serum (FBS), 1% penicillin-streptomycin, 1% non-essential amino acid stock solution, and %1 L-glutamine (all from Biological Industries, USA), transferred to 6-well plates and propagated at 37 °C, 5% CO_2 and 95% relative humidity conditions. The cells were passed when reaching 80-90% confluency. The spindle-shape fibroblastic morphology of hPDLF cells was observed by an inverted-phase contrast microscope (PrimoVert, Zeiss, Germany). Cells in the passages between 2 – 5 were used in the experiments.

Cell seeding on JC and miswak extract-laden JC scaffolds

JC and miswak extract-laden JC scaffolds were sterilized under UV (254 nm) exposure for 2 hours in a laminar air flow cabinet (Bio II Advance, Telstar, Spain). hPDLF cells were then seeded at a density of 2.4 x 10^5 cells/scaffolds and growth in DMEM high glucose supplemented with 10% fetal bovine serum (FBS), 1% penicillin-streptomycin, 1% nonessential amino acid stock solution, and 1% L-glutamine by replenishing the growth medium every 2 – 3 days. The culture was maintained under standard culture conditions (at 37 °C, 5% CO_2 and 95% relative humidity) for 3, 7 and 14 days. Cell proliferation was quantified using MTT assay kit (Cell Growth Determination Kit, MTT based, CGD1, Merck) by following manufacturer's instructions at a wavelength of 570 nm on days 3, 7 and 14.

Scanning electron microscopy

The surface morphology of fabricated JC and miswak extract-laden JC scaffolds and cellular behaviors on these surfaces were observed by field-emission scanning electron microscopy (FE-SEM JFM 7100F EDS, JEOL, Japan). After being fixed with 2.5% glutaraldehyde (prepared in PBS) for at least 24 hours, the specimens were rinsed repeatedly with PBS (pH 7.2 – 7.4) and immersed in an ethanol series (50, 70, 80, 90, 95, and 100 %) for dehydration. Samples dried at RT were then sputter-coated with Pd-Au for 90 seconds so as to improve the electron conductivity in order to achieve better SEM micrographs. Images were taken at 10 kV and different magnification levels in a high vacuum.

Statistical analysis

One-way analysis of variance (ANOVA) by followed Tukey tests were performed using Origin Pro8SR0 (v8.0724, Origin Lab Corporation, MA, USA) software to evaluate the results. Only variables with a confidence level higher than 95 % ($p \leq 0.05$) were considered to be statistically significant. The mean ± standard deviation of variables was also calculated with Microsoft Office Professional Plus 2016 Excel. The results presented in this study are the average of at least three independent measurements.

RESULTS AND DISCUSSION

The performance of the extraction processes

The techniques and also solvents used in the extraction process could affect the quantity and composition of bioactive compounds of miswak extract. According to the results, the extraction yields were found to be 14.2 ± 0.9 % and 17.1 ± 0.4 % for the Method I and II, respectively. In other studies related to the miswak extraction, various solvents or their mixtures were studied to achieve maximum crude extract. To this end, Mohamed and Khan (31) have tested 80% methanol, 80% ethanol, 80% acetone and water to determine the effects of such solvents on extraction yield of dried miswak (origin of Saudi Arabia). They have reported that highest yield was obtained when using 80% methanol (1.02 ± 0.05 %, w/w) compared to water (0.56 ± 0.01 %, w/w). Interestingly, another study found that the yield of methanolic extract of *Salvadora persica* L. (origin of South of Algeria) was 45% (32).

Evaluating the GC-MS results

The biologically active constituents of aqueous miswak extract (Method II) were assessed with GC-MS. Six major compounds representing 95.1% of the aqueous miswak extract were detected. The main compound was found to be 1,8-cineole (49.3%) in addition to benzyl nitrile (36.2%), benzyl isothiocyanate (5.9%), limonene (2.4%), eugenol (0.8%) and palmitic acid (0.3%) (Figure 2A). These findings correspond with the results reported by Noumi et al. (33) and Naeini et al. (34). Among these compounds, benzyl nitrile and benzyl isothiocyanate have a significant role in the antibacterial repertoire of miswak extract (35). On the other hand, the differences in the yields (%) and chemical composition might be related to geological conditions, the season of the plant collection and in particular climate (36).

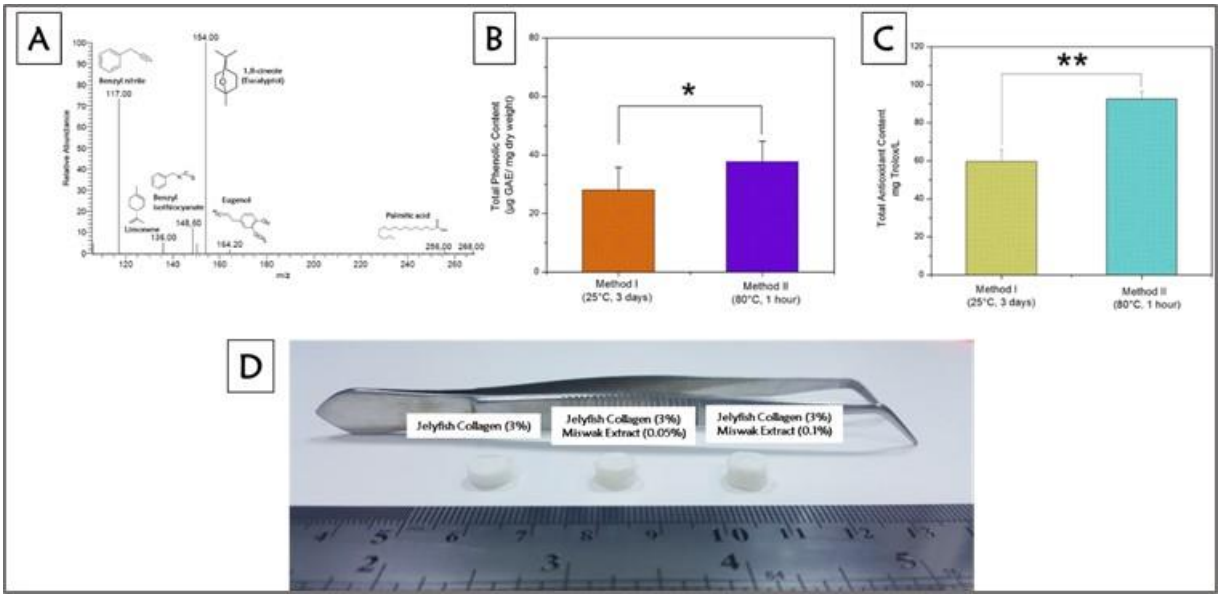

Figure 2. GC-MS analysis (A), total phenolic content (B), total antioxidant activity (C) and macroscopic images of the fabricated scaffolds (D).

Total Extractable phenolics

The total extractable phenolics of *Salvadora persica* were evaluated through total phenolic content (TPC) analysis. TPC of *Salvadora persica* was found to be 28.79 ± 7.79 and 37.7 ± 4.0 µg GAE/mg dry weight for Method I and II, respectively. No significant difference (* $p > 0.05$, $n = 3$) was found when evaluating the data concerning Methods I and II statistically (Figure 2B). According to the study reported by Chelli-Chentouf et al. (32), the TPC of Hoggar *Salvadora persica* was 70 µg GAE/mg dried weight. Similarly, a study by Taha et al. (37) ascertained that TPC of *Salvadora persica* was calculated as 52.6 µg GAE/mg dried weight.

The Trolox equivalent antioxidant capacity of extract

Oxidative stress stimulated by free radicals might cause many problems in the human body. Antioxidant intake is thus crucial to protect the body from free radicals. Cupric reducing antioxidant capacity (CUPRAC) method was performed to determine the antioxidant levels of aqueous miswak extracts in terms of mg Trolox/L. The study revealed that the antioxidant activity of the aqueous extract was found to be 59.17 ± 6.23 and 92.5 ± 4.09 mg Trolox/L for Method I and II, respectively (Figure 2C). This difference is probably due to the high temperature applied in Method II (** $p < 0.05$, $n = 3$). The antioxidant activities of the miswak species have been determined by applying different methods such as DPPH and ABTS in the literature (31,33). The present study reports the antioxidant activity levels of *Salvadora persica* extracts in terms of mg Trolox/L for the first time in the literature. When comparing the results with another study published by our group (21), we concluded that a sufficient antioxidant capacity was achieved in Method II.

Construction of bioengineered scaffolds

The results related to the isolation and characterization of JC were discussed in depth in the studies previously published by our group (18,19). Structural integrity is one of the main challenges to be overcome when using jellyfish-derived atelocollagen to fabricate novel bioengineered scaffolds which have a proper pore size, mechanical stability, and so on. To address this challenge, MES buffer containing at least 80-90 % ethanol (15) or acetone (38) (v/v) is essential for successful cross-linking of such scaffolds. On the other hand, when aqueous miswak extracts were loaded into cross-linked JC scaffolds at ratios of 0.05 and 0.1 %, the morphology of miswak extract-laden JC scaffolds slightly shrunk depending on the loaded extract ratio (Figure 2D). It has been a well-known issue that swelling ratio decreases as the degree of cross-linking increases (39). So as to enlighten the effect of the cross-linking process on interconnected pores in the scaffolds, swelling rates (%) of JC and miswak extract-laden JC scaffolds were investigated. The swelling ratio of JC scaffold was found to be 3291.23 ± 309.74%, whereas 0.05 and 0.1% miswak extract-laden JC scaffolds were 2836.75 ± 341.31% and 2822.52 ± 376.16%, respectively. According to results presented by Tronci et al. (40), the highest swelling ratio of collagen type I-based scaffold (derived from rat tail) was found as 1996 ± 182%. Our findings indicate that JC-based scaffolds have shown remarkable swelling properties when comparing to mammalian-derived alternatives. Lastly, the changes in the morphology and swelling ratio might have arisen from the sticky organic compounds

(such as terpenes) in the miswak extract (34,41).

In vitro study

Periodontal layers of healthy premolars were scraped and digested with collagenase type I to isolate the primary hPDLF cells (Figure 3A – C). The isolated cells were then expanded at standard culture conditions. While hPDLF cells in the culture environment showed spindle or stellate-shaped morphology at early passages, the appearances of the most cells changed to a spindle-shaped fibroblastic morphology (42,43) and organized in a swirl pattern (44). The microscopic images of isolated hPDLF cells are seen in Figure 3D. The cells were seeded onto JC and miswak extract-laden JC scaffolds, and the cell viability was determined by MTT assay on the 3rd, 7th and 14th days. Figure 4 reveals the fabricated scaffolds to have no cytotoxic effects on hPDLF cells. Although cell attachment was observed both JC and miswak extract-laden JC scaffolds, it was seen that the cell viability on miswak extract-laden JC scaffolds, unexpectedly, remained slightly low compared to JC scaffold (* $p < 0.05$, $n = 3$). Furthermore, there was no remarkable change in cell viability on 0.05 and 0.1% miswak extract-laden JC scaffolds (** $p > 0.05$, $n = 3$) depending on time points. We believe that the pore size of the miswak extract-laden JC scaffolds has affected cell proliferation (45).

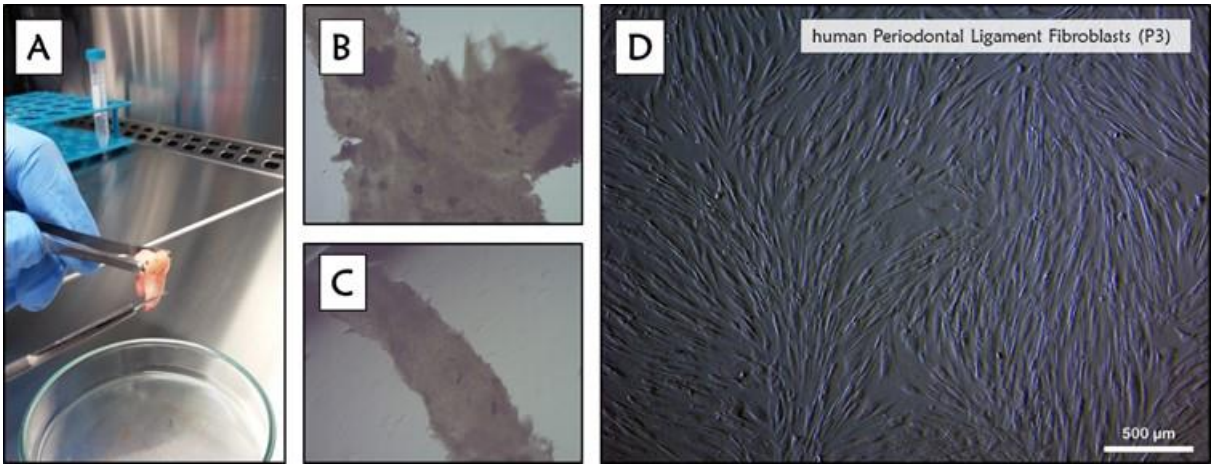

Figure 3. Healthy premolar (A), scraped periodontal layers (B, C) and human periodontal ligament fibroblast cells at Passage 3 (D). Scale bar: 500 µm.

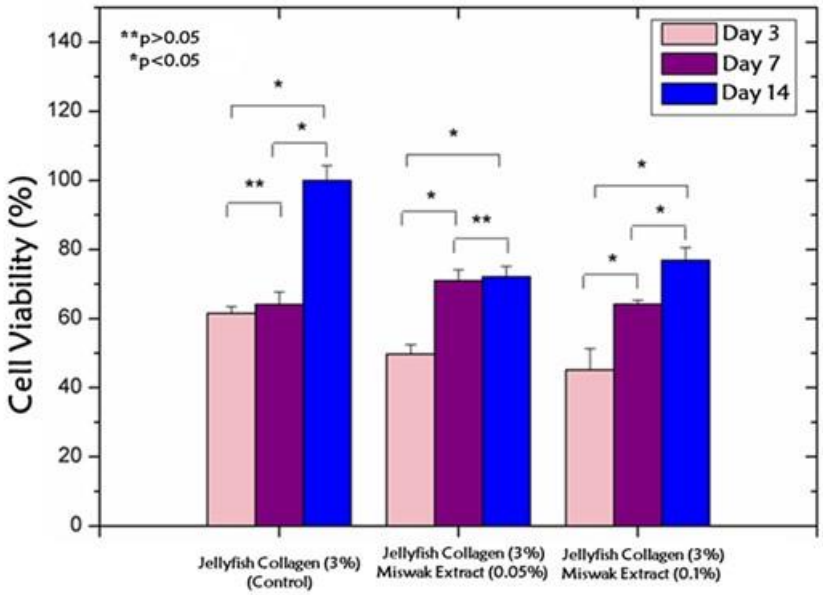

Figure 4. Cell viability assay (MTT-based) for jellyfish collagen (3%), 0.05% and 0.1% miswak extract-laden jellyfish collagen (3%) scaffolds on days 3, 7 and 14.

Morphology of scaffolds and cell adhesion

The pore size distributions, 3D interconnections between pores, surface roughness, and so on are the fundamental parameters to be considered in the construction of useful scaffolds for tissue engineering and regenerative medicine. The macroporosity of JC, 0.05 and 0.1 % miswak extract-laden JC scaffolds were measured in the range of 70 – 100 µm, 30 – 60 µm, and 20 – 50 µm, respectively (Figure 5). The results are also consistent with swelling test measurements. As can be seen in Figure 5, although JC scaffolds are highly porous, the

pore size of miswak extract-laden JC scaffolds slightly shrunk depending on the increase in miswak ratio loaded into scaffolds. On the other hand, SEM micrographs revealed hPDLF cells to spread and cover the surfaces of prepared scaffolds on days 3, 7 and 14 to the extent allowed by pore size. These findings are also in close agreement with the MTT results.

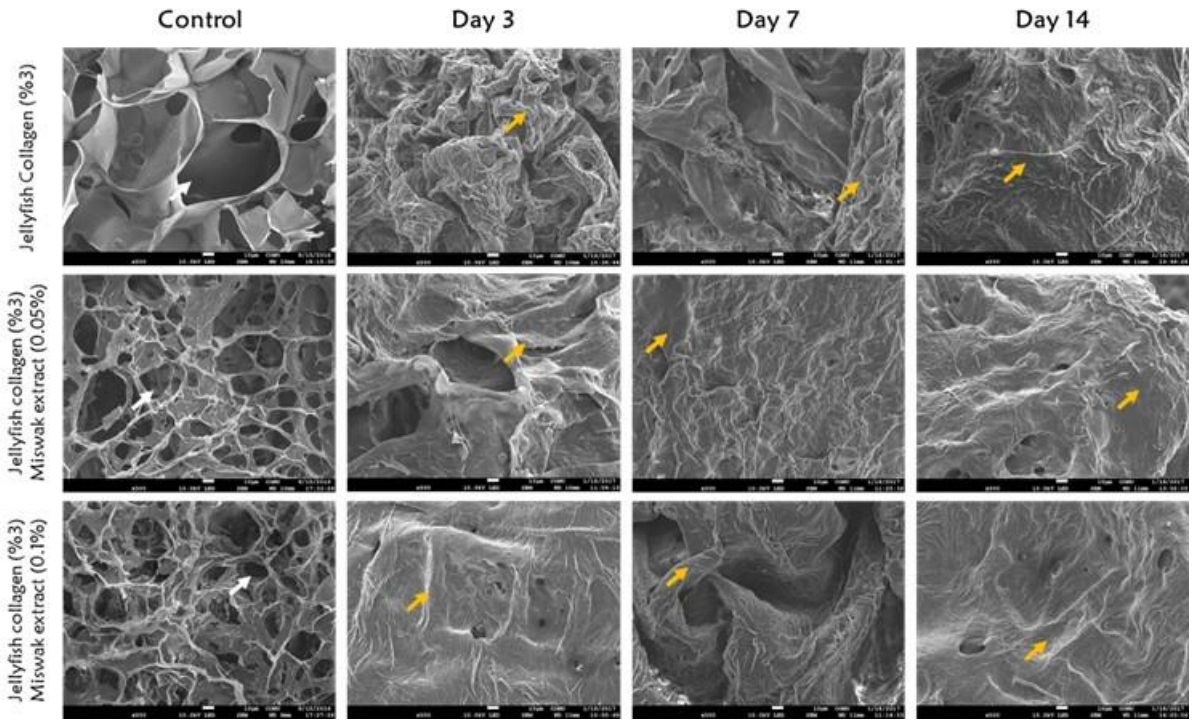

Figure 5. Scanning electron microscopy micrographs (500x) demonstrate the microarchitecture (white arrows) of the prepared scaffolds and hPDLF cell proliferation (yellow arrows) on these surfaces on days 3, 7 and 14. Scale bars: 10 μm.

CONCLUSION

Understanding the role of bioactive molecules derived from medicinal plants in cellular behaviors is substantial with regard to transferring this knowledge to translational medicine concept. Among many medicinal plants, *Salvadora persica* has the remarkable potential in maintaining and regulating the oral health due to the presence of some unique constituents. To that aim, we fabricated hybrid bioengineered scaffolds using jellyfish collagen and miswak extract. We then sought to evaluate the cellular behaviors of hPDLF such as attachment, growth, and proliferation in both JC and miswak extract-laden JC scaffolds. Miswak extract-laden JC scaffolds supported to cell attachment, but could not affect sufficient cell proliferation and growth compared to JC scaffolds. These results demonstrate that miswak extract has a significant influence on the pore size distribution of JC-based scaffolds. On the other hand, the antimicrobial effects of miswak extracts have been intensely studied in the literature, but there are no studies regarding the use of miswak extracts in periodontal tissue engineering applications. As a result, we believe that miswak extract-laden JC scaffolds could be a notable candidate for periodontal tissue regeneration in the future.

ACKNOWLEDGMENTS

The research reported here was financially supported by Çanakkale Onsekiz Mart University, Scientific Research Projects Coordination Unit (Project ID. FYL-2016-632). The authors wish to thank Çanakkale Onsekiz Mart University, Science and Technology Application & Research Center for analyses.

REFERENCES

1. Inanç B, Arslan YE, Seker S, Elçin AE, Elçin YM. Periodontal ligament cellular structures engineered with electrospun poly(DL-lactide-co -glycolide) nanofibrous membrane scaffolds. J Biomed Mater Res Part A. 2009 Jun;90A(1):186–95. Available from: http://doi.wiley.com/10.1002/jbm.a.32066

2. Sokos D, Everts V, de Vries TJ. Role of periodontal ligament fibroblasts in osteoclastogenesis: a review. J Periodontal Res. 2015 Apr;50(2):152–9. Available from: http://doi.wiley.com/10.1111/jre.12197

3. Kim JH, Park CH, Perez RA, Lee HY, Jang JH, Lee HH, et al. Advanced Biomatrix Designs for Regenerative Therapy of Periodontal Tissues. J Dent Res. 2014 Dec 19;93(12):1203–11. Available from:

http://journals.sagepub.com/doi/10.1177/0022034514540682

4. Özdoğan AI, İlarslan YD, Kösemehmetoğlu K, Akca G, Kutlu HB, Comerdov E, et al. In vivo evaluation of chitosan based local delivery systems for atorvastatin in treatment of periodontitis. Int J Pharm. 2018 Oct;550:470–6. Available from: https://linkinghub.elsevier.com/retrieve/pii/S0378517318306446

5. Hajishengallis G. Immunomicrobial pathogenesis of periodontitis: keystones, pathobionts, and host response. Trends Immunol. 2014 Jan;35(1):3–11. Available from: http://dx.doi.org/10.1016/j.it.2013.09.001

6. Han J, Menicanin D, Gronthos S, Bartold P. Stem cells, tissue engineering and periodontal regeneration. Aust Dent J. 2014 Jun;59(SUPPL. 1):117–30. Available from: http://doi.wiley.com/10.1111/adj.12100

7. Chahal S, Hussain FSJ, Kumar A, Rasad MSBA, Yusoff MM. Fabrication, characterization and in vitro biocompatibility of electrospun hydroxyethyl cellulose/poly (vinyl) alcohol nanofibrous composite biomaterial for bone tissue engineering. Chem Eng Sci. 2016 Apr;144:17–29. Available from: http://dx.doi.org/10.1016/j.ces.2015.12.030

8. Chen F-M, Zhao Y-M, Jin Y, Shi S. Prospects for translational regenerative medicine. Biotechnol Adv. 2012 May;30(3):658–72. Available from: http://dx.doi.org/10.1016/j.biotechadv.2011.11.005

9. Inanc B, Elcin AE, Elcin YM. Osteogenic Induction of Human Periodontal Ligament Fibroblasts Under Two- and Three-Dimensional Culture Conditions. Tissue Eng. 2006 Feb;12(2):257–66. Available from: https://www.liebertpub.com/doi/10.1089/ten.2006.12.257

10. Qasim SB, Delaine-Smith RM, Fey T, Rawlinson A, Rehman IU. Freeze gelated porous membranes for periodontal tissue regeneration. Acta Biomater. 2015 Sep;23:317–28. Available from: http://dx.doi.org/10.1016/j.actbio.2015.05.001

11. Wu C, Zhou Y, Lin C, Chang J, Xiao Y. Strontium-containing mesoporous bioactive glass scaffolds with improved osteogenic/cementogenic differentiation of periodontal ligament cells for periodontal tissue engineering. Acta Biomater. 2012 Oct;8(10):3805–15. Available from: http://dx.doi.org/10.1016/j.actbio.2012.06.023

12. Hatayama T, Nakada A, Nakamura H, Mariko W, Tsujimoto G, Nakamura T. Regeneration of gingival tissue using in situ tissue engineering with collagen scaffold. Oral Surg Oral Med Oral Pathol Oral Radiol. 2017 Oct;124(4):348–54. Available from: https://doi.org/10.1016/j.oooo.2017.05.471

13. Kuttappan S, Mathew D, Nair MB. Biomimetic composite scaffolds containing bioceramics and collagen/gelatin for bone tissue engineering - A mini review. Int J Biol Macromol. 2016 Dec;93:1390–401. Available from: http://dx.doi.org/10.1016/j.ijbiomac.2016.06.043

14. Montalbano G, Toumpaniari S, Popov A, Duan P, Chen J, Dalgarno K, et al. Synthesis of bioinspired collagen/alginate/fibrin based hydrogels for soft tissue engineering. Mater Sci Eng C. 2018 Oct;91:236–46. Available from: https://doi.org/10.1016/j.msec.2018.04.101

15. Hoyer B, Bernhardt A, Lode A, Heinemann S, Sewing J, Klinger M, et al. Jellyfish collagen scaffolds for cartilage tissue engineering. Acta Biomater. 2014 Feb;10(2):883–92. Available from: https://linkinghub.elsevier.com/retrieve/pii/S1742706113005394

16. Jongjareonrak A, Benjakul S, Visessanguan W, Nagai T, Tanaka M. Isolation and characterisation of acid and pepsin-solubilised collagens from the skin of Brownstripe red snapper (Lutjanus vitta). Food Chem. 2005 Dec;93(3):475–84. Available from: http://linkinghub.elsevier.com/retrieve/pii/S0308814604007666

17. Pustlauk W, Paul B, Gelinsky M, Bernhardt A. Jellyfish collagen and alginate: Combined marine materials for superior chondrogenesis of hMSC. Mater Sci Eng C. 2016 Jul;64:190–8. Available from: http://dx.doi.org/10.1016/j.msec.2016.03.081

18. Arslan YE, Sezgin Arslan T, Derkus B, Emregul E, Emregul KC. Fabrication of human hair keratin/jellyfish collagen/eggshell-derived hydroxyapatite osteoinductive biocomposite scaffolds for bone tissue engineering: From waste to regenerative medicine products. Colloids Surfaces B Biointerfaces. 2017 Jun;154:160–70. Available from: http://linkinghub.elsevier.com/retrieve/pii/S0927776517301522

19. Derkus B, Arslan YE, Bayrac AT, Kantarcioglu I, Emregul KC, Emregul E. Development of a novel aptasensor using

jellyfish collagen as matrix and thrombin detection in blood samples obtained from patients with various neurodisease. Sensors Actuators B Chem. 2016 Jun;228:725–36. Available from: https://linkinghub.elsevier.com/retrieve/pii/S0925400516300958

20. Putra ABN, Nishi K, Shiraishi R, Doi M, Sugahara T. Jellyfish collagen stimulates maturation of mouse bone marrow-derived dendritic cells. J Funct Foods. 2015 Apr;14:308–17. Available from: http://dx.doi.org/10.1016/j.jff.2015.02.008

21. Efe B, Galata YF, Arslan YE. Assessment of the Cytotoxicity of Melia azedarach L. Extracts on Human Adipose-derived Mesenchymal Stem Cells. Hacettepe J Biol Chem. 2018;46(1):121–8.

22. Khan H. Medicinal Plants in Light of History. J Evid Based Complementary Altern Med. 2014 Jul;19(3):216–9. Available from: http://journals.sagepub.com/doi/10.1177/2156587214533346

23. Petrovska B. Historical review of medicinal plants' usage. Pharmacogn Rev. 2012;6(11):1–5. Available from: http://www.phcogrev.com/text.asp?2012/6/11/1/95849

24. Farag MA, Fahmy S, Choucry MA, Wahdan MO, Elsebai MF. Metabolites profiling reveals for antimicrobial compositional differences and action mechanism in the toothbrushing stick "miswak" Salvadora persica. J Pharm Biomed Anal. 2017 Jan;133:32–40. Available from: http://dx.doi.org/10.1016/j.jpba.2016.11.018

25. Halawany HS. A review on miswak (Salvadora persica) and its effect on various aspects of oral health. Saudi Dent J. 2012 Apr;24(2):63–9. Available from: http://dx.doi.org/10.1016/j.sdentj.2011.12.004

26. Abhary M, Al-Hazmi A-A. Antibacterial activity of Miswak (Salvadora persica L.) extracts on oral hygiene. J Taibah Univ Sci. 2016 Oct 16;10(4):513–20. Available from: http://linkinghub.elsevier.com/retrieve/pii/S1658365515001661

27. Singleton VL, Rossi JA. Colorimetry of Total Phenolics with Acid Reagents. Am J Enol Vitic. 1965;16(3):144–58.

28. Apak R, Güçlü K, Özyürek M, Çelik SE. Mechanism of antioxidant capacity assays and the CUPRAC (cupric ion reducing antioxidant capacity) assay. Microchim Acta. 2008 Apr 21;160(4):413–9. Available from: http://link.springer.com/10.1007/s00604-007-0777-0

29. Buttafoco L, Kolkman NG, Engbers-Buijtenhuijs P, Poot AA, Dijkstra PJ, Vermes I, et al. Electrospinning of collagen and elastin for tissue engineering applications. Biomaterials. 2006 Feb;27(5):724–34. Available from: http://linkinghub.elsevier.com/retrieve/pii/S0142961205005910

30. Kaczmarek B, Sionkowska A, Stojkovska J. Scaffolds based on chitosan and collagen with glycosaminoglycans cross- linked by tannic acid. Polym Test. 2018 Jul;65:163–8. Available from: https://doi.org/10.1016/j.polymertesting.2017.11.026

31. Mohamed SA, Khan JA. Antioxidant capacity of chewing stick miswak Salvadora persica. BMC Complement Altern Med. 2013 Dec 21;13(40):1–6. Available from: BMC Complementary and Alternative Medicine

32. Chelli-Chentouf N, Tir Touil Meddah A, Mullié C, Aoues A, Meddah B. In vitro and in vivo antimicrobial activity of Algerian Hoggar Salvadora persica L. extracts against microbial strains from children's oral cavity. J Ethnopharmacol. 2012 Oct;144(1):57–66. Available from: http://linkinghub.elsevier.com/retrieve/pii/S0378874112005508

33. Noumi E, Snoussi M, Trabelsi N, Hajlaoui H, Ksouri R, Valentin E, et al. Antibacterial, anticandidal and antioxidant activities of Salvadora persica and Juglans regia L. extracts. J Med Plants Res. 2011 Jul 1;5(17):4138–46.

34. Naeini A, Jalayer Naderi N, Shokri H. Analysis and in vitro anti- Candida antifungal activity of Cuminum cyminum and Salvadora persica herbs extracts against pathogenic Candida strains. J Mycol Med. 2014 Mar;24(1):13–8. Available from: http://dx.doi.org/10.1016/j.mycmed.2013.09.006

35. Sofrata A, Santangelo EM, Azeem M, Borg-Karlson A-K, Gustafsson A, Pütsep K. Benzyl Isothiocyanate, a Major Component from the Roots of Salvadora Persica Is Highly Active against Gram-Negative Bacteria. Heimesaat MM, editor. PLoS One. 2011 Aug 1;6(8):e23045. Available from: https://dx.plos.org/10.1371/journal.pone.0023045

36. Daferera DJ, Ziogas BN, Polissiou MG. GC-MS Analysis of Essential Oils from Some Greek Aromatic Plants and Their Fungitoxicity on Penicillium digitatum. J Agric Food Chem.

2000 Jun;48(6):2576–81. Available from: http://pubs.acs.org/doi/abs/10.1021/jf990835x

37. Taha E, Mariod A, Abouelhawa S, El-Geddawy M, Sorour M, Matthäus B. Antioxidant activity of extracts from six different Sudanese plant materials. Eur J Lipid Sci Technol. 2010 Nov;112(11):1263–9. Available from: http://doi.wiley.com/10.1002/ejlt.201000326

38. Song E, Yeon Kim S, Chun T, Byun H-J, Lee YM. Collagen scaffolds derived from a marine source and their biocompatibility. Biomaterials. 2006 May;27(15):2951–61. Available from: http://linkinghub.elsevier.com/retrieve/pii/S0142961206000147

39. Rehakova M, Bakos D, Vizarova K, Soldan M, Jurickova M. Properties of collagen and hyaluronic acid composite materials and their modification by chemical crosslinking. J Biomed Mater Res. 1996 Mar;30(3):369–72. Available from: http://doi.wiley.com/10.1002/%28SICI%291097-4636%28199603%2930%3A3%3C369%3A%3AAID-JBM11%3E3.0.CO%3B2-F

40. Tronci G, Grant CA, Thomson NH, Russell SJ, Wood DJ. Multi-scale mechanical characterization of highly swollen photo-activated collagen hydrogels. J R Soc Interface. 2014 Nov 19;12(102):20141079. Available from: http://rsif.royalsocietypublishing.org/cgi/doi/10.1098/rsif.2014.1079

41. Tabatabaei F, Moezizadeh M, Javand F. Effects of extracts of Salvadora persica on proliferation and viability of human dental pulp stem cells. J Conserv Dent. 2015;18(4):315–20. Available from: http://www.jcd.org.in/text.asp?2015/18/4/315/159740

42. Şeker Ş, Elçin AE, Yumak T, Sınağ A, Elçin YM. In vitro cytotoxicity of hydrothermally synthesized ZnO nanoparticles on human periodontal ligament fibroblast and mouse dermal fibroblast cells. Toxicol Vitr. 2014 Dec;28(8):1349–58. Available from: https://linkinghub.elsevier.com/retrieve/pii/S0887233314001313

43. Zhan D, Guo L, Zheng L. Inhibition of the receptor for advanced glycation promotes proliferation and repair of human periodontal ligament fibroblasts in response to high glucose via the NF-κB signaling pathway. Arch Oral Biol. 2018 Mar;87:86–93. Available from: https://doi.org/10.1016/j.archoralbio.2017.12.011

44. Duan X, Ji M, Deng F, Sun Z, Lin Z. Effects of connective tissue growth factor on human periodontal ligament fibroblasts. Arch Oral Biol. 2017 Dec;84(51):37–44. Available from: https://linkinghub.elsevier.com/retrieve/pii/S0003996917302819

45. O'Brien FJ, Harley BA, Yannas IV, Gibson LJ. The effect of pore size on cell adhesion in collagen-GAG scaffolds. Biomaterials. 2005 Feb;26(4):433–41. Available from: http://linkinghub.elsevier.com/retrieve/pii/S0142961204002017.

JOTCS A
Journal of the Turkish Chemical Society Section: A Chemistry
TURKISH CHEMICAL SOCIETY

Design, synthesis and biological evaluation of 1,3-diaryltriazene-substituted sulfonamides as antioxidant, acetylcholinesterase and butyrylcholinesterase inhibitors

Suleyman Akocak[1*], Mehmet Boga[2*], Nabih Lolak[1], Muhammed Tuneg[2], Rajesh K.K. Sanku[3],

[1]Adiyaman University, Faculty of Pharmacy, Department of Pharmaceutical Chemistry, 02040, Adiyaman, Turkey.
[2]Dicle University, Faculty of Pharmacy, Department of Pharmaceutical Technology,21280, Diyarbakir, Turkey.
[3]University of Pennsylvania, Perelma School of Medicine, Department of Systems Pharmacology and Translational Therapeutics, 19104, Philadelphia, United States

Abstract: 1,3-diaryltriazenes are one of the most useful and important linkers for many pharmaceutical applications. Therefore, in the current work, a series of 1,3-diaryltriazene sulfonamides **4(a-k)** were synthesized by reacting diazonium salt of sulfanylamide and substituted aromatic amine derivatives **3(a-k)**. The obtained compounds were investigated for antioxidant properties by using different methods such as a DPPH radical scavenging assay, ABTS radical decolarization, cupric reducing antioxidant capacity (CUPRAC) and metal chelating methods. The cholinesterase inhibition activities (acetylcholinesterase and butyrylcholinesterase) of synthesized compounds were also tested. In general, compounds showed weak antioxidant activity, except compounds **4d** (IC_{50} =114.89 µM for DPPH activity), **4i** (IC_{50} =25.31 µM for ABTS activity), **4a** (IC_{50} = 86.33 µM for metal chelating activity), and **4k** (absorbance value 1.229 µM for CUPRAC). Some of the compounds showed great % inhibition against both acetylcholinesterase and butyrylcholinesterase with % inhibition values ranging from 11.54 to 93.67 and 62.24 to 98.47, respectively.

Keywords: Sulfanylamide, 1,3-diaryltriazene, antioxidant, anticholinesterase.

Submitted: January 22, 2019. **Accepted:** February 01, 2019.

Cite this: Akocak S, Boga M, Lolak N, Tuneg M, Sanku R. Design, synthesis and biological evaluation of 1,3-diaryltriazene-substituted sulfonamides as antioxidant, acetylcholinesterase and butyrylcholinesterase inhibitors. JOTCSA. 2019;6(1):63–70.

DOI: https://dx.doi.org/10.18596/jotcsa.516444.

***Corresponding authors.** E-mail: akocaksuleyman@gmail.com, mehmetboga1980@gmail.com.

INTRODUCTION

Sulfur-containing drugs, especially sulfonamides, are used for various pharmaceutical applications. Their importance can be dated back from the first use of sulfonamide containing antibacterial drugs. Sulfonamides are used for a wide range of biological applications such as antibacterial (1-3), anti-inflammatory (4, 5), antioxidant (6-8), anticancer (9-14), carbonic anhydrase inhibitors (10, 15-17) and for Alzheimer's disease (18, 19). There are more than 112 FDA approved drugs containing sulfonamide group (20).

Alzheimer's disease (AD) is a neurodegenerative disorder featured with cognitive dysfunction and dementia (20). According to the present estimation, about 50 million people are going through this disease and this number might triple up to 152 million by 2050 (World Alzheimer report). Unfortunately, the medicines used for the cure of AD and its progression are not discovered yet. There are some pathophysiology factors like beta-amyloid deposits, inflammation, oxidative stress, dyshomeostasis of biometals, tau-protein aggregation, deficiencies of acetylcholine (ACh) and butyrylcholine (BCh) which are believed to be responsible for the disease progression (21-23).

Inhibition of ACh and BCh hydrolysis by using acetylcholinesterase (AChE) and butyrylcholinesterase (BChE) inhibitors has been considered to increase the level of the ACh and BCh in synapses aiding the restoration of the cholinergic neurotransmission and cognitive capabilities (24, 25). First-line drugs in the symptomatic treatment of AD treatment involve the use of cholinesterase inhibitors such as rivastigmine, galantamine and donepezil (24), but these drugs are reported to have side effects like nausea, gastrointestinal upset, diarrhea, muscular weakness, syncope and weight loss (26). On the other hand, antioxidants are thought to offer a good possibility of combating neurodegeneration and protection against Alzheimer's disease (27,28). Therefore, there is a need for less toxic cholinesterase inhibitors along with antioxidant properties for AD treatment.

More recently, our research group showed the efficient human carbonic anhydrase II (hCA II) inhibition profile of 1,3-diaryltriazene sulfonamides (29, 30). The nanomolar potency was obtained against one of the most abundant isoform hCA II. In the current study, we are focusing on the role of 1,3-diaryltriazene sulfonamides as antioxidant, acetylcholinesterase and butyrylcholinesterase inhibitors, prompted by the potent carbonic anhydrase inhibition results.

EXPERIMENTAL SECTION

Chemistry

General synthetic route for the preparation of 1,3-diaryltriazene-substituted sulfonamides **4(a-k)** are depicted in Figure 1. The synthesis of the compounds was done as previously described by us (29, 30). Briefly, a solution of sulfanylamide **1** (5 mmol) in ~1-1.5 ml of conc. hydrochloric acid and 5 ml of water was cooled to 0-5 ^{0}C. Then, sodium nitrite (7 mmol) in 5 mL of water was added dropwise to the solution under continuous stirring. The mixture was stirred about 15-20 min at 0-5 ^{0}C, and diazonium solution was added to aromatic amines (prepared by 5 mmol anilines in 5 mL of MeOH) by adjusting the pH around 6-7 with a saturated sodium acetate solution. After that, the reaction mixture was stirred 5-6 h at 0-5 ^{0}C and overnight at room temperature in dark. The obtained colorful mixture was filtered off, washed several times with cold water, and then crystallized from ethanol. Physicochemical and spectroscopic characterization of all compounds **4(a-k)** have been previously described by us (29).

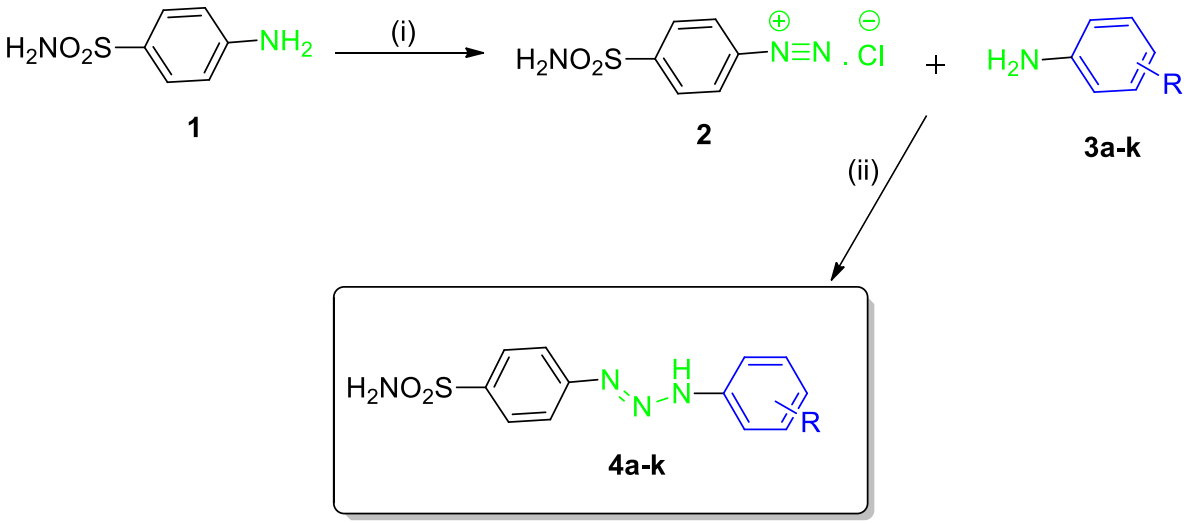

Figure 1. General synthetic route for the synthesis of 1,3-diaryltriazene sulfonamides **4a-k**.

DPPH Free radical scavenging assay

The DPPH (2,2-diphenyl-1-picrylhydrazyl) radical scavenging activity of the synthesized compounds was determined by spectrophotometric method based on the reduction of a ethanolic solution of DPPH (31). 2, 5, 10, 20 µL of 1mM stock solution of each compound were completed to 40 µL with DMSO and mixed with 160 µL of 0.1 mM of DPPH free radical solution. The mixture was left to stand for 30 min in the dark and the absorbance was then measured at 517 nm against a blank. Inhibition of free radical, DPPH, in percent (I%) was calculated according to the formula:

$$I\,\% = (A_{control} - A_{sample})/A_{control} \times 100;$$

where $A_{control}$ is the absorbance of the control reaction (containing all reagents except for the tested compounds), and A_{sample} is the absorbance of the test compounds. Tests were carried out in triplicate. BHA (butylated hydroxyanisole), BHT (butylated hydroxytoluene) and α-Toc (α-Tocopherol) were used as positive control.

ABTS cation radical scavenging assay

The $ABTS^{\cdot+}$ (2,2`-azino-bis(3-ethylbenzothiazoline-6-sulfonic acid)), cationic radical scavenging activity assay determines the inhibition percentage as a function of time and concentration, and evaluated relative to the activity of BHT, BHA and α-Toc (32). 2, 5, 10 and 20 µL of 1 mM stock solutions were completed to 40 µL with the DMSO. Then 160 µL of 7 mM ABTS

solutions were added into each well in the micro plate. After keeping them for 6 min in dark at room temperature, the absorbances were measured at 734 nm. ABTS cation radical scavenging activities as % inhibition were determined by using the below equation:

$$\%Inhibition = (A_{control} - A_{sample})/A_{control} \times 100$$

where A is the absorbance. Tests were carried out in triplicate. BHA, BHT and α-Toc were used as positive control.

Metal Chelating Activity

The chelating ability of synthesized compounds was examined according to the method of Dinis et al. (33). 2, 5, 10 and 20 µL of 1 mM stock solutions were completed to 188 µL with the DMSO. Then, each sample was mixed with 4 µL of 2 mM iron(II) chloride. The reaction was started by adding 8 µL of 5 mM ferrozine. The mixture was left to stand for 10 min at room temperature, then the absorbance was measured at 562 nm against a blank. The results were expressed as percentage of inhibition of the ferrozine -Fe^{2+} complex formation. EDTA was used as a positive control. The percentage inhibition of the ferrozine -Fe^{2+} complex formation was calculated using the formula given below:

$$\text{Chelating ability } (\%) = (A_{control} - A_{sample})/A_{control} \times 100$$

Cupric reducing antioxidant capacity (CUPRAC) assay

CUPRAC method comprises the reduction of Cu(II)-Neocuproine into its colored form Cu(I)-Neocuproine chelate in the presence of antioxidant compounds (34). The absorbance at 450 nm was measured when the complex was obtained. 61 µL of 10 mM $CuCl_2$, 61 µL of 7.5 mM Neocuproine and 61 µL of 1 M of NH_4OAc solutions were added into the prepared solutions to adjust the concentrations as 10, 25, 50, and 100 µM. The absorbance values were compared with the standard molecules BHA, BHT and α-Toc. Each of samples was applied three times to verify the results.

Anticholinesterase inhibition assay

The inhibitory effect of 1,3-diaryltriazene-substituted sulfonamide derivatives **4(a-k)** on AChE and BChE activities was determined according to the slightly modified spectrophotometric method of Ellman et al. (35). All compounds were dissolved in DMSO to prepare stock solutions at 4 mM concentration. Aliquots of 150 µL of 100 mM sodium phosphate buffer (pH 8.0), 10 µL of sample solution and 20 µL AChE (or BChE) solution were mixed and incubated for 15 min at 25 °C, and DTNB (5,5'-dithio-bis(2-nitrobenzoic acid)) (10 µL) is added. The reaction was then initiated by the addition of acetylthiocholine iodide (or butyrylthiocholine iodide) (10 µL). 30 minutes after addition of substrates (acetylthiocholine iodide or butyrylthiocholine iodide), the absorbances were measured at 412 nm. The final concentration of the tested compounds' solution was 200 µM.

$$\%Inhibition = (A_{control} - A_{sample})/A_{control} \times 100$$

where A is the absorbance. Tests were carried out in triplicate. Galantamine was used as positive control.

Statistical analysis

The results of the antioxidant and anticholinesterase activity assays are expressed as the mean ± SD of three parallel measurements. The statistical significance was estimated using a Student's t-test, where p-values < 0.05 were considered significant.

RESULTS AND DISCUSSION

In the present study, we report the synthesis, antioxidant, acetylcholinesterase and butyrylcholinesterase inhibition activities of 1,3-diaryltriazene-substituted sulfonamide derivatives **4(a-k)** obtained from sulfanylamide as a lead molecule. The compounds were obtained via the reaction of diazonium salt of sulfanylamide with substituted aromatic amine derivatives **3(a-k)**. These compounds were previously synthesized and fully characterized by us a potent and selective human carbonic anhydrase II (hCA II) inhibitors.

The antioxidant capacities of prepared 1,3-diaryltriazene-substituted sulfonamides are assayed by using several antioxidant methods, including DPPH free radical scanvenging, ABTS cation radical scavenging, cupric reducing (CUPRAC) and metal chelating methods. Also, acetylcholinesterase (AChE) and butyrylcholinesterase (BChE) inhibitory activities were investigated.

The DPPH free radical scavenging activity of the synthesized compounds was assayed and compared with BHT, BHA and α-TOC used as standards. The DPPH free radical scavenging activity of the synthesized compounds is given in Table 1 as an IC_{50} values. As depicted in Table 1, three compounds show better DPPH activity than the standard BHT, which are **4d** (4-CN), **4f** (4-BuO) and **4j** (2,3,4,5,6-F) with IC_{50} values of 114.89, 162.29, and 219.88 µM, respectively. In case of compounds **4a** (4-F), **4b** (4-Cl), **4c** (4-MeO), **4e** (4-Acetyl), **4g** (2-CN), **4h** (3-NO_2), and **4i** (3,4-diMeO), there was no significant DPPH activity with IC_{50} values of >1000 µM. On the other hand, all compounds displayed lesser DPPH activity than other standards BHA and α-TOC.

The results revealed that some of the compounds from the series show good ABTS cation radical scanvenging activity. The compound **4i** (3,4-diMeO) showed the best ABTS activity with IC_{50} value of 25.31 µM, which is more active than the standards BHA, BHT and α-TOC. The compounds **4f** (4-BuO) and **4j** (2,3,4,5,6-F) were also sensitive to ABTS cation radical scavenging activity with IC_{50} values of 53.01 and 50.79 µM, respectively. The IC_{50} values of the remaining

compounds were ranging from 108.89 to 610.34 μM, except the compound **4d** (4-CN) which has no ABTS cation radical scavenging activity (IC_{50} >1000 μM) as demonstrated in Table 1.

The metal chelating properties of the 1,3-diaryltriazene-substituted sulfonamide derivatives **4(a-k)** on iron(II) ions were presented in Table 1 and compared with standard EDTA. It was considered that compound **4a** (4-F) and **4e** (4-acetyl) were the most active compounds with IC_{50} values 86.33 and 99.10 μM, respectively, which showed chelating activity similar to standard compound EDTA (IC_{50}= 52.35 μM). Also, compounds **4c** (4-MeO), **4d** (4-CN), **4g** (2-CN) and **4h** (3-NO_2) showed moderate activity with IC_{50} values ranging from 120.52 to 198.86 μM. The remaining compounds had no activity in metal chelating assay with IC_{50} values >1000 μM (Table 1).

Table 1. DPPH free radical scavenging, ABTS cation radical scavenging and metal chelating activities of 1,3-diaryltriazene-substituted sulfonamides **4(a-k)** and controls BHA, BHT, α-Toc, and EDTA.

Comp.	R	IC_{50} (μM)[a]		
		DPPH Free Radical Scavenging Activity	**ABTS Cation Radical Scavenging Activity**	**Metal Chelating Activity**
4a	**4-F**	>1000	146.33±1.76	86.33±1.70
4b	**4-Cl**	>1000	176.97±1.67	>1000
4c	**4-MeO**	>1000	108.89±1.53	121.31±1.88
4d	**4-CN**	114.89±2.50	>1000	198.86±1.80
4e	**4-Acetyl**	>1000	610.34±3.07	99.10±1.02
4f	**4-BuO**	162.29±2.76	53.01±0.25	>1000
4g	**2-CN**	>1000	460.17±3.05	120.52±1.58
4h	**3-NO_2**	>1000	369.50±1.03	147.13±1.14
4i	**3,4-diMeO**	>1000	25.31±0,21	>1000
4j	**2,3,4,5,6-F**	219.88±2.92	50.79±1.62	>1000
4k	**3,4-diCl**	813.65±1.18	394.08±1.10	>1000
BHA[b]	**---**	61.72±0.85	45.40±1.08	-
BHT[b]	**---**	232.11±3.01	26.54±0.18	-
α-TOC[b]	**---**	56.86±0.77	34.12±0.41	-
EDTA[b]	**---**	-	-	52.35±1.15

[a] IC_{50} values represent the means (standard deviation of three parallel measurements) ($p < 0.05$).
[b] Reference compounds.

Table 2. Cupric ion reducing antioxidant capacity (CUPRAC) of the 1,3-diaryltriazene-substituted sulfonamides **4(a-k)** and controls BHA, BHT, and α-Toc.

Comp.	R	Absorbance Values (μM)[a]			
		10 μM	**25 μM**	**50 μM**	**100 μM**
4a	**4-F**	0.102±0.013	0.119±0.002	0.155±0.008	0.168±0.006
4b	**4-Cl**	0.079±0.004	0.111±0.036	0.127±0.021	0.168±0.009
4c	**4-MeO**	0.271±0.088	0.224±0.008	0.418±0.058	0.744±0.051
4d	**4-CN**	0.095±0.003	0.099±0.005	0.188±0.062	0.244±0.043
4e	**4-Acetyl**	0.340±0.001	0.406±0.001	0.549±0.004	0.889±0.008
4f	**4-BuO**	0.166±0.064	0.236±0.036	0.366±0.044	0.882±0.046
4g	**2-CN**	0.102±0.004	0.098±0.012	0.134±0.002	0.151±0.001
4h	**3-NO_2**	0.131±0.057	0.127±0.036	0.250±0.083	0.301±0.019
4i	**3,4-diMeO**	0.176±0.006	0.328±0.004	0.626±0.016	1.083±0.022
4j	**2,3,4,5,6-F**	0.122±0.006	0.156±0.005	0.197±0.008	0.290±0.024
4k	**3,4-diCl**	0.599±0.001	0.726±0.008	0.965±0005	1.229±0.002
BHA[b]		0.288±0.015	0.572±0.046	1.026±0.013	1.984±0.035
BHT[b]		0.303±0.010	0.610±0.010	1.167±0.024	2.000±0.173
α-TOC[b]		0.179**±**0.001	0.296**±**0.012	0.482**±**0.017	0.912**±**0.065

[a]Values expressed are means ± SD of three parallel absorbance measurements ($p<0.05$) [b] Reference compounds

The cupric reducing antioxidant capacity (CUPRAC) method was also applied to identify the antioxidant capacity of the prepared 1,3-diaryltriazene-substituted sulfonamide derivatives. As expected, the activity of the compounds increased with increasing concentration as summarized in Table 2. The compounds **4i** (3,4-diMeO) and **4k** (3,4-diCl) showed a better CUPRAC capacity than standard α-TOC. The compound **4k** had better activity at concentrations 10 and 25 μM than all three standards. Interestingly, these two active

compounds have 3,4-disubstitution on the phenyl ring make them different from the rest of the compounds.

Table 3. Anticholinesterase activities of the 1,3-diaryltriazene-substituted sulfonamides **4(a-k)** at 200 µM and standard drug galanthamine.

Comp.	R	AChE (Inhibition %)[a]	BChE (Inhibition %)[a]
4a	**4-F**	11.54±0.26	84.18±1.20
4b	**4-Cl**	13.55±0.76	67.26±1.39
4c	**4-MeO**	25.16±0.64	90.22±0.88
4d	**4-CN**	33.50±0.49	79.00±0.46
4e	**4-Acetyl**	84.48±1.02	77.21±0.20
4f	**4-BuO**	67.07±0.48	82.14±4.33
4g	**2-CN**	69.60±0.67	62.24±1.16
4h	**3-NO_2**	67.70±0.27	71.51±1.80
4i	**3,4-diMeO**	85.01±0.78	90.22±0.10
4j	**2,3,4,5,6-F**	93.67±0.30	98.47±0.56
4k	**3,4-diCl**	55.35±0.32	97.00±0.61
Galantamine[b]		84.20±0.74	87.86±0.24

[a] 200 µM, [b] Standard drug

In the current series of 1,3-diaryltriazene sulfonamides, most of the compounds showed great potency against both cholinesterase enzymes (AChE and BChE). In general, all compounds had higher BChE inhibition activity than AChE inhibition activity, except the compounds **4e** (4-acetyl) and **4g** (4-CN). In case of AChE inhibition, the compounds **4e**, **4i** and **4j** showed better activity than standard drug galanthamine with %inhibition values of 84.48, 85.01 and 93.67, respectively. The compounds **4f** (4-BuO), **4g** (2-CN), **4h** (3-NO_2) and **4k** (3,4-diCl) were moderate inhibitors of this enzyme with %inhibition values ranging from 55.35 to 69.60. For BChE activity, compounds **4j** (2,3,4,5,6-F) and **4k** (3,4-diCl) showed the highest %inhibition at 200 µM with 98.47 and 97.00, respectively. The remaining compounds also showed good inhibition against BChE enzyme with %inhibition values ranging from 62.24 to 90.22.

CONCLUSIONS

In the present study, 1,3-diaryltriazene sulfonamides **4(a-k)** were synthesized from the reaction of diazonium salt of sulfonamide and substituted aromatic amines. The antioxidant activities of the compounds were investigated by DPPH, ABTS, metal chelating and CUPRAC methods. The AChE and BChE inhibition studies were also examined. In general, compounds showed weak DPPH, ABTS, metal chelating and CUPRAC activity. However, several compounds were good and promising antioxidant capacity, such as compounds **4d** (IC_{50} =114.89 µM for DPPH activity), **4i** (IC_{50} =25.31 µM for ABTS activity), **4a** (IC_{50} = 86.33 µM for metal chelating activity), and **4k** (absorbance value 1.229 µM for CUPRAC). The best biological results were obtained against BChE enzyme inhibition in this study. Specifically, compounds **4j** and **4k** showed excellent %inhibition against this enzyme with %inhibition values of 98.47 and 97.00, respectively. Since the AChE and BChE enzymes are related with neurodegenerative disorders and their inhibition is important for this type of brain disorders, these 1,3-diaryltriazene sulfonamides may be considered of interest for *in vivo* studies.

ACKNOWLEDGMENTS

This work was partially funded by The Scientific and Technological Research Council of Turkey (TUBITAK) with Grant no. 216S907.

REFERENCES

1. Konda S, Srujana R, Bhaskar K, Munaganti RK, Gugloth V, Nagarapu L, Akkewar DM. Synthesis and antimicrobial activity of novel benzoxazine sulfonamide derivatives. Bioorg Med Chem Lett. 2015;25(7):1643-6.

2. Durgun M, Turkmen H, Zengin G, Zengin H, Koyunsever M, Koyuncu I. Synthesis, characterization, *in vitro* cytotoxicity and antimicrobial investigation and evaluation of physicochemical properties of novel 4-(2-methylacetamide)benzenesulfonamide derivatives. Bioorg Chem. 2017;70:163-72.

3. Genc Y, Ozkanca R, Bekdemir Y. Antimicrobial activity of some sulfonamide derivatives on clinical isolates of *Staphylococus aureus*. Ann Clin Microbiol Antimicrob. 2008 Aug;(7):17-23.

4. Chandna N, Kumar S, Kaushik P, Kaushik D, Roy SK, Gupta GK, Jachak SM, Kapoor JK, Sharma PK. Synthesis of novel celecoxib analogues by bioisosteric

replacement of sulfonamide as potent anti-inflammatory agents and cyclooxygenase inhibitors. Bioorg Med Chem. 2013;21(15):4581-90.

5. Bano S, Javed K, Ahmad S, Rathish IG, Singh S, Alam MS. Synthesis and biological evaluation of some new 2-pyrazolines bearing benzene sulfonamide moiety as potential anti-inflammatory and anti-cancer agents. Eur J Med Chem. 2011;46(12):5763-8.

6. Gocer H, Akincioglu A, Oztaskin N, Goksu S, Gulcin I. Synthesis, antioxidant, and antiacetylcholinesterase activities of sulfonamide derivatives of dopamine-related compounds. Arch Pharm. 2013 Oct;346(11):783-92.

7. Ning X, Guo Y, Ma X, Zhu R, Tian C, Zhang Z, Wang X, Ma Z, Liu J. Design, synthesis and pharmacological evaluation of (E)-3,4-dihydroxy styryl sulfonamides derivatives as multifunctional neuroprotective agents against oxidative and inflammatory injury. Bioorg Med Chem. 2013;21(17):5589-97.

8. Garibov E, Taslimi P, Sujayev A, Bingol Z, Cetinkaya S, Gulcin I, Beydemir S, Farzaliyev V, Alwasel SH, Supuran CT. Synthesis of 4,5-disubstituted-2-thioxo-1,2,3,4-tetrahydropyrimidines and investigation of their acetylcholinesterase, butyrylcholinesterase, carbonic anhydrase I/II inhibitory and antioxidant activities. J Enzyme Inhib Med Chem. 2016;31:1-9.

9. Lu XY, Wang ZC, Ren SZ, Shen FQ, Man RJ, Zhu HL. Coumarin sulfonamides derivatives as potent and selective COX-2 inhibitors with efficacy in suppressing cancer proliferation and metastasis. Bioorg Med Chem Lett. 2016;26(15):3491-8.

10. Akocak S, Alam MR, Shabana AM, Sanku RKK, Vullo D, Thompson H, Swenson ER, Supuran CT, Ilies MA. PEGylated Bis-sulfonamide carbonic anhydrase inhibitors can efficiently control the growth of several carbonic anhydrase IX-expressing carcinomas. J Med Chem 2016;59(10):5077-88.

11. Lolak N, Akocak S, Bua S, Supuran CT. Design, synthesis and biological evaluation of novel ureido benzenesulfonamides incorporating 1,3,5-triazine moieties as potent carbonic anhydrase IX inhibitors. Bioorg Chem. 2019;82:117-22.

12. Casini A, Scozzafava A, Mastrolorenzo A, Supuran CT. Sulfonamides and sulfonylated derivatives as anticancer agents. Curr Cancer Drug Targetd. 2002;2(1):55-75.

13. Canakci D, Koyuncu I, Lolak N, Durgun M, Akocak S, Supuran CT. Synthesis and cytotoxic activities of novel copper and silver complexes of 1,3-diaryltriazene-substituted sulfonamides. J Enzyme Inh Med Chem. 2019;34(1):110-6.

14. Zhao C, Rakesh KP, Ravidar L, Fang WY, Qin HL. Pharmaceutical and medicinal significance of sulfur (S^{VI})-containing motifs for drug discovery: A critical review. Eur J Med Chem. 2019;162:679-734.

15. Akocak S, Lolak N, Nocentini A, Karakoc G, Tufan A, Supuran CT. Synthesis and biological evaluation of novel aromatic and heterocyclic bis-sulfonamide Schiff bases as carbonic anhydrase I, II, VII and IX inhibitors. Bioorg Med Chem. 2017;25(12):3093-7.

16. Akocak S, Lolak N, Bua S, Turel I, Supuran CT. Synthesis and biological evaluation of novel N,N`-diaryl cyanoguanidines acting as potent and selective carbonic anhydrase II inhibitors. Bioorg Chem. 2018;77:245-1.

17. El-Gazzar MG, Nafie NH, Nocentini A, Ghorab MM, Heiba HI, Supuran CT. Carbonic anhydrase inhibition with a series of novel benzenesulfonamide-triazole conjugates. J Enzyme Inhib Med Chem. 2018;33(1):1565-74.

18. Bag S, Tulsan R, Sood A, Cho H, Redjeb H, Zhou W, LeVine H, Torok B, Torok M. Sulfonamides as multifunctional agents for Alzheimer's disease. Bioorg Med Chem Lett. 2015;25(3):626-30.

19. Rishton GM, Retz DM, Tempest PA, Novontny J, Kahn S, Treanor JJ, Lile JD, Ciltron M. Fencyhylamine sulfonamide inhibitors of amyloid beta peptide production by the gamma-secretase proteolytic pathway: potential small-molecule therapeutic agents for the treatment of Alzheimer's disease. J Med Chem. 2000;43(12):2297-9.

20. Wang J, Gu BJ, Masters CL, Wang YJ. A systemic view of Alzheimer disease-insights from amyloid-β metabolism beyond the brain. Nat Rev Neurol. 2017;13(10):612-23.

21. Swerdlow RH. Pathogenesis of Alzheimer's disease. Clin Interv Aging. 2007;2(3):347-59.

22. Dong S, Duan Y, Hu Y, Zhao Z. Advances in the pathogenesis of Alzheimer's disease: a re-evaluation of amyloid cascade hypothesis. Transl Neurodegener. 2012;1(1):1-18.

23. Greig NH, Lahiri DK, Sambamurti K. Butyrylcholinesterase: an important new target in Alzheimer's disease therapy. Int Psychogeriatr. 2002;14:77-91.

24. Gulcin I, Scozzafav A, Supuran CT, Akincioglu H, Koksal Z, Turkan F, Alwasel S. The effect of caffeic acid phenethyl ester (CAPE) on metabolic enzymes including acetylcholinesterase, butyrylcholinesterase, glutathione S-transferase, lactoperoxidase, and carbonic anhydrase isozymes I, II, IX, and XII. J Enzyme Inhib Med Chem. 2016;31(6):1095-101.

25. Oztaskin N, Cetinkaya Y, Taslimi P. Goksu S, Gulcin I. Antioxidant and acetylcholinesterase inhibition properties of novel bromophenol derivatives. Bioorg Chem. 2015;60:49-57.

26. Casey DA, Antimisiaris D, O'Brien J. Drugs for Alzheimer's disease: are they effective?. P T. 2010;35(4):208-11.

27. Klatte ET, Scharre DW, Nagaraja HN, Davis RA, Reversdorf DQ. Combination therapy of donepezil and vitamin E in Alzheimer disease. Alzheimer Dis Assoc Disord. 2003;17(2):113-6.

28. Cai P, Fang SQ, Yang HL, Yang XL, Liu QH, Kong LY, Wang XB. Donepezil-butylated hydroxytoluene (BHT) hybrids as Anti-Alzheimer's disease agents with cholinergic, antioxidant, and neuroprotective properties. Eur J Med Chem. 2018;5(157):161-76.

29. Lolak N, Akocak S, Bua S, Koca M, Supuran CT. Design and synthesis of novel 1,3-diaryltriazene-substituted sulfonamides as potent and selective carbonic anhydrase II inhibitors. Bioorg Chem. 2018;77:542-7.

30. Akocak S, Lolak N, Bua S, Supuran CT. Discovery of novel 1,3-diaryltriazene sulfonamides as carbonic anhydrase I, II, VII, and IX inhibitors. J Enzyme Inhib Med Chem. 2018;33(1):1575-80.

31. Blois MS. Antioxidant determinations by the use of a stable free radical. Nature. 1958;181:1199-200.

32. Pellegrini RRN, Proteggente A, Pannala A, Yang M, Rice-Evans C. Antioxidant activity applying and improved ABTS radical cation decolorization assay. Free Rad Bio Med. 1999;26:1231-7.

33. Dinis TCP, Maderia VMC, Almedia LM. Action of phenolic derivatives (acetoaminophen, salycilate and 5-aminosalycilate) as inhibitors of membrane lipid preoxidation and as preoxyl radical scavengers. Arc Biochem Biophy. 1994;315:161-9.

34. Apak R, Guclu K, Ozyurek M, Karademir SE. Novel total antioxidant capacity index for dietary polyphenols and vitamine C and E, using their cupric ion reducing capability in the presence of neocuproine: CUPRAC method. J Agric Food Chem. 2004;52:7970-81.

35. Ellman GL, Courtney KD, Andres V, Featherstone RM. A new and rapid colorimetric determination of acetylcholinesterase activity. Biochem Pharmacol. 1961;7:88-95.

JOTCS A
Journal of the Turkish Chemical Society
Section: A
Chemistry
TURKISH CHEMICAL SOCIETY

Discovery of New DNA Topoisomerase II Inhibitors using Structure Based Virtual Screening Method

Tugba Ertan-Bolelli[1]*, Kayhan Bolelli[1,2]

[1]Department of Pharmaceutical Chemistry, Faculty of Pharmacy, Ankara University, TR-06560 Ankara Turkey
[2]LumiLabs, TR-06050 Ulus Ankara Turkey

Abstract: DNA topoisomerases are proved therapeutic targets of antibacterial and anticancer drugs. Structures of topoisomerase–DNA and inhibitor ternary complexes have revealed the exact binding sites and mechanisms of topoisomerase poisons. There are two isoforms of Human Topoisomerase II; α and β. Both of them perform similar functions and their levels differ depending on the replicative activity and type of tissue. Topo IIα is preferentially expressed in proliferating cells. Thus, selective Topo IIα inhibitors have been of particular interest in cancer therapy, as they may represent a more targeted approach to highly proliferative cells. In this study, we use structure-based virtual screening method with molecules which are commercially available in the ZINC database. Docking studies were performed by Glide module available in Schrödinger software, to obtain an efficient collection of hit molecules ligand filtration was also done by employing Lipinski's "rule of five" and pharmacokinetic properties were tested using Qikprop module. From approximately ten thousand compounds from Zinc database we selected 4 top chemical structures with suitable ADME/Tox properties and good inhibiting profile for topo II. Thus compounds 1-4 could be the promising inhibitors of human topo IIα enzyme.

Keywords: anticancer activity, docking, topoisomerase, virtual screening.

Submitted: October 02, 2018. **Accepted:** February 04, 2019.

Cite this: Ertan-Bolelli T, Bolelli K. Discovery of New DNA Topoisomerase II Inhibitors using Structure Based Virtual Screening Method. JOTCSA. 2019;6(1):71–8.

DOI: https://dx.doi.org/10.18596/jotcsa.466457.

***Corresponding author. E-mail:** tbolelli@ankara.edu.tr

INTRODUCTION

Topoisomerases are ubiquitous enzymes in key cellular processes such as DNA replication, transcription, recombination, and repair processes such as supercoiled, relaxed, catenated, and knotted DNA (1). All type of topoisomerases shows their biochemical functions by catalyzing DNA cleavage and relegation (2). DNA topoisomerases are proved therapeutic targets of antibacterial and anticancer drugs. Structures of topoisomerase–DNA and inhibitor ternary complexes have revealed the exact binding sites and mechanisms of topoisomerase poisons. α and β Human Topoisomerase II are two available isoforms. Both of them perform similar functions and their levels differ depending on the replicative activity and type of tissue (3-6). Human topo IIα and β sharing a similar tertiary structure and primary sequence but they distribute in various cells and tissues. They also show various cellular functions, topo IIα overexpressed in proliferating cells and generally located in the nuclear plasma. Topoisomerase IIβ plays apparent roles in transcriptional regulation, cell development, and differentiation, but not essential for cell proliferation and survival. Although human topo IIα relaxes negatively supercoiled plasmid slower than positively supercoiled plasmids, but topo IIβ is not. Because of all these reasons, topo IIα seems to be the more attractive target for new anticancer drugs. Thus selective Topo IIα inhibitors have been of particular interest in

cancer therapy, as they may represent a more targeted approach to highly proliferative cells (7-10).

Recently, computational protein–ligand docking process has been used to predict the affinities and optimal binding modes of the compounds with the target proteins. Ligand docking method enables the visualization of an optimal complex that can be predicted from a target protein structure and a candidate drug compound. Structure-based virtual screening method focus on the therapeutic targets three-dimensional (3D) information for docking method. In order to select the hits that exhibit chemical, structural and electronic characteristics, docking procedures are used. The information of the target protein can be obtained from *in silico* technique or experimental data. In order to exploring lead compounds for target proteins all these advantages have encouraged the usage of computational methods in drug discovery (11-13).

Human topo IIα has a homodimer structure and its monomer is composed of 1531 amino acids including four sections DNA-gate, N-gate, C-gate, and CTD (14). The X-ray crystallographic structure of this enzyme (PDB: 5GWK) is available in Protein Data Bank (www.rcsb.org) and we used this structure for *in silico* studies (15). In this work, we use structure-based drug design method, in order to predict the binding modes and calculate the ADME/Tox properties to propose new anti-cancer candidates which have suitable properties to be promising oral human topo IIα inhibitors.

MATERIAL AND METHODS

Structure-based virtual screening method focus on the therapeutic targets 3D information. In order to select the hits that exhibit chemical, structural and electronic characteristics, docking procedures are used. The information of the target protein can be obtained from *in silico* technique or experimental data (13). Docking calculations were performed using Schrödinger 2018-2, with Maestro 11.5 and the Glide module (16-18).

Protein Preparation

The X-ray crystallographic structure of human topoisomerase II enzyme complex with etoposide (PDB: 5GWK) was obtained from Protein Data Bank (www.rcsb.org) and prepared for docking process. To prepare the enzyme (PDB: 5GWK), we used the protein preparation wizard module. We use OPL5-2005 force field and pH =7.0 to minimize hydrogen atoms. Bond orders were assigned, with zero order bonds to disulfide bonds and metals as well.

Ligand preparation

For virtual screening study, 10,241 commercially available compounds were obtained from ZINC database. All of these ligands were prepared by using Schrödinger, LigPrep module. The bond angles and bond orders were assigned after ligand minimization step. For the minimization OPLS 2005 force field was used. In order to keep the ligands in the right protonation state in biological conditions, epik option was used.

Grid preparation

The active site of the topo II enzyme, was defined for generating the grid in Maestro. The grid box was limited to the size of 20 Å at the active site. Firstly, docking procedure was validated by extracting ligand etoposide from the binding site and re-docking it to the topo II (PDB: 5GWK). Glide had successfully reproduced the experimental binding conformations of etoposide in topo II enzyme with an acceptable root-mean-square deviation (RMSD) value of 0.42Å.

Virtual Screening

Docking studies were carried out using high throughput virtual screening (HTVS) option, SP screening (standard-precision) and XP screening (extra-precision) mode of Glide module, respectively. We considered ring conformations, nitrogen inversions, input partial charges and, for amides, a penalty for nonplanar conformations was applied. Epik state penalties were added to docking scores. We did not use any similarities or constraints for the docking calculations. 10,241 commercially available compounds from ZINC database were screened. The compounds were redocked via postprocessing. The best pose was output on the basis of Glide score. After visual inspection we retained four inhibitor candidates, compounds 1-4 (ZINC000131302839, ZINC000119841605, ZINC000131302897, ZINC000119841475). Docking scores of these compounds were shown in Table 1.

ADME/Tox Analyses

To obtain an efficient *in silico* collection of hit molecules, ligand filtration was done by employing Lipinski's "rule of five" and ADME properties using Qikprop module of Schrödinger (19). Calculated ADME properties of the comp. 1-4 (ZINC000131302839, ZINC000119841605, ZINC000131302897, ZINC000119841475) which have best docking scores, were shown in Table 2. This analysis includes, brain/blood partition coefficient (QPlog BB), aqueous solubility (QPlog S), total solvent accessible surface area (SASA),

octanol/water partition coefficient (QP log Po/w), predicted apparent MDCK cell permeability (QPMDCK), Lipinski Rule of 5 violations, and human oral absorption.

RESULT AND DISCUSSION

In this study, we use structure based virtual screening method with 10,241 commercially available compounds in the ZINC database. To obtain an efficient collection of hit molecules, docking studies were performed using Glide module available in Schrödinger software, ligand filtration was also done by employing Lipinski "rule of five" using Qikprop module (12, 13). Docking scores of the best topo II inhibitor candidate compounds are shown in Table 1 and QikProp Properties Predictions topo II inhibitor candidate compounds were also shown in Table 2. According to the docking studies, binding energies of the comp. 1-4 (ZINC000131302839, ZINC000119841605, ZINC000131302897, ZINC000119841475) were found −12.692, −12.417, −11.082, −11.058 respectively, and all of these compounds showed better docking score than standard drug etoposide (−10.193). All of the pharmacokinetic properties conducted by Qikprop were within the permissible range. From approximately ten thousand compounds from Zinc database we selected 4 top chemical structures with suitable ADME/Tox properties and good inhibiting profile for human topo IIα. The structures of the compounds 1-4 are shown in Figure 1.

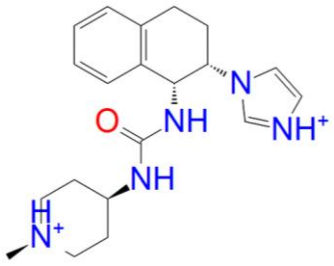

Compound 1 (ZINC000131302839)

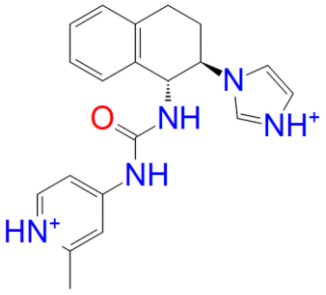

Compound 2 (ZINC000119841605)

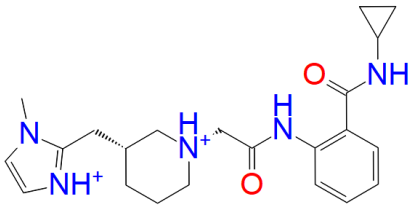

Compound 3 (ZINC000131302897)

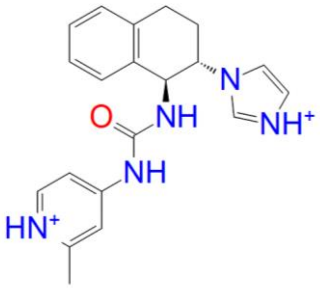

Compound 4 (ZINC000119841475)

Figure 1 Structures of the topo II inhibitor candidate compounds

Table 1. Docking scores of the topo II inhibitor candidate compounds.

Code	Docking Score	Glide Score
Comp. 1 (ZINC000131302839)	-12.692	-12.885
Comp. 2 (ZINC000119841605)	-12.417	-13.093
Comp. 3 (ZINC000131302897)	-11.082	-11.403
Comp. 4 (ZINC000119841475)	-11.058	-11.734
Etoposide	-10.193	-10.193

Table 2. QikProp Properties Predictions topo II inhibitor candidate compounds.

Code	Molecular Weight	Percent Human Oral Absorption	SASA	QPlog BB	QPlog S	QPlog Po/w	QPMDCK	Rule of Five
Comp. 1	353.466	91.03	630.508	0.278	-3.575	2.663	346.748	0
Comp. 2	347.419	100	648.084	-0.372	-5.438	3.457	866.085	0
Comp. 3	395.503	95.33	683.098	-0.168	-3.572	3.457	252.772	0
Comp. 4	347.419	100	649.387	-0.365	-5.475	3.468	886.651	0
Etoposide	588.564	47.524	773.724	-1.481	-3.453	0.606	111.019	2

According to the docking results; comp. 1 (ZINC000131302839) revealed H-bonds with deoxythymidine DT9, and Glu461; pi-pi stacking with deoxyadenosine DA12, deoxyguanosin DG13; salt bridges with deoxycytidine DC8 and Glu 461; comp. 2 (ZINC000119841605) revealed H-bond with Glu461; π-π stacking with deoxythymidine DT9 and deoxyguanosine DG13; salt bridges with deoxythymidine DT9 and Glu 461; comp. 3 (ZINC000131302897) revealed H-bonds with deoxythymidine DT9, and Gly488; π - π stacking with deoxyadenosine DA12, deoxyguanosine DG13; salt bridges with deoxythymidine DT9, π -cation interaction with deoxythymidine DT9, deoxyguanosine DG10 and deoxyadenosine DA12; comp. 4 (ZINC000119841475) revealed H-bonds with deoxythymidine DT9; π - π stacking with deoxythymidine DT9, and deoxyguanosine DG13; salt bridges with deoxythymidine DT9 and Glu 461 and etoposide revealed H-bond with deoxyguanosine DG13, and Asp463; π - π stacking with deoxyguanosine DG13; π - cation interactions with Arg487 (Figure 2). According to the docking studies, it can be concluded that compounds 1-4 showed better docking scores than standard drug etoposide. The binding energies of compounds 1-4 were found −12.692, −12.417, −11.082, −11.058 respectively, and for etoposide it was −10.193. These results showed that, compounds 1-4 have strong interactions with human topo IIα and they could be the promising inhibitors of this enzyme, thus compounds 1-4 were selected for the further studies as human topo IIα candidate drugs.

According to the Qikprop Properties Predictions, the human oral absorption percentage of the selected compounds was in the appropriate excretion range of 91 to 100%. Compound 2, and compound 4 showed 100% oral absorption. For selected lead compounds, the partition coefficient (QP log Po/w) was within the permissible range of 0.6-3.47. SASA and brain/blood partition coefficient (QP log BB) were also found to be within satisfactory range. Violations of Lipinski's rule of five were also calculated (20). For all selected compounds have no violations of the Lipinski's Rule of 5, thus indicating their potential as a drug-like molecule. Additionally, compounds are in the acceptable range for predicted apparent MDCK cell permeability (QPMDCK) and predicted aqueous solubility (QPLog S). Table 1 showed some pharmacokinetic properties calculated for compound 1-4 by Qikprop simulation.

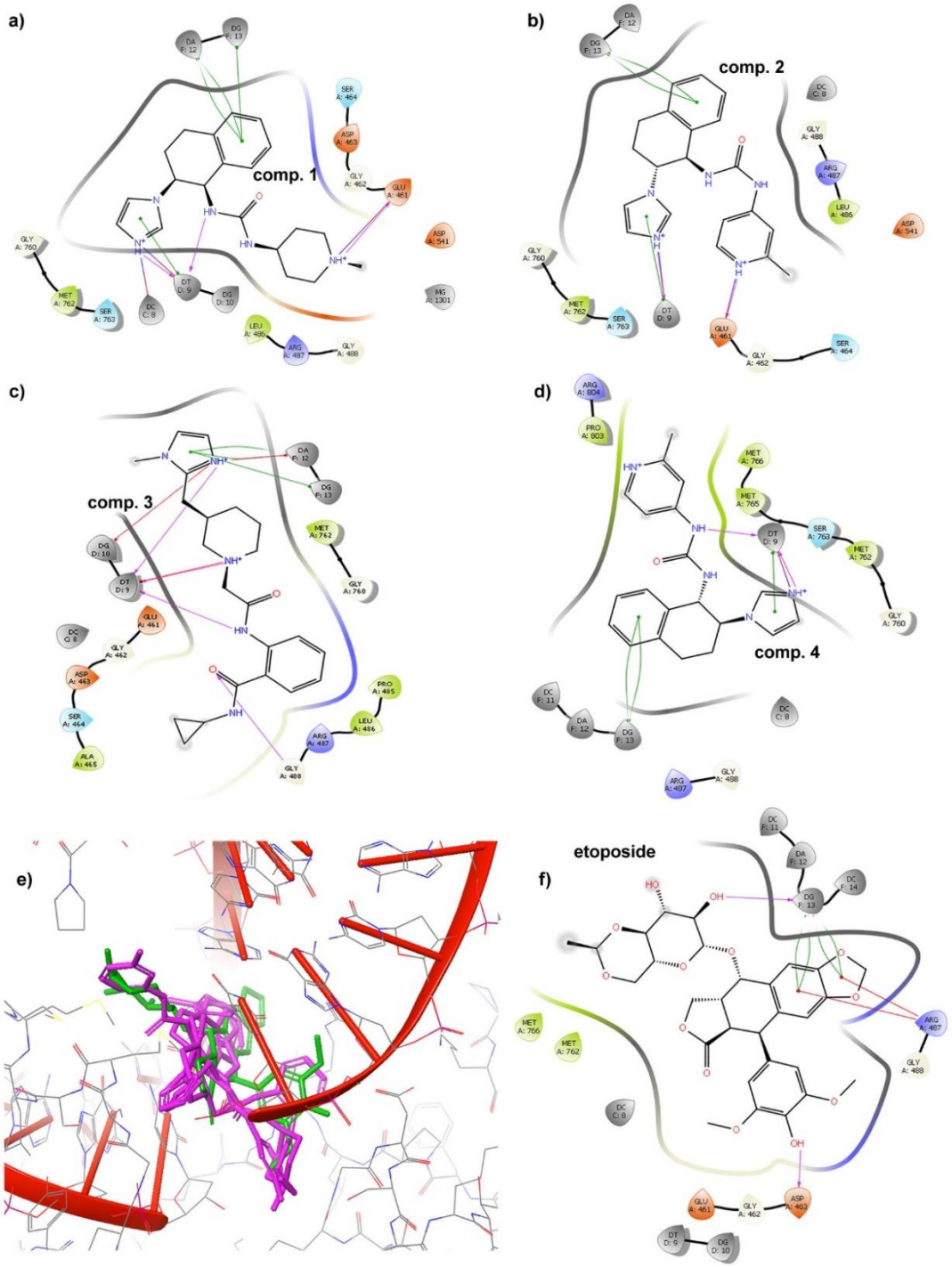

Figure 2 **a)** Docked position of comp.1 (ZINC000131302839): compound revealed H-bonds with deoxythymidine DT9, and Glu461; π- π stacking with deoxyadenosine DA12, deoxyguanosine DG13; salt bridges with deoxycytidine DC8 and Glu 461. **b)** Docked position of compound 2 (ZINC000119841605): compound revealed H-bond with Glu461; π - π stacking with deoxythymidine DT9 and deoxyguanosine DG13; salt bridges with deoxythymidine DT9 and Glu 461. **c)** Docked position of compound 3 (ZINC000131302897): compound revealed H-bonds with deoxythymidine DT9, and Gly488; π - π stacking with deoxyadenosine DA12, deoxyguanosine DG13; salt bridges with deoxythymidine DT9, π -cation interaction with deoxythymidine DT9 , deoxyguanosine DG10 and deoxyadenosine DA12. **d)** Docked position of comp.4 (ZINC000119841475): compound revealed H-bonds with deoxythymidine DT9; π - π stacking with deoxythymidine DT9, and deoxyguanosine DG13; salt bridges with deoxythymidine DT9 and Glu 461. **e)** Structure of topoisomerase IIα (pdb ID:5gwk) complex with etoposide (green) and docking poses of inhibitor candidate compounds (magenta) in active site. **f)** Docked position of etoposide: compound revealed H-bond with deoxyguanosine DG13, and Asp463; π - π stacking with deoxyguanosine DG13; π -cation interactions with Arg487.

CONCLUSION

Virtual screening methods have been an important tool for new hit compound search. In this study, from approximately ten thousand compounds from Zinc database, it was possible to select 4 top chemical structures with good inhibiting profile for topo II. According to the docking studies, it can be concluded that compounds 1-4 (ZINC000131302839, ZINC000119841605, ZINC000131302897, ZINC000119841475) showed better docking score than standard drug etoposide. The binding energies of compounds 1-4 were found −12.692, −12.417, −11.082, −11.058 respectively, and for etoposide it was −10.193. These compounds showed strong interactions with human topo IIα, they bound to the active site residues of the enzyme and DNA. Besides, all of the predicted pharmacokinetic properties conducted by Qikprop were within the permissible range. As a conclusion, we selected 4 top chemical structures with suitable ADME/Tox properties and good inhibiting profile for topo II, thus compounds 1-4 could be the promising inhibitors of topoisomerase IIα enzyme.

ACKNOWLEDGMENTS

This study is supported by a grant (Project Number: 18H0237001) from Scientific Research Projects Committee of Ankara University and it was presented in the International Chemistry & Biology Conference'18 on July 12th, 2018 in Sharm El-Sheikh, Egypt.

REFERENCES

1. Wang JC. Cellular roles of DNA topoisomerases: A molecular perspective. Nat. Rev. Mol. Cell Biol. 2002, (3):430−40.

2. Cowell IG, Sondka Z, Smith K, Lee KC, Manville CM, Sidorczuk-Lesthuruge M, Rance HA, Padget K, Jackson GH, Adachi N, Austin CA. Model for MLL translocations in the rapyrelated leukemia involving topoisomerase II β-mediated DNA strand breaks and gene proximity. Proc. Natl. Acad. Sci. U. S. A. 2012, (109):8989−94.

3. Nitiss JL. DNA topoisomerase II and its growing repertoire of biological functions. Nat. Rev. Cancer. 2009, (9):327−33.

4. Tiwari VK, Burger L, Nikoletopoulou V, Deogracias R, Thakurela S, Wirbelauer C, Kaut J, Terranova R, Hoerner L, Mielke C, Boege F, Murr R, Peters AH, Barde YA, Schübeler D. Target genes of topoisomerase II β regulate neuronal survival and are defined by their chromatinstate. Proc.Natl.Acad.Sci.U.S.A. 2012, (109):E934−43.

5. Pogorelcnik B, Perdih A, Solmajer T. Recent advances in the development of catalytic inhibitors of human DNA topoisomerase IIα as novel anticancer agents. Curr. Med. Chem. 2013, 20(5):694-709.

6. Schmidt, B.H.; Osheroff, N.; Berger, J.M. Structure of a topoisomerase II-DNA-nucleotide complex reveals a new control mechanism for ATPase activity. Nat. Struct. Mol. Biol., 2012, 19(11): 1147-54.

7. Larsen AK, Escargueil AE, Skladanowski A. Catalytic topoisomerase II inhibitors in cancer therapy. Pharmacol. Ther. 2003, (99):167−81.

8. Farr CJ, Antoniou-Kourounioti M, Mimmack ML, Volkov A, Porter AC. The α isoform of topoisomerase II is required for hyper compaction of mitotic chromosomes in human cells. Nucleic Acids Res. 2014, (42):4414−26.

9. D'Arcy N, Gabrielli B. Topoisomerase II Inhibitors and Poisons, and the Influence of Cell Cycle Checkpoints. Curr. Med. Chem. 2017, (24):1504-19.

10. McClendon, A. K.; Rodriguez, A. C.; Osheroff, N. Human topoisomerase IIalpha rapidly relaxes positively supercoiled DNA: implications for enzyme action ahead of replication forks. J.Biol.Chem. 2005, (280):39337−45.

11. Diniz EMLP, Poiani JGC, Taft CA, da Silva CHTP. Structure-Based Drug Design, Molecular Dynamics and ADME/Tox to Investigate Protein Kinase Anti-Cancer Agents. Curr. Bioact. Comp. 2017, 13(3):213–22.

12. Verma P, Tiwari M, Tiwari V. *In silico* high-throughput virtual screening and molecular dynamics simulation study

to identify inhibitor for AdeABC efflux pump of *Acinetobacter baumannii*. J Biomol. Struct. Dyn. 2018, 36(5):1182-94.

13. Taft CA, da Silva CHTP. Current State-of-the-art for Virtual Screening and Docking Methods New Developments in Medicinal Chemistry, Bentham Science: Dubai, 2014, (2):3-169.

14. Wendorff TJ, Schmidt BH, Heslop P, Austin CA, Berger JM. The structure of DNA-bound human topoisomerase II alpha: conformational mechanisms for coordinating inter-subunit interactions with DNA cleavage. J. Mol. Biol. 2012, (424):109−24.

15. Wang YR, Chen SF, Wu CC, Liao YW, Lin TS, Liu KT, Chen YS, Li TK, Chien TC, Chan NL. Producing irreversible topoisomerase II-mediated DNA breaks by site-specific Pt (II)-methionine coordination chemistry. Nucleic Acids Res. 2017, (45):10861-71.

16. Friesner RA, Banks JI, Murphy RB, Halgren TA, Kicic JJ, Maung DAT, Repasky MP, Knowll EH. Glide: A new approach for rapid, accurate docking and scoring: Method and assessment of docking accuracy. J. Med. Chem. 2004, (47):1739-49.

17. Schrödinger LLC. New York, USA: Schrodinger Inc.; 2008. http://www.schrodinger.com

18. Friesner RA, Murphy RB, Repasky MP, Frye LL, Greenwood JR, Halgren TA, Sanschagrin PC, Mainz DT. Extra Precision Glide: Docking and Scoring Incorporating a Model of Hydrophobic Enclosure for Protein-Ligand Complexes, J. Med. Chem. 2006, (49):6177–96.

19. Schrödinger Release 2018-2: QikProp, Schrödinger, LLC, New York, NY, 2018.

20. Lipinski CA, Lombardo F, Dominy BW, Feeney PJ. Experimental and computational approaches to estimate solubility and permeability in drug discovery and development settings. Adv Drug Deliv Rev. 2012, 64(1-3):4-17.

JOTCS A
Journal of the Turkish Chemical Society
Section: A
Chemistry
TURKISH CHEMICAL SOCIETY

Doping Agent Naphazoline Hydrochloride: Development of Simple and Fast Voltammetric Method for Its Determination in Human Serum

Tuğçe Çetinkol[1], Funda Öztürk[1*], Pınar Esra Erden[2]

[1]Department of Chemistry, Faculty of Science and Arts, Tekirdağ Namık Kemal University, Tekirdağ, Turkey
[2]Department of Chemistry, Polatlı Faculty of Science and Arts, Ankara Hacı Bayram Veli University, Ankara, Turkey

Abstract: Electrochemical behavior of naphazoline hydrochloride on a carbon paste electrode that was modified with aluminium oxide nanoparticles (Al_2O_3NPs) was investigated in a Britton-Robinson (BR) buffer (pH 7.0) using various voltammetric techniques. The results support the presence of an irreversible and diffusion-controlled electrochemical oxidation signal of naphazoline hydrochloride which is approximately at 0.9 V *vs.* Ag/AgCl. A selective, accurate, and simple square-wave anodic adsorptive stripping voltammetric method was proposed for naphazoline hydrochloride detection. The linear response was within the range of 5.0×10^{-8} – 3.0×10^{-5} mol L^{-1} with a detection limit of 2.6×10^{-9} mol L^{-1} (0.642 µg L^{-1}). In addition, the proposed method was also utilized for naphazoline hydrochloride determination in human serum sample.

Keywords: Aluminum oxide nanoparticles, doping agent, electrochemical techniques, naphazoline, human serum

Submitted: August 03, 2018. **Accepted:** February 08, 2019.

Cite this: Çetinkol T, Öztürk F, Erden P. Doping Agent Naphazoline Hydrochloride: Development of Simple and Fast Voltammetric Method for Its Determination in Human Serum. JOTCSA. 2019;6(1):79–88.

DOI: https://dx.doi.org/10.18596/jotcsa.450793.

***Corresponding author. E-mail**: fozturk@nku.edu.tr.

INTRODUCTION

Naphazoline, 2-(1-naphthylmethyl)-2-imidazoline hydrochloride (NZ HCl) (Figure 1), is a relatively long-lasting vasoconstrictor, which realizes its action by interacting with the alpha receptors of vascular smooth muscle. It is used as an important ingredient of various pharmaceutical preparations especially in nasal and ophthalmic solutions (1,2). Its empirical formula is $C_{14}H_{15}ClN_2$. NZ HCl is a white crystalline powder and it is soluble in water and ethanol. NZ HCl belongs to the group of α-sympatomimetics that are agonists of α-adrenergic receptors (3). When NZ HCl is found in a serum sample from an athlete, the athlete is charged for doping, therefore, determination of it in serum samples is crucial.

Different analytical techniques including spectrophotometry (4-9), fluorimetry (10), high performance liquid chromatography (11,12), gas chromatography (13), potentiometry (3,14,15) and liquid chromatography-mass spectrometry (16) were used for the determination of NZ HCl separately or in the presence of other drugs. However, all these methods were generally used for nasal and eyes drops and not for serum samples in the determination of NZ HCl. Only one report was found that designates NZ HCl in serum (16).

The electrochemical method has many advantages, such as instrumental simplicity, high sensitivity and selectivity, short analysis time, and moderate cost, hence various methods such as cyclic voltammetry (CV), differential pulse voltammetry (DPV) and square-wave voltammetry (SWV) (17,18) were proposed for the analysis of drugs and drug related molecules in pharmaceutical dosage forms and biological fluids. Oliveira et al. developed, a batch-injection analysis technique with square-wave voltammetric detection for the simultaneous

determination of zinc and naphazoline species. In this study boron-doped diamond electrode was employed as the working electrode. The linear working range and detection limit of the method for naphazoline were reported as 3.0-21.0 µmol L^{-1} and 0.04 µmol L^{-1}, respectively. Analytical application of this method was investigated in pharmaceutical samples (19).

Carbon paste electrodes (CPEs) have the advantage of quick and easy preparation and their surface is easily renewable and reproducible. They also offer a low residual current. Therefore, these electrodes are widely used for the voltammetric analysis in many electrochemical studies (20). Metal oxide nanoparticles (MONPs) have gained much attention in the fabrication of modified electrodes due to their unique properties (21-23). As electrode modification material MONPs present large surface-to-volume ratio, high surface reaction activity and good catalytic efficiency (21). Therefore, incorportion of MONPs into carbon paste matrix can be a good approach to improve the analytical characteristics of the resulting electrode. In this study Al_2O_3NPs were used for the modification of carbon paste electrode and the resulting electrode was applied to the electrochemical analysis of NZ HCl. To the best of our knowledge, there is no method reported for the voltammetric analysis of NZ HCl in biological fluids. This study introduces a simple, rapid, reliable and sensitive, square wave anodic adsorptive stripping voltammetric (SWAAdSV) method which can be used in determination of NZ HCl in human serum samples using an aluminium oxide nanoparticles modified carbon paste electrode (Al_2O_3-NPs-CPE).

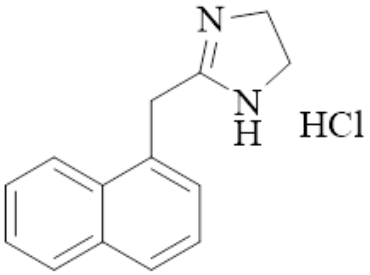

Figure 1. Structure of naphazoline hydrochloride.

EXPERIMENTAL SECTION

Materials

Al_2O_3-NPs (2-4 nm×2800 nm), and paraffin oil were purchased from Sigma-Aldrich (St. Louis, MO, USA). NaOH, methanol, H_3BO_3, H_3PO_4, and CH_3COOH were supplied from Merck (Darmstadt, Germany). Graphite powder (<20 µm) was acquired from Fluka. (Britton-Robinson (BR) buffer solution was prepared by mixing 0.04 mol L^{-1} of H_3PO_4–CH_3COOH–H_3BO_3 solution and adding 0.2 mol L^{-1} of NaOH to the required pH value. NZ HCl stock solution was prepared at a concentration of 1.5×10^{-3} mol L^{-1} in water. Standard working solutions of NZ HCl were obtained by diluting the stock solution with BR buffer and pH values of the diluted solutions were adjusted to the desired values (such as 2.0, 4.0, 6.0, 7.0, 8.0, 9.0 and 10.0) for pH studies with 0.2 mol L^{-1} NaOH. All aqueous solutions were prepared using double-distilled water.

Apparatus and measurements

CV, SWV and SWAAdSV experiments were performed on a Drop Sens µstat 400 electrochemical analyzer (Lianera, Spain). A computerized IVIUM electrochemical analyzer (Ivium Technologies, Netherlands) was used for the electrochemical impedance spectroscopy (EIS) experiments. A modified carbon paste electrode, a platinum wire and Ag/AgCl electrode were employed as working, counter and reference electrodes, respectively. Thermo Scientific Orion Model 720A Benchtop pH meter with an Orion combination pH electrode (Waltham, USA) was used for the pH measurements. EIS experiments were performed in the frequency range from 10^5 Hz–0.05 Hz with 10 mV as the amplitude in 0.1 M KCl with 5.0 mM $K_3[Fe(CN)_6]/K_4[Fe(CN)_6]$ (1:1). All experiments were performed under ambient conditions.

10.0 mL of NZ HCl solutions in BR buffer were used in all voltammetric studies. The test solution was purged with high purity nitrogen (99.99%) for 60 s before the first run and 30 s between all individual successive runs. Voltammograms were obtained by applying a positive-going scan (frequency (Hz): 10; E_{step} (V): 0.005; $E_{amplitude}$ (V): 0.005) after 3 s equilibration time.

Preparation of unmodified and modified electrodes

Al_2O_3-NPs-CPE was constructed by mixing the graphite powder (12.0 mg) with the Al_2O_3-NPs (3.0 mg) and then adding paraffin oil (10 µL). The resulting mixture was homogenized in a mortar for 30 minutes. CPE without modification (UCPE) was constructed by mixing 15.0 mg graphite powder with 10 µL paraffin oil. The homogenized paste was inserted into the electrode and the CPE surface was smoothed. The CPEs were washed with double distilled water and BR buffer between experiments.

Analysis of real samples

Serum samples, supplied from healthy individuals, were analyzed to investigate the practical use of the proposed method. 1.0 mL of serum sample was transferred to the electrochemical cell containing 10.0 mL of BR buffer solution and then aliquots from stock NZ HCl solution were added. Calibration curve method was utilized to determine the NZ HCl concentration in serum samples.

RESULTS AND DISCUSSION

Electrochemical behavior of NZ HCl on CPE modified with Al_2O_3-NPs

CV and SWV techniques were used to investigate the electrochemical behavior of NZ HCl. Figure 2 depicts the CVs of NZ HCl at pH 7.0 at UCPE and Al_2O_3-NP-CPE. A single well-defined oxidation peak was obtained at a potential of 0.93 V and 0.94 V at UCPE and Al_2O_3-NPs-CPE at pH 7.0, respectively. As expected, no peak was observed in blank BR buffer scanned under the same operational conditions. No cathodic peak was observed at the reverse scan indicating a totally irreversible electrode reaction (Figure 2). The oxidation peak of NZ HCl was higher at Al_2O_3-NPs-CPE compared with that of the peak at UCPE. The increase in peak current confirms a higher electron transfer rate for NZ HCl at Al_2O_3-NPs-CPE. It can be concluded that Al_2O_3 nanoparticles are suitable modifiers for the electrochemical determination of NZ HCl.

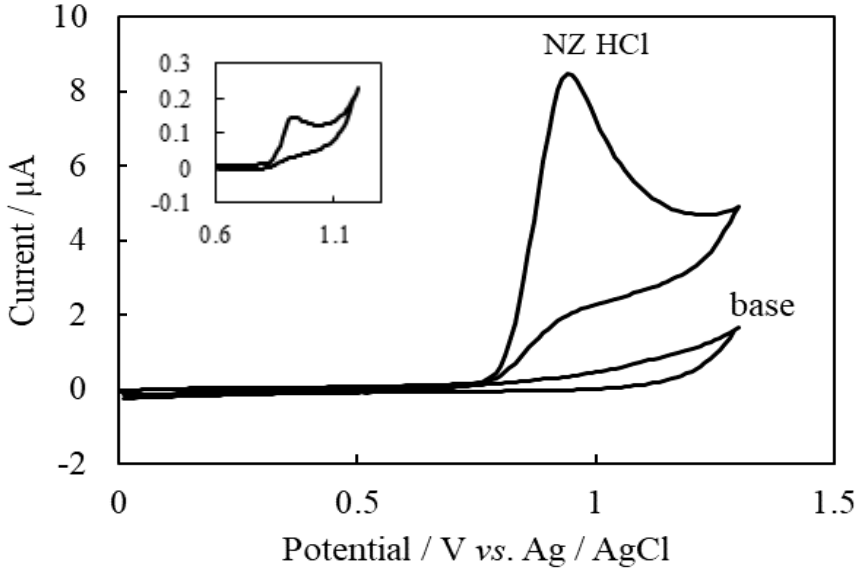

Figure 2: Cyclic voltammograms of 1.5×10^{-3} mol L^{-1} NZ HCl solutions at Al_2O_3-NPs-CPE in BR buffer solution pH 7.0 and scan rate 0.1 V s^{-1} (inset: cyclic voltammograms of NZ at bare CPE at the same condition).

More detailed experimental studies were also done to reveal the characteristic of oxidation. First of all, the effect of scan rate (*v*) on the anodic peak current (*ip,a*) was studied by CV (Figure 3). The peak potential shifts to more positive potential values with the increasing scan rate from 0.01 to 0.225 V s^{-1} which indicates that the electrooxidation step is not reversible.

The plot of the peak current versus square root of scan rate (Figure 3; inset A) reveals a linear relationship (R^2 = 0.9802). This relationship indicates a diffusion-controlled process for the electrochemical reaction mechanism.

Linear relationships of logarithm of peak current ip,a versus logarithm of scan rate (V s^{-1}) following the regression equation with R^2= 0.9796 were obtained (Figure 3; inset B). In this equation the value of the slope was found to be very close to the theoretical value of 0.5 for diffusion species (24). The result further confirms that the diffusion phenomenon is dominant.

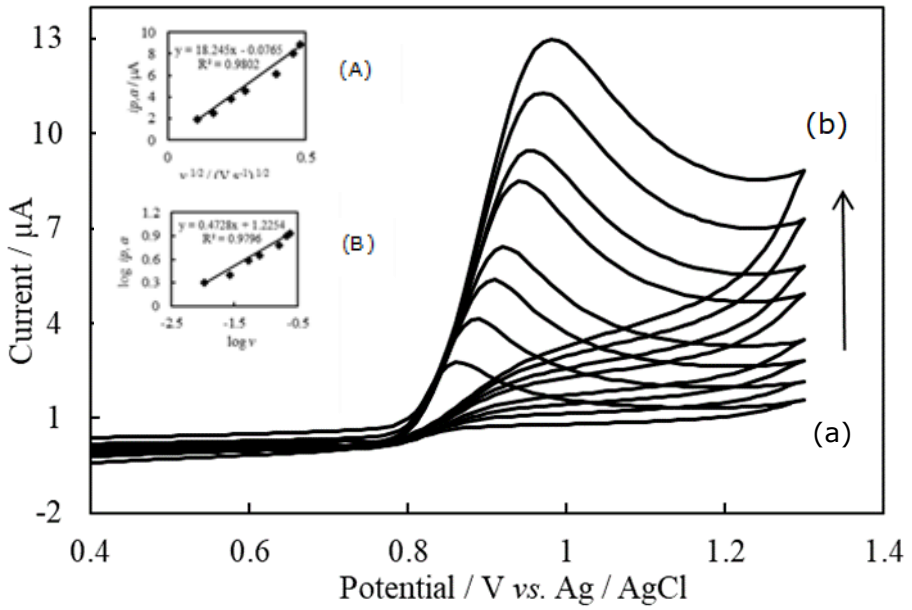

Figure 3: Effect of potential scan rate on both anodic peak current and anodic peak potential of 1.5×10^{-3} mol L^{-1} NZ HCl at pH 7.0 (inset: (A) Curve of peak current versus square root of scan rate, (B) curve of logarithm of peak current versus logarithm of scan rate (a: 0.01 V s^{-1}, b: 0.025 V s^{-1}, c: 0.05 V s^{-1}, d: 0.075 V s^{-1}, e: 0.1 V s^{-1}, f: 0.175 V s^{-1}, g: 0.2 V s^{-1}, h: 0.225 V s^{-1})

EIS studies of UCPE and Al_2O_3-NPs-CPE were conducted in 0.1M KCl solution with 5.0 mM $[Fe(CN)_6]^{3-/4-}$ in the frequency range, $0.05–10^5$ Hz with 10 mV as the amplitude (Figure 4). In the Nyquist plot of impedance spectra the semicircle part represents the electron transfer limited process and its diameter is equal to the electron transfer resistance, R_{ct} (25). The R_{ct} for Al_2O_3-NPs-CPEs (curve B) is smaller than that of UCPE (curve A) indicating that incorporation of Al_2O_3 nanoparticles into carbon paste matrix facilates electron transfer.

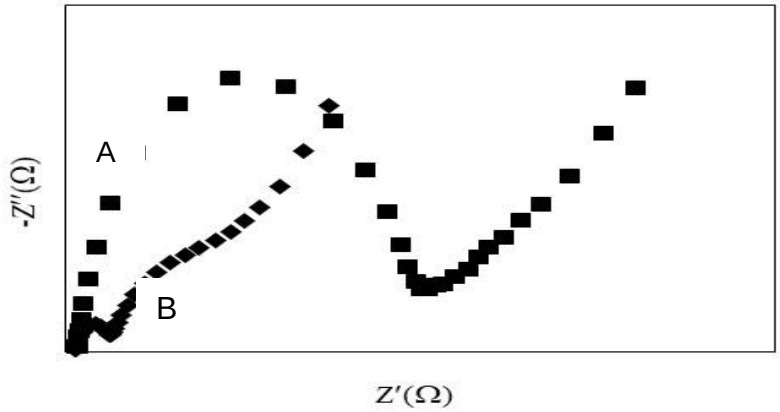

Figure 4: The Nyquist curves of (A) UCPE and (B) Al_2O_3-NP-CPE in 0.1 M KCl solution containing 5.0 mM $Fe(CN)_6^{3-/4-}$.

Influence of pH

pH of the test solution is an important parameter that has a significant influence on the electrochemical behaviors of molecules. Thus, the influence of pH on the electrochemical behavior of NZ HCl was investigated in the pH range of 2.0–10.0 (Figure 5). Two different trends can be observed in the SW voltammograms as the pH varies between 2.0–7.0 and 7.0–10.0. The first trend is that the anodic peak potential shifts to more cathodic values and peak current increases as pH varies from 2.0 to 7.0. Conversely, as the second trend, the peak potential shifts to more anodic values when pH varies from 7.0 to 10.0, and the peak current decreases. The greatest peak current was obtained at pH 7.0 (data not shown), and it was chosen as the optimum pH.

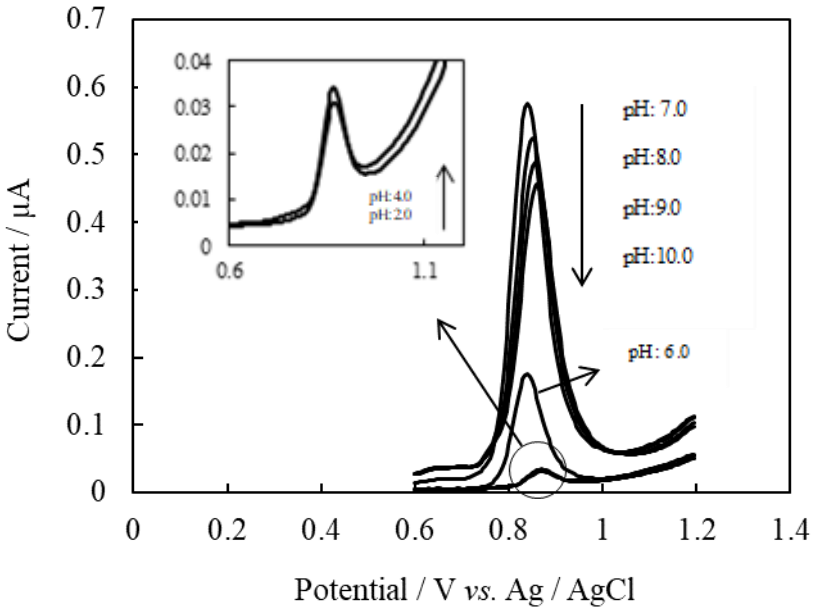

Figure 5: Effect of pH on SWVs of 1.0×10^{-5} mol L^{-1} NZ HCl.Inset:SWVs obtained at pH 2 to 4.

Optimization of the experimental variables

In order to specify the optimum working conditions, instrumental parameters and experimental variables were investigated and optimized. Various instrumental parameters including frequency (f), scan increment (ΔE_i) and pulse amplitude (ΔE_a) were optimized for 1.0×10^{-6} mol L^{-1} NZ HCl in a BR solution at pH 7.0 and found to be f: 10 Hz, ΔE_i: 5 mV, ΔE_a: 5 mV.

The effect of the deposition potential on the SWAAdSV signal was evaluated in the range of 0.0 V – 0.8 V for a 1.0×10^{-6} mol L^{-1} NZ HCl solution. The maximum peak current was obtained at 0.6 V (data not shown). The effect of deposition time on peak current was also studied in the range from 15 to 150 s for 1.0×10^{-6} mol L^{-1} NZ HCl and 90 s was found as the optimum deposition time (data not shown).

Linear working range and detection limit

In this study, electrochemical determination of NZ HCl with adsorptive techniques was achieved and a lower limit of detection than studies reported in the literature was obtained.

After the operating conditions were optimized, SWAAdSV was conducted in the BR buffer solution (pH 7.0) containing different NZ HCl concentrations in order to obtain the analytical curve. The obtained values for the peak current gave a linear relationship with the NZ HCl concentrations in the range from 5.0×10^{-8} mol L^{-1} (0.0123 mg L^{-1}) to 3.0×10^{-5} mol L^{-1} (7.40 mg L^{-1}) (Figure 6). The calibration plots are represented by the equation $I_{p,a}$ (µA) = 0.0667 [NZ HCl] (µmolL^{-1}) + 0.0298 with a correlation coefficient of 0.9949 (Figure 7). The high value of the correlation coefficient indicates a good linearity, confirming the validity of the SWAAdSV method for NZ HCl determination. Table 1 depicts the characteristics of the calibration plot.

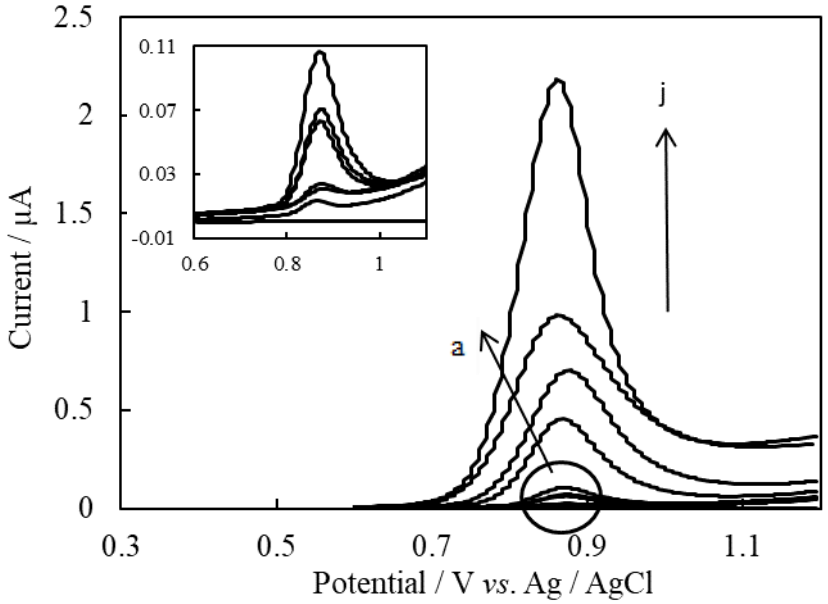

Figure 6: SWAAdS voltammograms of NZ HCl at different concentrations (in µmol L^{-1}) a: 0.05, b: 0.08, c: 0.1, d: 0.5, e: 0.8, f: 1.0, g. 5.0, h: 8.0, i: 10.0, j: 30. Inset: SWAAdS voltammograms from a to f.

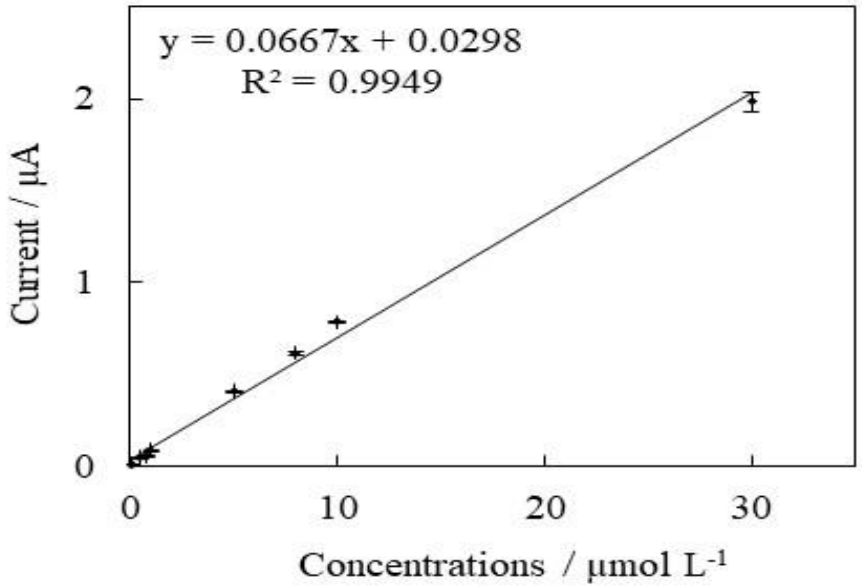

Figure 7: Calibration curve for NZ HCl solutions in BR buffer of pH 7.0 ($t_{deposition}$: 90.0 s, $E_{deposition}$: 0.6 V). Error bars show the standard deviation of three measurements.

Limit of detection (LOD) and limit of quantification (LOQ) values were estimated according to the following equations: $LOD = 3\frac{s}{m}$ $LOQ = 10\frac{s}{m}$ (18) where *s* refers to the standard deviation of intercept of calibration curve and *m* refers to the slope of the related calibration curve. *LOD* and *LOQ* values were calculated as 2.6×10^{-9} mol L^{-1} (0.642 µg L^{-1}) and 8.7×10^{-9} mol L^{-1} (2.147 µg L^{-1}), respectively (Table 1). These low LOD and LOQ values indicates that the presented method can be utilized to analyze the NZ HCl concentration of highly diluted samples. It is also important to highlight that the LOD obtained in our study was lower than the detection limits previously obtained for potentiometric methods (3,14,15,19).

Stability of the proposed method

The stability of NZ HCl in the BR buffer at pH 7.0 was investigated under the optimum working conditions by observing the changes in both the anodic peak potential and the anodic peak current of standard NZ HCl solution. Relative standard deviation (RSD) of peak current and peak potentials obtained after three series of measurements were calculated as 1.1% and 0.1%, respectively (Table 1). It can be concluded that the absence of notable change in peak potential and peak current indicates the excellent stability of the method. Moreover, the stability of standard stock solution was investigated for 2 weeks. The standard stock solution of NZ HCl was

kept in dark at +4 ˚C. No changes were observed in the peak potential or peak current of NZ HCl and it was found to be stable during this period.

Table 1: Regression data of the calibration curve for assay of NZ HCl by SWAAdSV.

Parameter	Value
Linear working range / mol L^{-1}	$5.0 \times 10^{-8} - 3.0 \times 10^{-5}$
Slope (m) / (μA L mol^{-1})	0.0667
Intercept / A	3.0×10^{-8}
Standard deviation of calibration (s_r) / A	4.74×10^{-8}
Standard deviation of slope / (μA L mol^{-1})	0.0017
Standard deviation of intercept (s) / A	3.53×10^{-8}
LOD / mol L^{-1}	2.6×10^{-9}
LOQ / mol L^{-1}	8.7×10^{-9}
Regression coefficient (R^2)	0.994
Repeatability of peak potential (RSD)[a] %	0.1
Repeatability of peak current (RSD)[a] %	1.12

[a]Calculated for 3 replicate measurements.

Analytical application of the presented method

NZ HCl was determined in spiked human serum samples to investigate the applicability of the presented method. Table 2 shows the results of the analysis of serum samples. The accuracy of the method was evaluated by its recovery values. The mean recoveries are in the range of 98.25 – 104.41% (Table 2). The recovery values are very close to 100% indicating that the method shows high accuracy. The reproducibility of the method was estimated from three replicate measurements of electrochemical signal of different NZ HCl solutions. The RSD of recovery values are within the range 0.85 – 3.81% (Table 2). It can be concluded that the precision of the method is very satisfactory for the analysis of serum samples. Hence, this method can be used safely in determination of NZ HCl content in human serum samples. t_{test} was also used to evaluate the performance of the method. The results presented in Table 2 shows that the t_{exp} values does not exceed the $t_{(critical)}$ values confirming that the results of the proposed method and the spiked amount show no difference at a confidence level of 95%.

Table 2: Results of NZ HCl amounts in human serum spiked by standard NZ HCl determined using the presented SWAAdSV method.

Sample	Spiked amount, μg	Found amount, μg	Recovery value, %[a]	RSD, %[b]	$t_{exp.}$
Standard in serum I	2.47	2.45; 2.34; 2.49	98.25 ± 7.75	3.18	0.024
Standard in serum II	12.34	12.88;12.99; 12.77	104.41 ± 2.21	0.85	1.06

[a]Results of recovery values are given as mean ± $\frac{ts}{\sqrt{N}}$ at 95% confidence level); [b]RSD Relative standard deviation; $t_{critical}$ value for 95% confidence level is 4.30 for two degrees of freedom.

Table 3 compares the characteristics of potentiometric and voltammetric methods reported for the analysis of NZ HCl with the proposed method. It is clear from the table that the method exhibits a low detection limit, wide linear range and good recovery. Among electrochemical methods for NZ HCl proposed method exhibits the best analytical characteristics.

Table 3: Comparison of electrochemical methods reported for the determination of NZ

Method	Working electrode	Linear range mol L^{-1}	Detection limit mol L^{-1}	Recovery pharmaceutical preparation %	Recovery serum %	Ref.
Potentiometric	ISPE ICPE	7.0×10^{-7}-1.0×10^{-2}	5.6×10^{-7} 5.9×10^{-7}	98.6-101.3 96.4-103.8	-	(3)
Potentiometric	NPZ-TPB ion pair (conventional) NPZ-TPB ion pair (Graphite coated)	1.0×10^{-5}-5.0×10^{-2} 5.0×10^{-6}-5.0×10^{-2}	4.0×10^{-6} 2.5×10^{-6}	97.9-101.8	-	(14)
Potentiometric	SPE CPE	1.0×10^{-6}-1.0×10^{-2}	3.5×10^{-6} 1.5×10^{-6}	98.3-99.0 97.20-97.30	-	(15)
BIA-SWV	BDD electrode	3.0×10^{-6}-2.1×10^{-5}	4.0×10^{-8}	-	-	(19)
SWAAdSV	Al_2O_3-NP-CPE	5.0×10^{-8}-3.0×10^{-5}	2.6×10^{-9}	-	98.2-104.4	This study

ISPE:*in situ* modified screen printed electrode; ICPE: *in situ* modified carbon paste electrode; NPZ-TPB: naphazoline tetraphenylborate; SPE: screen printed electrode; CPE: Carbon paste electrode; Al_2O_3-NP-CPE: aluminium oxide nanoparticles modified carbon paste electrode; BIA- SWV: batch-injection analysis system with square wave voltammetry; BDD: boron- doped diamond.

CONCLUSION

Electrochemical determination of NZ HCl in human serum was achieved with SWAAdSV method for the first time. Al_2O_3-NPs-CPE electrode enhanced the analytical performance of the proposed method in terms of LOD, LOQ and linear working range. The proposed method offers a simple, sensitive, rapid and low-cost approach to the analysis of NZ HCl in human serum samples. Moreover, the method was successfully applied to serum samples, with the advantage of no requirement of time consuming extraction step.

ACKNOWLEDGEMENTS

This work was funded by Namık Kemal University Research Fund. Project No. NKU BAP. 00.10.YL.14.03. The authors would like to thank to Prof. Esma Kılıç at Ankara University for helpful discussions.

REFERENCES

1. Meloun M, Syrový T, Vrána A. The thermodynamic dissociation constants of ambroxol, antazoline, naphazoline, oxymetazoline and ranitidine by the regression analysis of spectrophotometric data. Talanta. 2004 62(3):511-22.

2. Manzoori J, Amjadi, M. Spectrofluorimetric and cyclodextrin-enhanced spectrofluorimetric methods for the determination of naphazoline in nasal and eye drops. Indian Journal of Chemistry. 2003 42A:2988-92.

3. Mohamed GG, El-Dien FN, Frag EY, Mohamed MEB. In situ modified screen printed and carbon paste ion selective electrodes for potentiometric determination of naphazoline hydrochloride in its formulation. Journal of Pharmaceutical Analysis *J. Pharm. Analysis*. 2013 *5*:367-75.

4. Souri E, Amanlou M, Farsam H, Afshari A. A rapid derivative spectrophotometric method for simultaneous determination of naphazoline and antazoline in eye drops. Chemical and Pharmaceutical Bulletin. 2006 54(1):119-22.

5. Goicoechea HC, Collado MS, Satuf ML, Olivieri AC. Complementary use of partial least-squares and artificial neural networks for the non-linear spectrophotometric analysis of pharmaceutical samples. Analytical and Bioanalytical Chemistry. 2002 374(3):460-5.

6. Joseph-Charles J, Bertucat M. Simultaneous determination of naphazoline nitrate and tetramethylthionine base in eye drops by first-derivative UV spectrophotometry. Analytical Letters. 1999 32:373-82.

7. Zhu S, Liu Y. Spectroscopic analyses on interaction of Naphazoline hydrochloride with bovine serum albumin. Spectrochimica Acta Part A: Molecular and Biomolecular Spectroscopy. 2012 98:142-7.

8. El deen Sayed N, Hegazy M, Abdelkawy M, Abdelfatah R. Spectrophotometric, chemometric and chromatographic determination of naphazoline hydrochloride and chlorpheniramine maleate in the presence of naphazoline

hydrochloride alkaline degradation product. Bulletin of Faculty of Pharmacy. Cairo University, 2013 51(1):57-68.

9. Ali NW, Hegazy MA, Abdelkawy M, Abdelfatah, RM. Simultaneous determination of naphazoline hydrochloride, chlorpheniramine maleate and methylene blue in their ternary mixture. Pakistan Journal of Pharmaceutical Sciences. 2013 26:641-8.

10. Díaz BC, Terrones SC, Carretero AS, Fernández JMC, Gutiérrez AF. Comparison of three different phosphorescent methodologies in solution for the analysis of naphazoline in pharmaceutical preparations. Analytical and Bioanalytical Chemistry. 2004 379:30-4.

11. Huang T, Chen N, Wang D, Lai Y, Cao Z. A validated stability-indicating HPLC method for the simultaneous determination of pheniramine maleate and naphazoline hydrochloride in pharmaceutical formulations. Chemistry Central Journal. 2014, 8, 7: 1-9.

12. Korodi T, Dulavová M, Urban E, Kopelent-Frank H, Lachmann B. A Stability-Indicating HPLC method for the determination of naphazoline and its degradation product and methyl parahydroxybenzoate in pharmaceutical preparations. Journal of Liquid Chromatography & Related Technologies. 2014 37:1321-33.

13. Massaccesi M. Gas chromatographic determination of some imidazolines in pharmaceutical preparations using the FFAP in stationary phase. Pharmaceutica Acta Helvetiae. 1987 62(10-11):302-5.

14. Ghoreishi SM, Behpour M, Nabi M. A novel naphazoline-selective membrane sensor and its pharmaceutical applications. Sensors and Actuators B: Chemical. 2006 113(2):963-9.

15. Frag EY, Mohamed GG, El-Dien FN, Mohamed ME. Construction and performance characterization of screen printed and carbon paste ion selective electrodes for potentiometric determination of naphazoline hydrochloride in pharmaceutical preparations. Analyst. 2011 *136*:332-9.

16. Saito T, Morita S, Kishiyama I, Miyazaki S, Nakamoto A, Nishida M, Namera, A, Nagao M, Inokuchi S. Simultaneous determination of dibucaine and naphazoline in human serum by monolithic silica spin column extraction and liquid chromatography–mass spectrometry. Journal of Chromatography B. 2008 872(1-2):186-90.

17. Öztürk F, Küçükkolbaşı S, Kaçar C, Kılıç E. Electrochemical studies of olmesartan medoxomil and its detection in pharmaceutical dosage forms and biological fluids by cathodic adsorptive stripping voltammetric method. Journal of the Brazilian Chemical Society. 2014 25(5):920-7.

18. Öztürk F, Taşdemir IH, Durmuş Z, Kiliç E. Electrochemical behavior of disopyramide and its adsorptive stripping determination in pharmaceutical dosage forms and biological fluids. Collection of Czechoslovak Chemical Communications. 2010 75(6):685-702.

19. Thiagoda CO, Jhonys MF, Rodrigo A, Abarza M, Eduardo MR. A batch injection analysis system with square-wave voltammetric detection for fast and simultaneous determination of naphazoline and zinc. Talanta. 2016 152:308-13.

20. Uslu B, Ozkan SA. Electroanalytical application of carbon based electrodes to the pharmaceuticals. Analytical Letters. 2007 40(5):817-53.

21. Shi X, Gu W, Li B, Chen N, Zhao K, Xian Y. Enzymatic biosensors based on the use of metal oxide nanoparticles. Microchimica Acta. 2014 181(1-2):1-22.

22. Öztürk FÖ, Erden PE, Kacar C, Kilic E. Amperometric biosensor for xanthine determination based on Fe_3O_4 nanoparticles. Acta Chimica Slovenica. 2014 61(1):19-26.

23. Karimi-Maleh H, Ahanjan K, Taghavi M, Ghaemy M. A novel voltammetric sensor employing zinc oxide nanoparticles and a new ferrocene-derivative modified carbon paste electrode for determination of captopril in drug samples. Analytical Methods. 2016 8(8)1:1780-8.

24. J. Wang, Analytical electrochemistry, 2 nd edition, Wiley-VCH, New York 2000.

25. Chang BY, Park SM. Electrochemical impedance spectroscopy. Annual Review of Analytical Chemistry. 2010 3: 207-9.